INL/EXT-20-58489

Light Water Reactor Sustainability Program

Risk Importance Ranking of Fire Data Parameters to Enhance Fire PRA Model Realism

May 2020

U.S. Department of Energy

Office of Nuclear Energy

INL/EXT-20-58489

Risk Importance Ranking of Fire Data Parameters to Enhance Fire PRA Model Realism

John M. Biersdorf (INL)
Ha Bui, (UIUC)
Tatsuya Sakurahara, (UIUC)
Seyed Reihani, (UIUC)
Chris LaFleur (SNL)
David L. Luxat (SNL)
Steven R. Prescott (INL)
Zahra Mohaghegh (UIUC)

May 2020

Prepared for the
U.S. Department of Energy
Office of Nuclear Energy

Light Water Reactor Sustainability Program

RISK-Informed Systems Analysis

Risk Importance Ranking of Fire Data Parameters to Enhance Fire PRA Model Realism

ABSTRACT

Fire is historically and analytically a significant contributor to nuclear power plant risk. The level of fire risk and the methods, tools, and data for modeling this risk are highly debated by experts. One area of debate is the input data used in fire modeling and how to deal with this data's high rate of uncertainty. This report outlines work performed for determining the key parameters causing this uncertainty and how it propagates into nuclear power plant PRA models. This research used the Integrated Probabilistic Risk Assessment (I-PRA) method and paves the way to correctly assess and reduce data uncertainty in fire modeling.

SUMMARY

The Nuclear Regulatory Commission requires that nuclear power plants evaluate fire risk, emphasizing the use of PRA modeling. However, there are several issues with the current risk modeling implementation that affect the results. Approved modeling methods can be overly conservative and often do not match plant experience. Also, the data used in the modeling can have many uncertainties and can be influenced by expert judgment.

To evaluate input data uncertainty, researchers performed an initial review of several fire experiments done at Sandia National Laboratories. Uncertainties for fire data can come from many sources, such as experiment design constraints, environmental conditions, or other plant-specific aspects. There are many different significant and insignificant parameters driving the uncertainty. Additionally, the uncertainty of the different input data used in the fire modeling could have a significant or insignificant effect on the entire plant risk.

A four-step methodology was developed to perform I-PRA Importance Ranking. A demonstration case using these steps was set up and three of the four steps were completed in fiscal year (FY) 2019. The fourth step was done in FY 2020. These steps included:

1. A qualitative analysis of potential sources of uncertainty. The following items were considered for the demonstration:
    - Maximum heat release rate
    - Time to maximum heat release rate
    - Duration of max heat release rate
    - Time to decay
    - Thermal conductivity of concrete
    - Specific heat of concrete
    - Density of concrete
    - Cable jacket thickness
    - Fire location
2. A quantitative characterization of dominant sources of uncertainty. A list of distributions and their parameters obtained for the dominant sources of uncertainty is shown in Appendix A.
3. A quantitative screening of the potential sources of uncertainty using Morris Elementary Effects (EE) analysis. A case study fire simulation model was developed and coupled with the Risk Analysis Virtual Environment (RAVEN). Compared to the one-way sensitivity analysis methods commonly used in the current PRA practices, the Morris EE

method provides a more robust distinction between influential vs. non-influential factors since it can explicitly address both main effects and the effects by nonlinearity and interaction through a randomized one-at-a-time sampling scheme. Among the sources of uncertainty associated with the nine input parameters of the fire simulation model, the Morris EE analysis was able to screen out four insignificant parameters, i.e., thermal conductivity of concrete, specific heat of concrete, density of concrete, and cable jacket thickness.

4. Global importance measure (Global IM) analysis to generate a comprehensive ranking based on their influence on the plant risk. In this research, a moment-independent Global IM is used since it can address (a) uncertainty in the input parameters of the fire model, (b) uncertainty in the risk outputs, and (c) non-linearity and interactions among input parameters in the fire model, more accurately than the correlation-based and variance-based global methods. The observations from the research showed that, depending on the initial and boundary conditions of the fire scenarios, fire-induced damage could have a very small probability and could be dominated by the tail of the uncertainty distribution; hence, the accuracy of the correlation-based and variance-based methods is questionable. The moment-independent Global IM analysis in this research provides a better understanding of how experimental uncertainty data affects industry's plant models and where improvements in that data will have the largest benefit for improving fire modeling accuracy in causing core damage. Among the five unscreened parameters obtained from the Morris EE analysis, the Global IM analysis results for the case study indicated that max heat release rate and fire location are the most important parameters.

The report also outlines benefits of using a unified computational platform that integrates the underlying simulations (e.g., a fire progression model), quantitative screening (using the Morris EE method), and the Global IM analysis. A unified platform can (i) facilitate the ranking of input parameters considering multiple key fire scenarios simultaneously, rather than considering one scenario at a time, (ii) contribute to more explicit and accurate treatment of dependencies at multiple levels of Fire PRA, (iii) facilitate the sampling-based uncertainty quantification for Fire PRA, and (iv) help generating both "industry-wide" and "plant-specific" ranking of uncertainty sources in Fire PRA.

Future research should be done to include additional parameters such as detection/suppression or cable fire spread. Adding a PRA software such as SAPHIRE to the RAVEN platform would help with plant model integration and improve treatment of fire-induced dependency. The I-PRA risk importance ranking methodology offered in this report can provide valuable information for efficiently (a) enhancing the realism of Fire PRA for existing plants and (b) supporting the development of Dynamic Fire PRA for advanced reactors and new plants.

CONTENTS

FIGURES

TABLES

ACRONYMS

3-D	Three-Dimensional
AC	Alternating Current
ANS	American Nuclear Society
ASME	American Society of Mechanical Engineers
BE	Basic Event
CAFTA	Computer Aided Fault Tree Analysis System
CAROLFIRE	Cable Response to Live Fire
CCDP	Conditional Core Damage Probability
CFAST	Consolidated Model of Fire Growth and Smoke Transport
CFD	Computational Fluid Dynamics
CFR	Code of Federal Regulations
CHRISTIFIRE	Cable Heat Release Ignition and Spread in Tray Installations During Fire
CI	Confidence Interval
DC	Direct Current
DESIREE-Fire	Direct Current Electrical Shorting in Response to Exposure Fire
DET	Dynamic Event Tree
DPRA	Dynamic Probabilistic Risk Assessment
EdF	Electricité de France
EE	Elementary Effects
EMRALD	Event Model Risk Assessment using Linked Diagrams
EPRI	Electric Power Research Institute
FDS	Fire Dynamics Simulator
FDT	Fire Dynamics Tools
F-V	Fussell-Vesely
FIVE-Rev1	Fire-Induced Vulnerability Evaluation Revision 1
FRP	First Responder Performance Module
FSM	Fire Simulation Module
HELEN-FIRE	Heat Release Rates of Electrical Enclosure Fires
HRR	Heat Release Rate
HVAC	Heating, Ventilation, and Air Conditioning
IE	Initiating Event
IF	Ignition Frequency
IM	Importance Measure

INL	Idaho National Laboratory
I-PRA	Integrated Probabilistic Risk Assessment
KATE-Fire	Kerite Analysis in Thermal Environment of Fire
KPM	Key Performance Measure
LWR	Light Water Reactor
MPI	Message Passing Interface
NEI	Nuclear Energy Institute
NFPA	National Fire Protection Association
NIST	National Institute of Standards and Technology
NPP	Nuclear Power Plant
NRC	Nuclear Regulatory Commission
NSP	Non-Suppression Probability
NUREG	Nuclear Regulatory Commission Regulation
OAT	One-At-A-Time
PRA	Probabilistic Risk Assessment
PWR	Pressurized Water Reactor
RACHELLE-FIRE	Refining and Characterizing Heat Release Rates from Electrical Enclosures during Fire
RAVEN	Risk Analysis Virtual Environment
RAW	Risk Achievement Worth
SAPHIRE	Systems Analysis Programs for Hands-on Integrated Reliability Evaluations
SF	Severity Factor
SSC	Structures, Systems, and Components
SNL	Sandia National Laboratory
SoTeRiA	Socio-Technical Risk Analysis
THIEF	Thermally-Induced Electrical Failure
UIUC	University of Illinois at Urbana-Champaign

1. INTRODUCTION

The 1976 fire at Brown's Ferry Nuclear Plant highlighted weaknesses in assessing and understanding the impacts of fire scenarios with respect to potential core damage events for nuclear reactors. To address the fire risk to the nuclear utilities, Appendix R to the Code of Federal Regulations (CFR) 10 CFR 50 was created. This was a deterministic approach to assessing the fire risk within the nuclear plants. A risk-informed performance-based standard, National Fire Protection Association (NFPA) 805 [1] was introduced in 2001 and led to the development of approved guidelines for the implementation within the nuclear plants themselves. The U.S. Nuclear Regulatory Commission (NRC) and Electric Power Research Institute (EPRI) created Nuclear Regulatory Commission technical report designation (NUREG) NUREG/CR-6850 (EPRI 1011989) which outlined guidelines for the nuclear plants to assess risk attributed to fire events within the plant that could cause core damage or a release of radionuclides. This NUREG outlines the methodology for using Probabilistic Risk Assessment (PRA) to assess and monitor fire risk to the plant.

There is a very strong interest in analysis of fire protection engineering practice, both domestically and worldwide. The NRC with EPRI and the National Institute of Standards and Technology (NIST) conducted a research project to verify and validate five fire models used for Nuclear Power Plant (NPP) applications. The results of this effort are documented in a seven-volume NUREG report, NUREG-1824 [2],[3], Verification & Validation of Selected Fire Models for NPP Applications. More recently, the NUREG-1934 [4] document provides information on the use of fire models in support of various commercial NPP fire hazard analysis applications.

The lack of realism in Fire PRA may generate biased risk information, which could impede the identification of truly critical risk-contributing factors and result in unnecessary and costly plant modifications. To better facilitate risk-informed decision making, the degree of realism in Fire PRA should be increased and the risk-contributing factors should be ranked based on their influence on the system risk.

Lack of realism may come from multiple areas. One of these areas is the limited sources and uncertainty of the data used to support fire risk modeling. To efficiently improve the realism of Fire PRA, it is critical to properly prioritize areas that need further industry, regulatory agency, and academic research/investigation. In current practice, the prioritization of Fire PRA research areas is mainly based on engineering judgments provided by experienced and knowledgeable experts from within the industry and regulatory agency [5],[6]. Although expert judgment helps provide valuable insights, the excessive reliance on the experts is vulnerable to various factors. Knowledge dependency among multiple experts and biases toward the occurrence of recent events are examples of the factors that could mislead the experts' judgments. To provide additional input for the decision making on prioritizing research areas in Fire PRA, this study develops a new methodology for identifying inputs/factors that are the most influential sources of uncertainty and conservatism in Fire PRA based on their contributions to the fire-induced plant risk.

2. BACKGROUND

The existing Fire PRA is developed using standard static PRA models, basically with the same general concepts as normal internal-events PRA. The major differences from the internal-events PRA come from what type of components are currently in scope and how scenarios are created and handled. A static PRA utilizes single failures or initiating events when beginning to analyze the plant's response and capabilities to respond to said event. All structures, systems, and components (SSCs) need to be incorporated into the PRA model to realistically assess the plant response to accident situations. However, it is not practical to model everything, so reasonable assumptions must be made to simplify the model and still get a realistic simulation.

In creating a Fire PRA, a risk analysis team of experts is required to help identify SSCs to be included and also to help develop the scenarios. The fire risk analysis team will include individuals with expertise in four key areas:

1. Fire analysis (basic fire behavior, fire modeling, fire protection engineering, and plant fire protection regulatory compliance practices and documentation)
2. General PRA and plant systems analysis (event tree/fault tree analysis, NPP systems modeling, reliability analysis, PRA practices as applied in the internal-events domain, and specific knowledge of the plant under analysis)
3. Human reliability analysis (emergency preparedness, plant operations, plant-specific safe-shutdown procedures, and operations staff training practices)
4. Electrical analysis (circuit failure modes and effects analysis and post-fire safe shutdown, including plant-specific regulatory compliance strategies and documentation).

While some of this expertise is generic, much of it is specific to the plant under analysis.

2.1 Risk-Informed Fire Assessments – Industry Fire PRA and Uses

2.1.1 Appendix R and Deterministic Approaches

The requirement to protect the public from nuclear accidents due to fire is addressed in CFR part 50, Appendix R. It lays out specifically how many protected systems need to be maintained at all times due to fire events. This includes all support components and cables that allow the components to perform their required safety function. This methodology is deterministic in its approach to stating whether components can provide the specific safety function. There is no use of risk-informed methodology and, as such, it is a more conservative assessment of fire's risk to the nuclear plant.

2.1.2 Risk-informed methodology – NUREG/CR 6850 and NFPA 805

The methodology for the static Fire PRA is built of the same event tree/fault tree approach as an internal-events PRA. The major differences lie in what is to be considered in scope for the Fire PRA, which includes a large selection of components and supporting equipment and scenario development. In addition to the safety system mitigation equipment, Fire PRAs must take into account fire-specific equipment, such as suppression and detection systems, fire barriers, and equipment credited for specific fire-related operator actions must also be addressed. Another unique major contributor to fire risk is the associated cabling for the credited equipment. Identifying the cabling is significant to ensure that fires do not prevent the specific equipment from performing their mitigation function. To create the overall fire scenarios, it is important to lay out the plant boundaries and identify where fires would originate, and what types of fires are possible. Once boundaries are established, scenarios need to be made that incorporate the heat release rates (HRRs) of fire types, fire spread from target to target and compartment to compartment, suppression and detection equipment, and additional operator actions. The goal of the Fire PRA is to analyze these scenarios to identify the risks to the plant, including the types and locations of fires that cause the most significant amount of risk to core damage or a release of radionuclides.

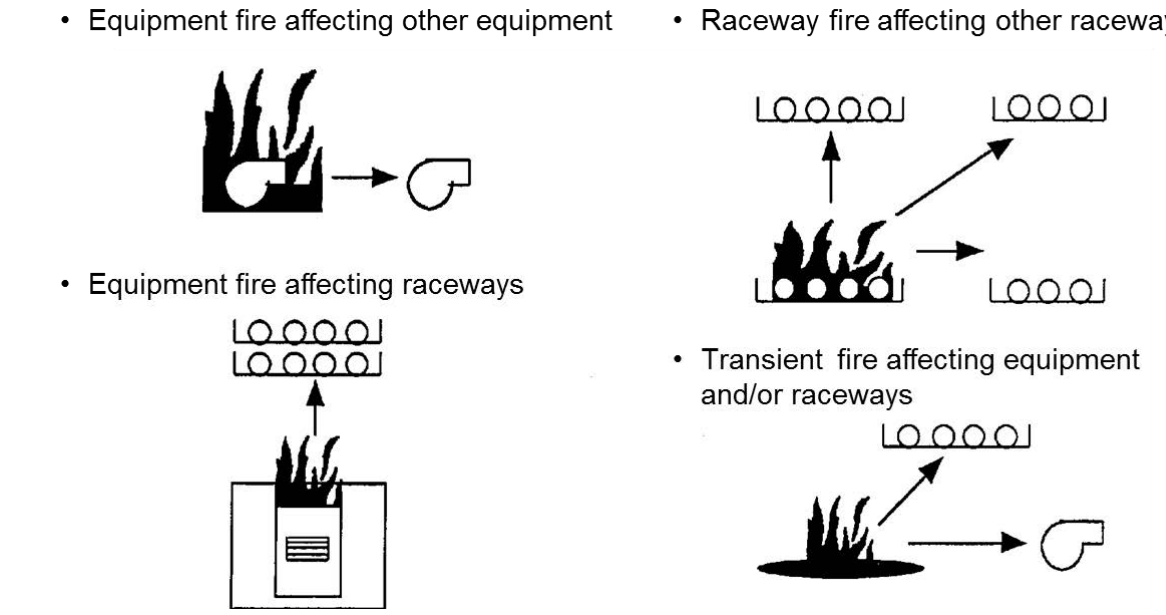

Figure 1: Sample scenarios for fire spread and impacts.

The components that can cause fire (e.g., electrical cabinets, pumps, oil reservoirs, transient combustibles, cable fires) and then impact targets around them are shown in Figure 1. Initially, the direct impact of fires on the component must be evaluated. Next, it must be determined if the fire can create a hot gas layer which can damage components indirectly. Finally, the scenarios about whether or not the fire (or hot gas layer) can spread into an adjacent compartment must be analyzed. These steps provide the immediate scope of the fire analysis and what it can directly impact in the scenario. Subsequently, the analysis needs to be expanded to see what components are affected by cable damage, the timing for failures, and other impedances for operator actions, and then incorporated into the scenarios.

There are multiple ways to incorporate the scenarios into the PRA model. A scenario can be added directly into fault trees or event trees. Also, a new PRA model does not need to be built for the Fire PRA, but rather scenarios can be incorporated directly into existing internal-events PRAs. There are different types of logic modeling software such as RISKMAN, Computer Aided Fault Tree Analysis System (CAFTA), and Systems Analysis Programs for Hands-on Integrated Reliability Evaluations (SAPHIRE). In this analysis, SAPHIRE [7] was used for examples.

To understand how current Fire PRA works within an internal-events model, an example is shown in an event tree (Figure 2) and fault tree (Figure 3).

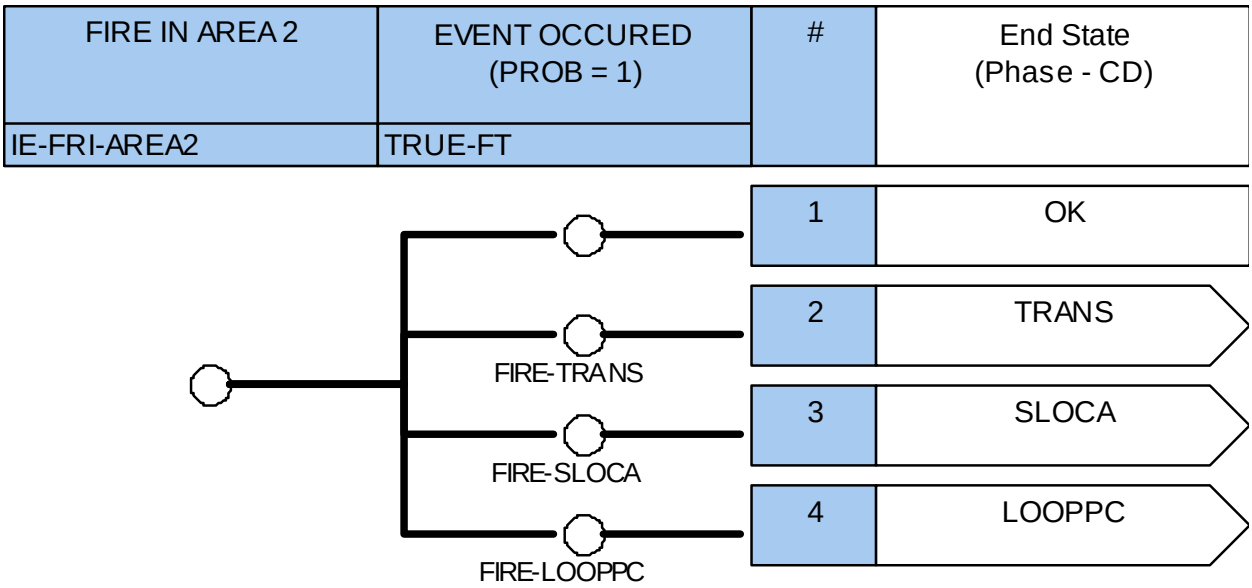

Figure 2: Example event tree with added fire branches into existing PRA.

The initiators are fires within the compartments that lead into their relevant internal-events event trees this is represented by the final TRANS, SLOCA, and LOOPPC boxes in Figure 2. Once the initiator occurs the fire event transfers into other initiators to assess the mitigation response if that fire managed to cause those types of events. The internal-events model will still analyze the individual random failures that can occur within the plant, but the fire failures must be accounted for as well. This is done by creating fire-specific failures within the fault tree, as shown in the HE-FIRE-AREA2 event in Figure 3. SAPHIRE produces cut-sets by quantifying the random failures and fire induced failures in the fault trees and the system failures of each accident sequence in the event trees. Once the cut sets are generated it removes redundant or non-minimal cut-sets using Boolean algebra to get the correct risk associated with each fire scenario. For more detail on this process or the specifics of how SAPHIRE works see [78].

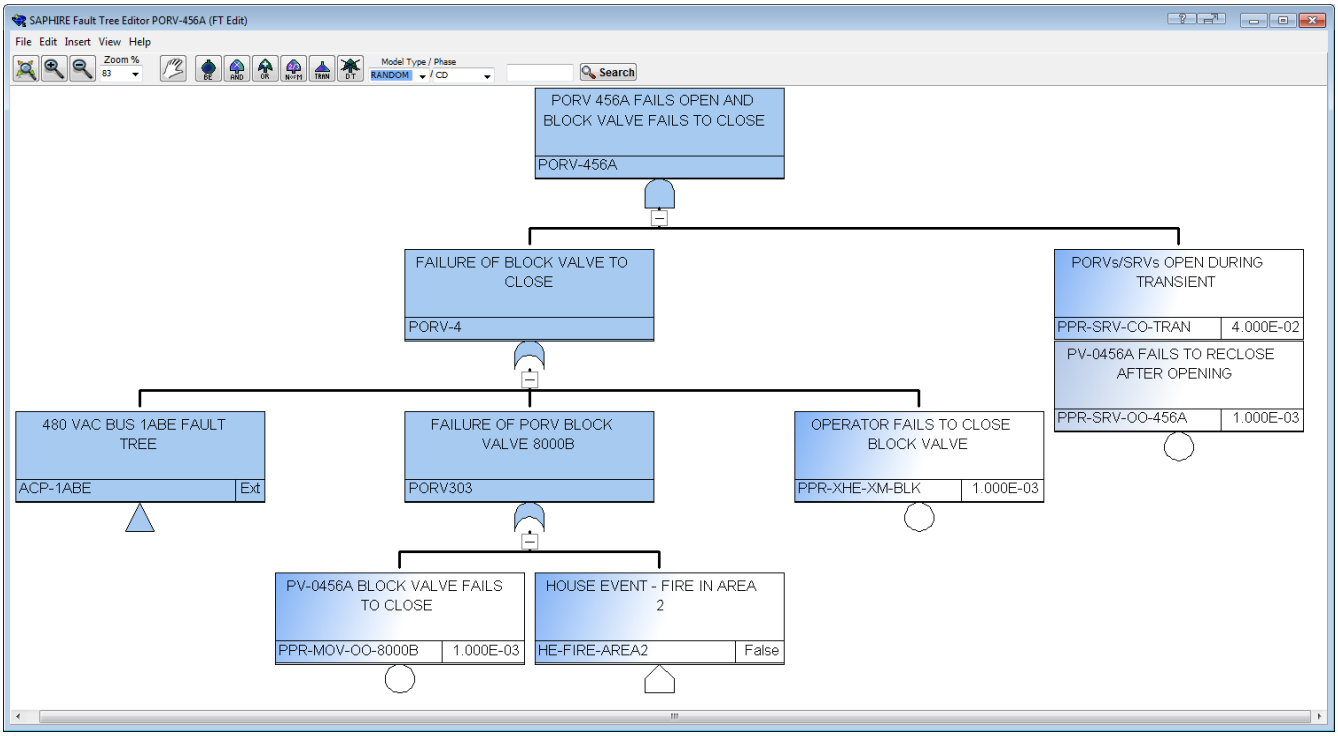

Figure 3: Example fault tree with specific fire failures added (HE-FIRE-AREA2).

This a common fire PRA modeling practice and seldom does it need to be more complicated than this. The PRA analyst will decide the level of detail that should be modeled in the PRA. The scenarios can be modeled from compartment level resolution down to the resolution of individual ignition sources and targets

2.1.3 Fire PRA

2.1.3.1 Fire Modeling

Improving the realism is beneficial for a variety of reasons. Namely, improving the uncertainty overall will allow for less variability in the results when quantifying our PRA models. It will allow the users to be more confident with the fire risk assessments overall. By identifying the key parameters driving the results, we can find the parameters that need to have improved uncertainties, improving the overall uncertainty of the model. Figure 4 [8] shows the uncertainty associated with Fire PRAs (included in the “other external events”) in relation to the more realistic internal-events model. Improving the uncertainty distributions would allow for more confidence in these models.

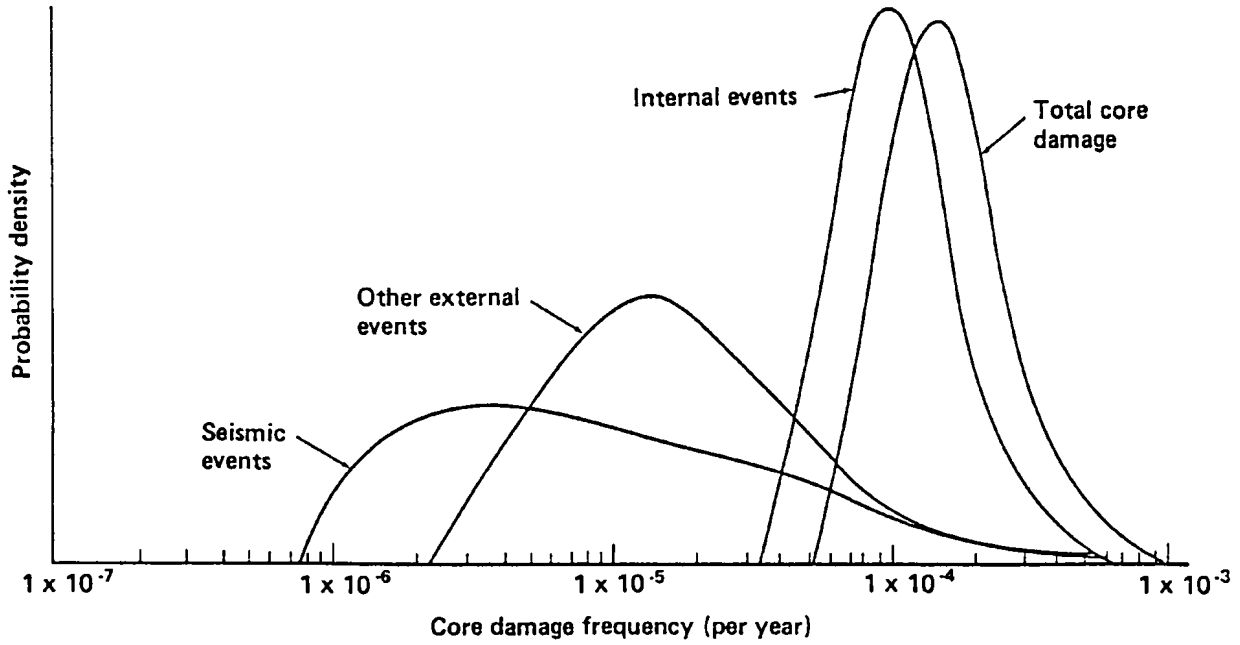

Figure 4: Uncertainty distribution for PRAs.

The second benefit would come from improved data collection and experiments, which may improve the mean probabilities or frequencies of our data sets. This may end up driving down the overall results in the future if the improved data can be utilized in the PRA model. As an example, a fire was simulated in the switchgear room to see how improving the HRR mean-point frequency would impact the scenario frequency and improve the model as a whole. The fire scenario was shown to fail both diesel generators using a generic pressurized water reactor (PWR) model. The logic that was modeled and inserted is shown below in Figure 5.

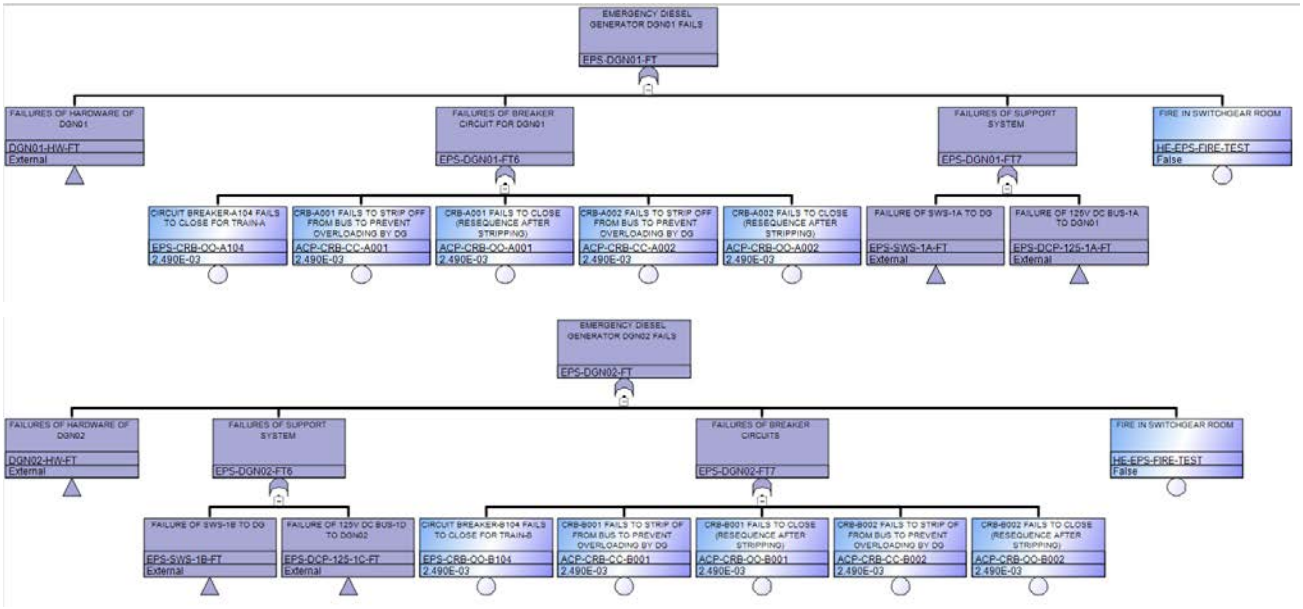

Figure 5: Example fire fault tree logic.

The “HE-EPS-FIRE-TEST” house event in the far-right of the diagram, will be triggered in the event of a switchgear fire failing both diesel generators.

Next, a flag set was created to change those house events from a “False” probability to a “True” probability after the occurrence of the switchgear fire. That flag set is shown below in Figure 6.

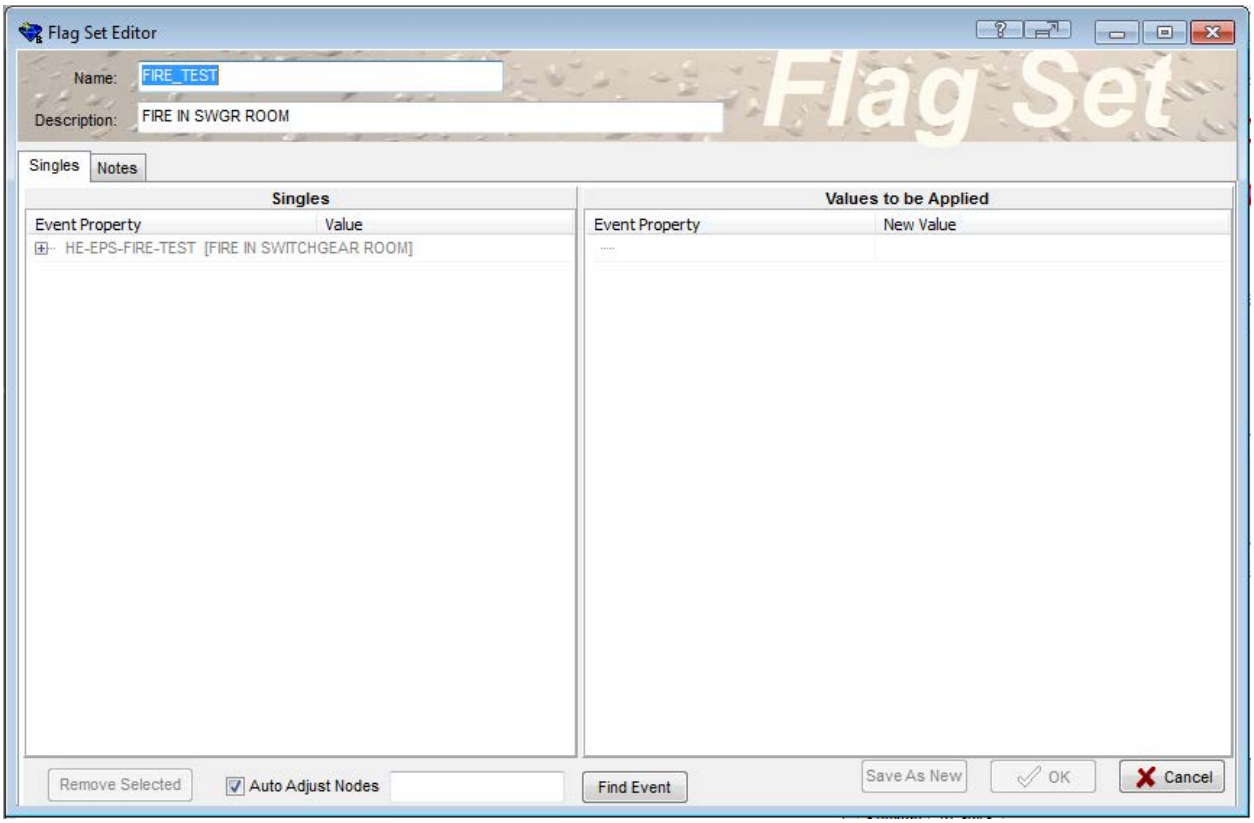

Figure 6: Example fire flag set.

Additional surrogate events could be placed here to fail additional components, or the house event can be placed directly into the logic.

Finally, the initiating event was created using test frequencies of 1.5E-2 (acquired from industry averages) and 1.0E-2 to show how a change may impact results. The fire initiating event tree is shown below in Figure 7.

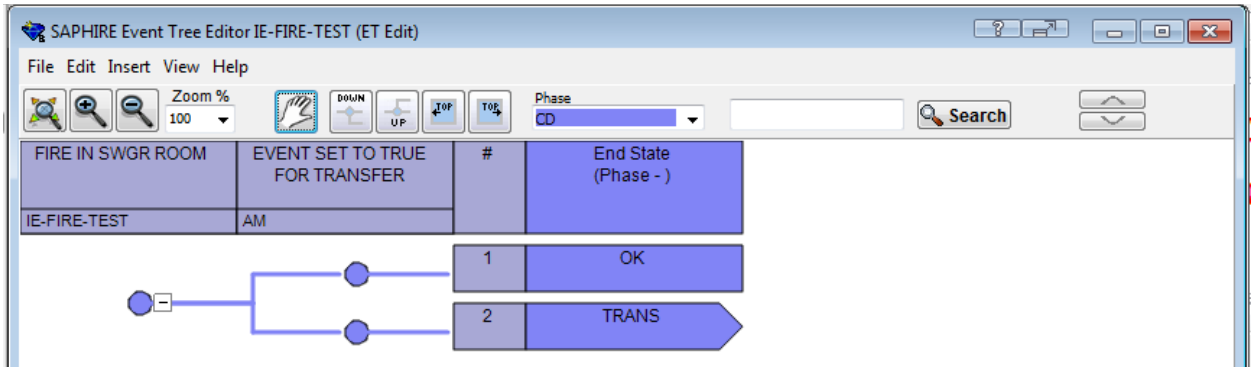

Figure 7: Example fire event tree logic.

Once the modeling is done, this specific initiator is quantified with the two different frequencies and the results are compared.

2.1.3.2 Input Data Areas

The impact of the HRR parameters was one area of interest on the initial phase of research. The maximum HRR value, the time to maximum HRR, duration of maximum HRR, and time to decay all impact the ignition frequencies of specific initiating event fires. Reducing the uncertainties surrounding those parameters will improve the level of realism and confidence in the specific HRR curves used in the PRA models. If the mean-point frequency can be improved, showing that fires of specific severity or duration are less likely to occur can improve the data used in the models for those types of fires. This is the example chosen in the previous section. Another area for data usage is identifying the uncertainty and improving the data around cable failure temperatures. This would improve the realism around exactly which fires would damage significant cables within the utility. If the data changes, it may change the severity of the fires that damage specific targets (reducing the severity factor or ignition frequency) or remove those targets from scenarios altogether. Finally, the parameters looking at properties of concrete will allow for better realism when modeling specific compartments in how hot those compartments will get and how fast they will heat up, as well as the possibility of fire spreading to adjacent compartments if the concrete fails. That information will be incorporated into the ignition frequencies or directly into what scenarios are possible and able to be modeled.

The four variables must be multiplied to solve the core damage frequency of each individual fire scenario. This new data would impact two of those variables—the ignition frequency and severity factor (sometimes included in ignition frequency), or eliminate the scenario entirely. The other variables included are NSP and the conditional core damage probability (CCDP).

$$(Core\ Damage\ Frequency)_i = IF_i * SF_i * NSP_i * CCDP_i \quad (5)$$

When solving a Fire PRA, first the core damage frequency is solved for each scenario and then added to find the total core damage frequency for the plant due to fire risk. This shows how reducing two of those variables or eliminating scenarios entirely would help reduce the overall core damage frequency of the plant.

2.1.3.3 Regulation Requirements

Currently, the industry either requires the utilities to be governed by 10 CFR 50 Appendix R, the deterministic approach, or they could have transitioned to NFPA 805 [1], the risk-informed methodology. This information could help improve the models developed to risk-inform the utilities of their fire risk for everyday operations, maintenance, or modification assessments. If this methodology is more accurate and shows improvements for facilities, it would help the utilities and the regulators have a better understanding and more confidence in the numbers to show just how risky certain actions would be. If the mean-point numbers were able to be adjusted through continued experimentation and additional data, it would allow the plants to have better numbers, which would encourage more utilities to make the shift to risk-informed governance or better utilize the models they allow for more configurations and online maintenance.

2.1.3.4 Data Change Insights

Using the example from Section 3.4.1, plugging the fire scenario into a generic PWR PRA model shows what reducing the mean-point frequency of a single scenario can accomplish. When quantifying a fire in the switchgear room scenario with a frequency of 1.5E-2, a single scenario gives a total core damage frequency of 2.948E-8. When we reduce the ignition frequency to just 1.0E-2, it drops the core damage frequency to 1.897E-8 for a single scenario. When there are thousands of scenarios within a Fire PRA, this can make a significant difference, especially if we can combine the possible elimination of a scenario.

2.2 Detailed Methods

For a more detailed model, broad fire scenarios that are concerned with fires at a compartment level can be broken down into a larger subset of scenarios that utilize more specific information within each compartment. For example, when deciding to model fire scenarios associated with the main control room, those scenarios can be divided into different sets by identifying unique ignition sources, target sets, or any other special separation that could create a unique situation that the user would like to analyze. The scenarios are typically divided by the type of initiator (electrical panels, motors, transients, hot work, etc.). Some of these initiators may need additional scenarios depending on the types of targets they can damage. In SAPHIRE, this would typically be done by modeling the scenarios directly as basic events in fault trees or by creating modifiers that manipulate the probabilities of existing basic events already within the model. The number of scenarios, targets, and ignition sources are unique to each plant. The approved identification, classification, and modeling methods are found within NUREG-6850.

2.3 Fire Simulation

Computational fire modeling aims to predict fire behavior in different environmental conditions. These computational models need to take into account the various physical processes of combustion, fluid dynamics, and heat transfer processes. The complexity in modeling the physical process of fire propagation arises from the dynamic turbulent nature of the internal processes. Computational Fluid Dynamics (CFD) is a branch of fluid mechanics that provides methods and tools that help in modeling, prototyping, testing, and analysis. NUREG-1824 documents the five software toolkits used in modeling fires in a typical NPP. They are (1) NRC's NUREG- 1805 Fire Dynamics Tools (FDT)[9], (2) EPRI's Fire-Induced Vulnerability Evaluation Revision 1, (FlVE-Rev1), (3) NIST’s Consolidated Model of Fire Growth and Smoke Transport (CFAST) [10], (4) Electricité de France's (EdF) MAGIC[11], and (5) NIST's Fire Dynamics Simulator (FDS)[12].

Algebraic models such as FDT and FIVE-Rev1, from NRC and EPRI, take minimal inputs and create quick analytical calculations. The advantages are that it is fast and easy to use. However, this might result in being too conservative. Zone models CFAST and MAGIC perform more detailed analysis than FDT and FIVE-Rev1. They can compute hot gas layers as well as target heat fluxes. A hot gas layer is a layer of smoke and heat that forms at the ceiling, filling the entire ceiling. It slowly descends, damaging additional targets as it lowers (see Figure 8). But these models also have limitations with respect to complex room geometries and large horizontal paths.

In terms of the types of analysis, FDS is broadest in scope. Moreover, its dynamic nature and simulations can be performed in three-dimensional (3-D) space. Chapter 3 of NUREG-1934 specifically lists seven generic scenarios which are considered for a fire at an NPP, and in many of those scenarios CFD models are either recommended or necessary to provide detailed analysis with obstacles in the path of the fire. Since FDS is a CFD model, it allows the analyst the ability to simulate fire conditions in complex geometries with complex vent conditions. However, it takes a significant effort to properly create the model for simulation, and computation times could be quite long. This modeling is used to simulate the types of fires that can cause damage to components by showing the specific HRRs that would damage nearby targets via direct impact or through a hot gas layer.

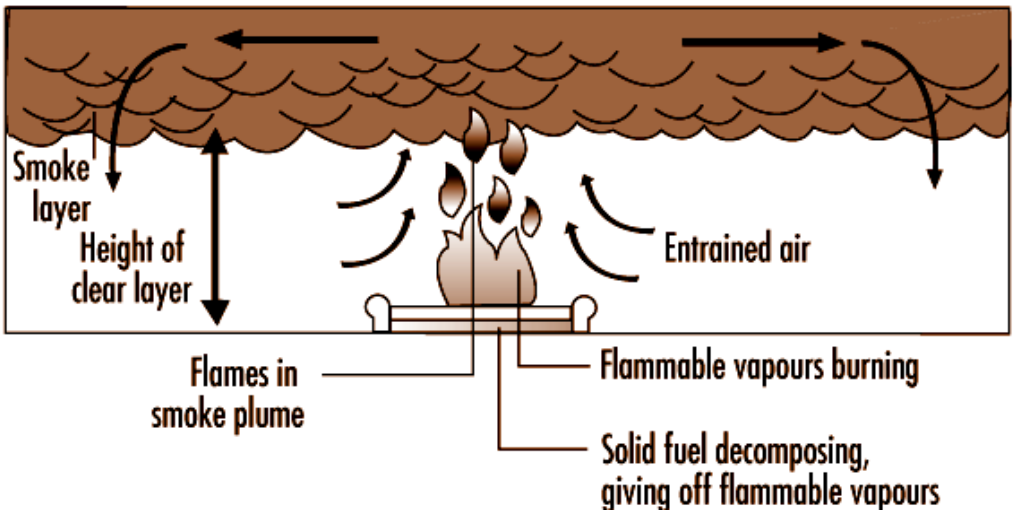

Figure 8: Smoke and hot gas layer formation and behavior.

Each simulation provides an estimate of the scope of damage and determines the components that will be available to help mitigate the specific fire scenario. Figure 9 shows the percentage or likelihood that a fire heat release will create a scenario needing further investigation because the resulting peak HRR can damage additional targets. These scenarios will be incorporated into the PRA. The fires that generate a peak HRR below this point only damage the ignition source itself and no other targets.

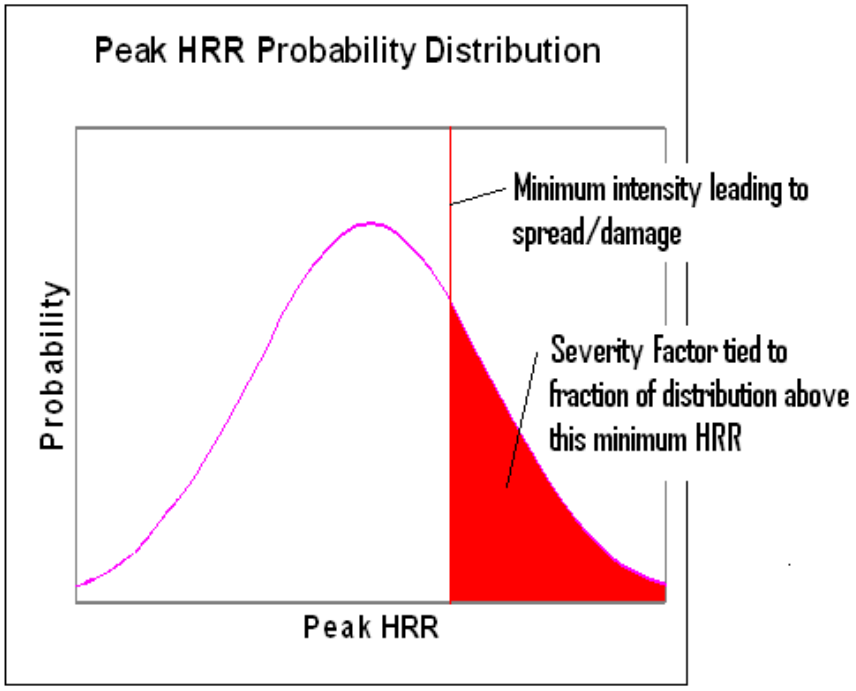

Figure 9: Example heat release rate with the severity factor for a particular component.

Computer modeling also provides information about the timing of the specific fire and how long it takes to damage targets or create a hot gas layer. It additionally provides an estimate of how long it takes for suppression and detection systems to actuate, which can be incorporated with plant procedures and training times. Further, the information can be used as time measurements for fighting the fire and preventing it from damaging targets. This timing information can be used to eliminate the impacts of fire scenarios within the PRA models because a non-suppression probability, in addition to the severity factor, is incorporated into the ignition frequencies. The graph in Figure 10 shows how the non-suppression probability (NSP) approaches 1 on the NSP axis as the time to detection approaches the time to damage. Removing the conservatism in either the time to damage and/or the time to detect can have a significant impact on the fire scenario in question.

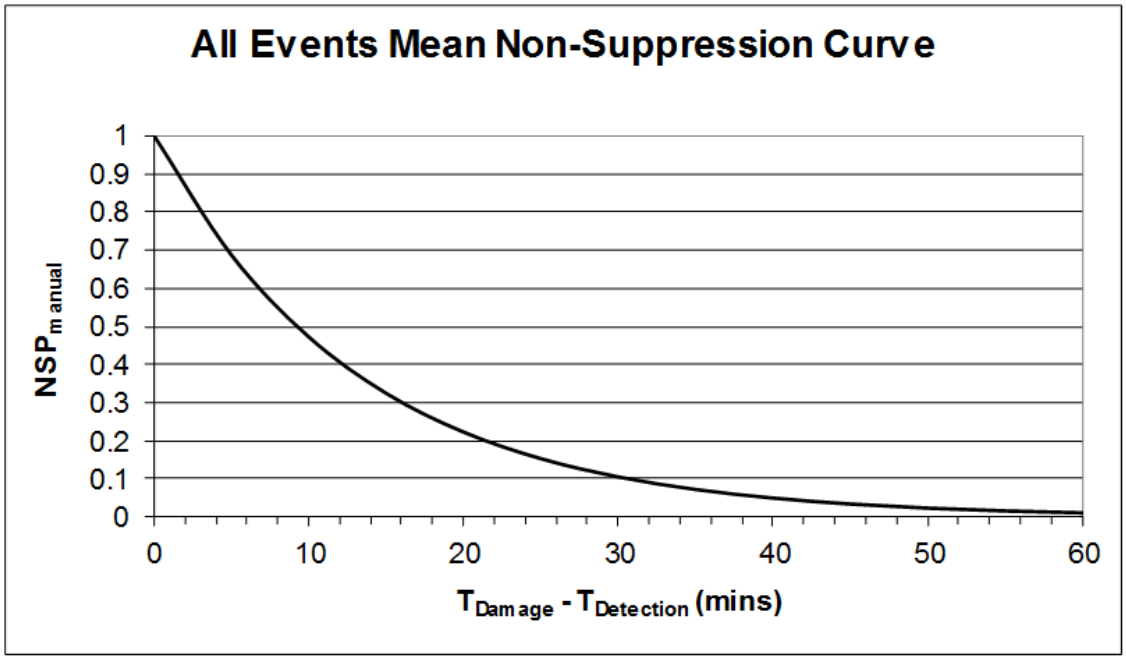

Figure 10: Example non-suppression probability over time.

2.3.1.1 Limitations

The primary limitations are due to the modeling assumptions and uncertainty within the model. Some are unique to fire modeling, while others are common limitations for PRA in general.

- **Modeling limitations** – This is a PRA limitation where not all components or subcomponents are incorporated into the PRA due to time and budget limitations for PRA staff. This limitation can prevent specific failure modes or actions from being performed if the component is not included into the PRA. This issue is mitigated by including enough detail in the model so that an adequate representation of the plant can be made with the components required to simulate it. Modeling conservative fire scenarios is simpler than creating more accurate individual fire scenarios. Excluding severity levels of the fires (what types of fires will damage what components), including failures of nearby equipment into scenarios, and assuming conservative failures of local fire suppression can all be examples of ways to reduce the detail in PRA modeling. However, this simplification introduces conservative assumptions into the modeling that increase the calculated level of risk to the plant. The modeling limitations can be reduced by incorporating more detail into the PRA model, but it is impossible to eliminate completely. It is up to the PRA developers to decide what level of assumptions and generalities are appropriate for a realistic model.

- **Operator action limitations** – The PRA currently can only take modest credit for operator actions and cannot take positive credit for actions that are implemented ahead of schedule. Gaining credit for sped-up actions that would improve the likelihood of successfully completing other actions is not considered within the PRA. Another limitation is the way in which an operator action is modeled as a singular step, or multiple actions as chains of simple steps. This limitation makes it difficult to create a basis for accuracy. When looking at firefighting activities for suppressing fires, being able to credit the timing of operator actions will help improve the time to detection and suppression of the fire. This will give the plant a larger credit for the number of fires that will be suppressed before the fire can cause damage to plant equipment. The credit will reduce the number of fires that create fire scenarios and reduce the overall plant risk.
- **Cable tracing issues** – Not all cables are precisely tracked within an NPP. When developing a scenario, cables that cannot be definitively excluded from a potential fire due to the uncertainty of their actual location must be included within the target sets. This issue is mitigated with better cable tracing to ensure specific cables (especially high-risk ones) are excluded from as many target sets as possible.
- **Fire modeling limitations** – There is significant uncertainty in the HRR profiles used in the PRA, which can have a substantial effect on the results since the HRRs are such a significant input[13, 14] . To mitigate this limitation, work to refine and characterize the maximum HRR of specific ignition sources is ongoing. Additional information on how fire spreads along cables and how power, instrument, and control cables respond during a fire can provide improved realism[15-17]. Also, improved realism of fire frequencies for individual ignition sources is an area of high uncertainty would improve the fire modeling.
- **Timing and spatial limitations** – Currently, it is easier to model conservative timing assumptions in potential fire scenarios. For example, for a fire scenario, it is often far simpler to conservatively assume immediate failure of components or not take credit for operator actions within the given area. This simplifies the modeling but reduces the precision of the model. Taking credit for timing or spatial considerations within the area can help reduce the conservative assumptions placed on the fire scenarios. Specifically, if a cable or manually-operated valve is located in a far corner of the room, it will take time to heat up to the point of damage, or make it incapable of being operated. Using more precise fluid dynamic modeling coupled with the timing of the scenario allows for additional credit to be taken. For example, components that are prematurely failed when using conservative timing assumptions may be credited for at least a specific amount of time as the scenario develops.

2.4 Historical Fire Testing

2.4.1 Experiments

There have been a series of six test programs to evaluate different aspects related to cable fires in NPPs between 2001 and the present. In 2001, Nuclear Energy Institute (NEI) and EPRI conducted 18 full-scale tests exposing energized low voltage electrical cables to a variety of thermal conditions to evaluate the electrical cable failure modes. Specifically, the test program wanted to investigate short-to-ground, inter- and intra-cable shorts, and open-circuit configurations. It was shown that, given cable damage, single and multiple spurious actuations are credible. Also, in a multiconductor cable, it is highly likely that multiple hot shorts will occur simultaneously. However, these results could not support the development of a failure mode prediction model[18],[19].

In 2006, the NRC and Sandia National Laboratory (SNL) conducted the Cable Response to Live Fire (CAROLFIRE) test program consisting of 78 small-scale radiant heating tests and 18 intermediate-scale tests, which were representative of in-plant conditions. These tests provided an experimental basis for resolving five of six items identified in RIS 2004-03, *Risk-informed Approach for Post-Fire Safe-Shutdown Circuit Inspections*. These tests showed that inter-cable shorting is plausible, but less likely than the intra-cable failure mode. However, more research was required to determine the number of failures assumed to be likely for configurations requiring failures of three or more cables[15],[16] ,[20].

The Kerite Analysis in Thermal Environment of FIRE (KATE-Fire) test series was conducted in 2011 to determine the fire-induced thermal failure limits of Kerite fire resistant cables. Based on the test results, the minimum threshold of electrical failure for Kerite FR cables was recommended to be 247°C. Thermoset materials are expected to provide adequate short-term electrical performance for temperatures of at least 330°C and some common thermoset insulation materials have failure thresholds of 390°C or higher. Also, it was determined that the lower bound failure temperature for thermoplastic cables is approximately 205°C and some common thermoplastic materials have failure thresholds in the 250–290°C range[21].

In 2012, the Direct Current Electrical Shorting in Response to Exposure Fire (DESIREE-Fire) test program conducted 59 small-scale tests and 17 intermediate-scale tests. The objective of this test program was to evaluate fire-induced cable failure modes and effects for direct current (DC) circuits to determine if they differ from alternating current (AC) circuits. It was shown that the faulting behavior of the DC-powered cables was more energetic than comparable AC-power cables observed in prior testing efforts. The DC-powered cables had substantial, sustained, and damaging arcs. Also, open circuits were noted to occur as the first failure mode while fuse sizing played a role in the duration of the hot short failures[22].

The Cable Heat Release Ignition and Spread in Tray Installations During Fire (CHRISTIFIRE) test program evaluated 26 horizontal and 17 vertical full-scale calorimetry tests in 2012. This program evaluated and quantified the burning characteristics of grouped electrical cables in horizontal and vertical configurations. As a result of these experiments, the FLASH-CAT model used for NUREG/CR-6850 analysis was validated. Also, it was discovered that fires are unlikely to spread upward indefinitely on a single tray of qualified cables; however, this was not true for multiple trays of qualified cables[23],[24].

In 2016, the Refining and Characterizing Heat Release Rates from Electrical Enclosures during Fire (RACHELLE-FIRE) test program evaluated 26 horizontal and 17 vertical full-scale calorimetry tests. The purpose of this test program was to classify enclosures in terms of function, size, contents, and ventilation. Additional objectives included determining the peak HRR probability distributions considering specific electrical enclosure characteristics, as well as developing a method to account for the impact of the enclosure on the vertical thermal zone of influence. This test program resulted in the development of peak HRR distributions for the different classification groups. Also, new fire plume temperature profiles were developed, which reflected the obstructed nature of fire plumes generated from fires inside electrical enclosures [13].

2.4.2 Experiment Uncertainty

NUREG-1855 [25] identifies two primary classes of uncertainty relevant to PRA models.

- Aleatory – Uncertainties that arise due to inherent randomness in the behavior of a system that can never be completely eliminated
- Epistemic – Uncertainties that arise due to state-of-knowledge and that can be realistically reduced by, for example, further experimental effort.

A PRA model typically captures a range of aleatory uncertainties that reflect inherent randomness in the realization of a future plant state. This could be due to the random failure of a set of SSCs to realize a plant state that poses the potential for either core damage or large early release—two key risk metrics commonly evaluated by PRA models of Light Water Reactors (LWRs) in the United States. Evaluation of the manner in which random failure of SSCs can lead to plant states that pose risk to public health and safety is the purpose of internal event PRAs. Other types of PRAs that capture the potential for external hazards to induce plant states that can lead to core damage or large early release are external event PRAs. These external hazards also reflect aleatory uncertainty due to the random occurrence of these external hazards. For example, a Fire PRA captures the impact of aleatory uncertainty associated with the occurrence of a fire at an NPP capable of causing damage that leads to either core damage or large early release.

Beyond the actual PRA logic model which is designed to capture the inherent randomness in realizing plant damage states posing risk to public health and safety, the characterization of event frequencies and probabilities for event occurrences (e.g., the probability that a fire in an electrical cabinet could lead to damage to neighboring equipment) often require development of supporting models. For example, the potential for a fire to lead to equipment damage in a room can be evaluated using deterministic fire simulation models such as CFAST or FDS. While these simulation models are often deterministic in nature, they can never completely specify the potential for damage due to uncertainties in numerous inputs. These models typically require the specification of:

- Initial conditions that can never be completely known or are inherently variable. For example, the severity and duration of a fire can be influenced by the initial temperature in a room. In the Heat Release Rates of Electrical Enclosure Fires (HELEN-FIRE) tests, the temperature in the facility where the tests were conducted was below the freezing temperature of water. This was identified as an important contributor in some tests to actually realizing a self-sustaining fire. In an NPP, temperatures in rooms vulnerable to fires are quite a bit higher than occurred in the HELEN-FIRE tests. However, they can exhibit variability based on the time of year, as well as the availability of heating, ventilation, and air conditioning (HVAC) systems. Thus, any deterministic fire modeling simulation of a plant room must account for the variability in initial room temperatures specific to that room in the plant. Variation in the initial room temperature, or other initial conditions, often arise due to aleatory contributors as noted above. This variability can typically be evaluated using historical data specific to the plant for the uncertain initial condition. However, there may also be limited knowledge of that specific initial condition due to a lack of observations at the plant. This type of epistemic variability may lead to use of a bounding uncertainty distribution to capture a realistic range over which the specific initial condition is thought to vary at the plant. It is important to note, however, that the uncertainty distribution capturing the variability in an initial condition must be specific to the plant. As in the case of the HELEN-FIRE tests, the initial temperature was significantly lower than what would be encountered in an NPP. Variability of this temperature from the tests is thus not relevant to analyzing a fire at an NPP.
- Boundary conditions for the model that can never be completely known or that exhibit inherent variability. As before, a model of a room fire may need to specify a temperature for a boundary volume to capture the degree of heat loss from the room throughout the course of a fire. This boundary temperature could be from a very large volume of a neighboring room, and again, may also vary due to natural fluctuations in temperature at an NPP throughout the year, or due equipment failures. As is the case with initial conditions, this type of uncertainty must be specified based on the variability at the plant for which the simulation is being performed.
- Event scenario perturbations represent inputs to models capturing the driving event that transiently moves the state of a collection of SSCs at a power plant away from normal operating conditions. The range of severity for perturbations realized is either variable based on aleatory uncertainty in the event occurrence or may exhibit an epistemic component that arises due to

imperfect knowledge of the type of event given available tests. In the case of a fire in a room, the HRR represents a parameter used to characterize the driving force for the scenario. HRRs used in deterministic fire analyses are typically established using available fire tests judged to be reasonably prototypic of fires that could be realized at a NPP. While HRRs exhibit an aleatory component, it has been acknowledged as containing an epistemic component of uncertainty due to imperfect knowledge of fire events in NPP. RACHELLE-FIRE represents an expert judgment process adopted to extrapolate the observations of parameters such as HRR made during the HELEN-FIRE tests to NPP events.

- Physical properties also must be specified in analytical models and introduce uncertainty that is typically epistemic in nature. For example, the thermal conductivity of concrete has variability that may be either due to an inability to completely specify the concrete composition used during construction of the plant (i.e., concrete samples are not available), or due to measurement uncertainty. These are both examples of epistemic sources of uncertainty.
- Model parameters represent another source of uncertainty that is typically epistemic for deterministic analyses. These types of model parameters could be, for example, parameters to the turbulence model. It is typical for these types of model inputs to be established based on validation exercises against experimental tests that are deemed to represent reasonably prototypic conditions for the scenario at the NPP being analyzed. These experimental tests may either be separate-effect (i.e., focused on experimental evaluation of a specific set of phenomena) or integral (i.e., focused on evaluating the interaction of multiple phenomena typically occurring during a transient event in an NPP). In using tests to establish modeling parameters for a simulation of an NPP event, it is necessary to establish the degree to which tests are representative of actual plant conditions to ensure that additional extrapolation uncertainty is not introduced. For example, in fire tests used to validate models and develop modeling parameter uncertainties, generally only tests with room temperatures similar to the plant room being simulated should be used. In situations where this is not the case, expert judgment processes have been employed to facilitate characterization of uncertainties from available tests to NPP conditions.

3. RISK IMPORTANCE RANKING OF FIRE PRA INPUT DATA

In Fire PRA, fire growth and its impact on SSCs are simulated using a fire model. The outputs from the fire model are used to estimate PRA inputs (e.g., initiating event frequencies, basic event probabilities) using the "severity factor" method [26]. In this setting, the classical Importance Measure (IM) analysis methods, such as Fussell-Vesely (F-V) IM and Risk Achievement Worth (RAW), cannot be used to identify the most critical risk-contributing factors at the failure-mechanism level (e.g., input variables of the fire model) for two reasons [27]: (i) input parameters at the failure-mechanism level are given in various units and wide ranges, unlike the basic event probabilities in classical PRA that have no units and only range from 0 to 1; and (ii) the underlying fire model may consist of a non-closed form of equations (e.g., a zone model or a CFD-based model) and may involve nonlinearity and complex interactions among input parameters, as opposed to the classical PRA model that is a linear function of basic event probabilities.

To address these challenges, the goal of this work is first to develop a new importance ranking methodology that can account for (a) uncertainty in the input parameters of the fire model, (b) non-linearity and interactions among input parameters in the fire model, and (c) uncertainty in the risk outputs. This study makes four key contributions:

i. A unified computational platform for Fire PRA is generated in a way that the relationships between the plant risk (as output from PRA) and the Fire PRA inputs at the failure-mechanism level are explicitly tracked. For this purpose, an Integrated PRA (I-PRA) methodological framework, (briefly explained in Section 3.1), previously developed by the Socio-Technical Risk

Analysis (SoTeRiA) research laboratory at the University of Illinois at Urbana-Champaign (UIUC) [28], is adopted. The new importance ranking methodology is hence referred to as the "I-PRA Importance Ranking Methodology" [29].

ii. Four methodological steps are designed as the core of the I-PRA Importance Ranking and are explained in Section 3.2.

iii. A computational platform is developed leveraging Risk Analysis Virtual Environment (RAVEN) [30] to operationalize the I-PRA Importance Ranking Methodology and is explained in Section 3.3.

iv. The I-PRA Importance Ranking Methodology is applied to a typical NPP fire case study (Section 3.4) to demonstrate its feasibility and value.

3.1 Integrated PRA (I-PRA) Methodological Framework

Fire I-PRA (Figure 11) is a multi-level risk analysis framework for analyzing layers of causal chains initiated by an internal fire that could cause a system-level initiating event (e.g., 'IE' in Figure 11), break down the defense-in-depth barriers against the progression of fire-induced damage to the safety-critical systems (e.g., systems 'A' and 'B' in Figure 11), and lead to core damage [28].

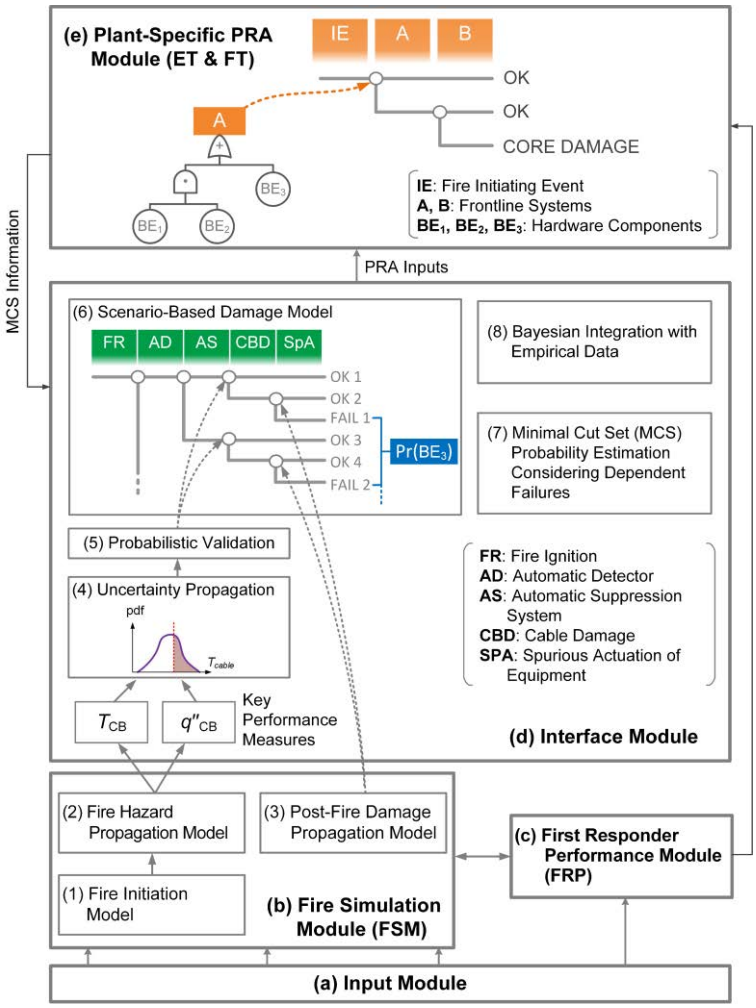

Figure 11: Integrated Probabilistic Risk Assessment (I-PRA) framework for Fire PRA [28].

In the I-PRA framework, simulation-based models of underlying phenomena are integrated with a plant PRA model by generating a probabilistic interface, the Interface Module ('d' in Figure 11), equipped with uncertainty analysis, dependency treatment, and Bayesian updating [28]. In Fire I-PRA, the fire-related simulation modules include the Fire Simulation Module (FSM), "b" in Figure 11) and the First Responder Performance Module (FRP, "c" in Figure 11). Interactions between these two modules are addressed by creating an explicit interface (represented by a two-directional arrow between 'b' and 'c' in Figure 11). Key Performance Measures (KPMs) predicted by FSM are associated with fire-induced damage, e.g., maximum temperature inside a target cable jacket (denoted by T_{CB} in Figure 11) and maximum heat flux at the surface of that cable jacket (q''_{CB} in Figure 11). Uncertainties associated with input parameters of these simulation modules are propagated via features equipped in the Interface Module to generate probabilistic results based on the simulation outputs (e.g., probability of a component-level failure, given fire-induced damage to target cables, represented by basic event 'BE_3' in Figure 11), and these probabilistic results are connected to the plant-specific PRA scenarios (in Module "e" in Figure 11) [28]. More details on the Fire I-PRA framework are provided by Sakurahara et al. [28, 31].

In the previous studies by the SoTeRiA laboratory at UIUC, Fire I-PRA was applied to a critical fire-induced scenario (i.e., a small-break loss-of-coolant accident due to stuck-open pressurizer valves induced by a switchgear room fire) in an NPP [31] that has improved the realism of PRA, leading to a 50% reduction in the total core damage frequency associated with the selected scenario. As compared to the current Fire PRA methodology based on NUREG/CR-6850 [26], Fire I-PRA advances three aspects [31]:

Table 1 summarizes four aspects that Fire I-PRA [30] has advanced, as compared to the current Fire PRA methodology based on NUREG/CR-6850 [25] and its subsequent NUREGs and Fire PRA FAQs.

Table 3-A: Comparison of Fire I-PRA with Existing Fire PRA Methodologies.

Fire PRA Methodological Areas	Current Fire PRA Methodology (NUREG/CR-6850)	I-PRA Framework
Connection between plant PRA and the fire physics model	"Passively" connected (i.e., fire-induced failure probabilities, externally computed by a fire model, are plugged into the plant PRA model)	Unified computational framework (i.e., information on relationships between fire-induced PRA events and underlying failure models is captured in the Interface Module, generating an automated linkage between the underlying simulations and the plant PRA)
Uncertainty propagation & computation of fire-induced cable damage probability	Severity factor method based on a predefined number of peak HRR bins	Monte Carlo simulation using Latin-Hypercube Sampling, equipped with a convergence study
Fire detection and suppression analysis	"Implicit" treatment by competition between time-to-damage and time-to-suppression	"Explicit," bidirectional interface between the Fire Simulation Module and the First Responder Response Module by modifying the time profile of HRR

Fire PRA Methodological Areas	Current Fire PRA Methodology (NUREG/CR-6850)	I-PRA Framework
Risk importance ranking	Ranking of the basic events in PRA using classical importance measures (e.g., Fussell-Vesely importance measure, Risk Achievement Worth)	Global importance ranking that allows for ranking factors at the level of underlying failure mechanisms (e.g., input parameters of the Fire Simulation Module and the First Responder Response Module).

As compared to the current Fire PRA methodology, the I-PRA framework creates a "unified" connection between the Plant-Specific PRA Module and the underlying physics and human performance models, where the communications of data and information among multiple levels of causality (i.e., fire growth, detection and suppression, cable damage, component failure, and system failure) are generated in a single computational platform [31]. In this unified framework, the relationships between the plant risk metrics and the input parameters associated with the underlying physics and human models can be traced and captured explicitly. The Interface Module in Fire I-PRA is designed so that the underlying physics and human models can be integrated with the existing plant PRA model developed in the commercial PRA software (e.g., RISKMAN [32], SAPHIRE [7]) without changes to the PRA software or significant modifications to the plant PRA structure. The unified connection between the underlying failure mechanisms and the plant PRA model allows for a comprehensive parametric study to explore the influences of changing the fire protection design parameters on the plant risk estimates. This feature of the I-PRA framework, together with the advancements in the global importance ranking [27], provides a basis for the development of the I-PRA Importance Ranking Methodology in this report (Section 3.2). In previous studies by the SoTeRiA laboratory at UIUC [31], Fire I-PRA was applied to a critical fire-induced scenario (i.e., a small-break loss-of-coolant accident due to stuck-open pressurizer valves induced by a switchgear room fire) in an NPP, which improved the realism of PRA, leading to a 50% reduction in the core damage frequency associated with the selected scenario. In the I-PRA framework, the Interface Module can treat multi-level dependencies by using the simulation-informed approach for dependency analysis developed in the previous research by the SoTeRiA Laboratory at UIUC [33].

3.2 Methodological Steps for the I-PRA Importance Ranking Methodology

Four methodological steps to implement the I-PRA Importance Ranking Methodology, developed in this work, are explained in the following sub-sections.

3.2.1 Step 1 – Qualitative analysis of potential sources of uncertainty and conservatism in Fire PRA

Step 1 provides a qualitative analysis to identify potential sources of uncertainty and conservatism in Fire PRA. This qualitative analysis is conducted based on a combined use of expert judgment, literature review, and insights from existing Fire PRAs (e.g., results of qualitative and quantitative screening in plant-specific Fire PRAs). A comprehensive search for potentially dominant sources of uncertainty and conservatism in Fire PRA requires a thorough inspection of all the tasks of the Fire PRA process documented in NUREG/CR-6850. When adding detailed simulation models (e.g., fire crew performance model [34]) into the scope of Fire PRA or when existing simulation models are utilized in an advanced framework (e.g., use of FDS/CFAST model in the Fire I-PRA framework [28, 31]) to generate simulation-based PRA inputs (e.g., fire-induced cable damage probabilities), the search for potentially

dominant sources of uncertainty and conservatism needs to consider additional factors, e.g., input parameters of those simulation models.

Within the scope of this project, the implementation of Step 1 involves a literature review that encompasses regulatory documents, academic research publications, and industry reports to identify potentially dominant sources of uncertainty and conservatism in fire progression modeling, focusing on electrical cabinet fire scenarios in NPPs. The review identifies, for example, that the HRR curves recommended for use in the current Fire PRA methodology are primarily derived from expert judgment and experimental data obtained from historical fire tests [13, 26]. Those supporting experiment data and expert judgment, therefore, should be included in the scope of Step 1 to identify potentially dominant sources of uncertainty and conservatism associated with fire progression. Based on the literature review and engineering judgment, all key parameters having potentially significant influences on fire progression are identified.

3.2.2 Step 2 – Quantitative characterization of dominant sources of uncertainty in Fire PRA based on experimental data

Step 2 uses available fire test and experiment data as well as engineering judgment to conduct a quantitative characterization for the potentially dominant sources of uncertainty and conservatism identified in Step 1. Within the scope of this project, the uncertainty characterization relies on historical fire test and experiment data collected by SNL. Results of Step 2 are the probability distributions characterizing those sources of uncertainty and conservatism extracted from historical fire tests and experiments, which, within the scope of this project, encompass key input parameters of the mechanistic fire models, commonly used for the Detailed Fire Modeling (Task 11 of NUREG/CR-6850).

In this step, for each key input parameter of the fire simulation model, an adequate parametric probability distribution is selected, and the parameters of the selected probability distribution (e.g., shape and scale parameters for a gamma distribution) are estimated. Two layers of uncertainty associated with each probability distribution should be considered. The first is the randomness or stochasticity associated with value of the input parameter being considered. This layer of uncertainty can be referred to as the aleatory uncertainty that characterizes the variability of the input parameter. Meanwhile, the second layer of uncertainty is associated with the type of the parametric probability distribution and the statistical estimation of the distribution parameters. This layer of uncertainty is categorized as an epistemic uncertainty source that is induced by lack of knowledge on the parametric probability distribution and the estimation of its unknown parameters based on limited empirical data. Using historical fire test and experiment data, the parametric probability distribution and its parameters can be determined using parameter estimation techniques (e.g., Maximum Likelihood Estimation (MLE) method, Bayesian approach), and tested with goodness-of-fit tests (e.g., Kolmogorov-Smirnov, Chi-squared tests). Within the scope of the project, the MLE method is used for parameter estimation, while the Kolmogorov-Smirnov method is used for goodness-of-fit test.

3.2.3 Step 3 – Quantitative screening of potential sources of uncertainty using Morris Elementary Effects Analysis

Step 3 performs a quantitative screening of the potentially dominant sources of uncertainty and conservatism using the Morris EE analysis method [35],[36]. The Morris EE analysis method provides an economical, randomized one-at-a-time (OAT) design of sensitivity analysis for screening out those input parameters of the simulation modules (in Fire I-PRA) that have negligible influence on the KPMs of interest obtained from the simulation output (e.g., T_{CB} and q''_{CB} in Figure 11). For predicting the KPMs of interest, the fire progression model can be developed using a CFD-based model (e.g., FDS code [37]) or a two-zone model (e.g., CFAST code [38]). Based on the results of this screening, input parameters whose influence on the KPMs cannot be ignored will be kept as random variables, and their uncertainties will be propagated through the Fire I-PRA framework during the Global IM analysis in Step 4 (Section 3.2.4).

This quantitative screening can help reduce the complexity of the problem and the total number of replications of the simulation runs required for implementing the Fire I-PRA framework.

In the Morris Elementary Effect (EE) analysis method, EE is an approximate local first derivative of the model output with respect to each input parameter. An EE distribution associated with a specific input parameter is computed by the individually randomized OAT design at different points in the input space [35, 36]. Suppose that the fire simulation model with output Y (representing the KPMs) can be expressed as a function of nX random key input parameters X_i (identified in Step 1), where $i \in \{1,2,\dots,nX\}$:

$$Y = g(X_1, X_2, \dots, X_{nX}). \tag{1}$$

For simplicity of description, assume that each input parameter X_i is a random variable between [0, 1]. To compute the EE, the state space of each input parameter is discretized into a p-level grid so that each input parameter X_i can be randomly sampled from its discretized values. Using two sets of input parameters where X_i has two different values (x_i and $x_i + \Delta$), while the other parameters are kept the same, the EE of input parameter X_i is defined as

$$EE_i = \frac{g(x_1, \cdots, x_{i-1}, x_i + \Delta, x_{i+1}, \cdots, x_{nX}) - g(x_1, \cdots, x_{i-1}, x_i, x_{i+1}, \cdots, x_{nX})}{\Delta}, \tag{2}$$

where Δ is an increment in x_i and is set to a predetermined value of $p/[2(p-1)]$ with p assumed to be even [35]. An empirical distribution F_i of the EE associated with input parameter X_i, i.e., $EE_i \sim F_i$, is obtained by randomly sampling different sets of values from the input space of X_i and repeating the calculation of EE_i using Eq. (2). Based on the resultant random samples of EE_i, two sensitivity measures suggested by Morris [35], i.e., the mean value μ_i and standard deviation σ_i of the distribution F_i of EE_i, can be estimated as follows:

$$\mu_i = \frac{1}{r}\sum_{j=1}^{r} EE_i^j, \tag{3}$$

$$\sigma_i^2 = \frac{1}{r-1}\sum_{j=1}^{r} (EE_i^j - \mu_i)^2, \tag{4}$$

where r is the number of observations of F_i per input parameter for each model output, estimated at a cost of $r * (nX + 1)$ model evaluations.

The measure μ assesses the overall influence of an input parameter on the model output, with higher values of μ implying a larger main effect that the parameter has on the model output. Meanwhile, the measure σ estimates the ensemble of that input parameter's effects and indicates the influences of nonlinearity and interactions among input parameters on the model output. A higher value of σ implies that the EEs of that input parameter varies considerably depending on the choice of the sample point where it is computed, i.e., depending on the choice of the values of other input parameters in the input space. It should be noted that the sole use of μ may fail to find a parameter that has considerable influence on the model output in situations where the EE distribution has both positive and negative elements, i.e., the model is non-monotonic or has interaction effects. In such situations, some effects may cancel out each other in the process of computing μ, producing a low value of μ for an important parameter. In this case, it is recommended that values of both μ and σ be simultaneously considered since a parameter with EE of different signs (i.e., that cancel each other out) would have a low value of μ but a considerable value of σ [35]. Alternatively, Campolongo et al. [36] suggest using another measure, μ^*, which is the mean of the absolute values of the EE, to solve the problem of different signs. The drawback is the loss of

information on the sign of the EE. To recover this loss of information, a simultaneous examination of both μ and μ^* can be performed with no extra computational cost. For example, if μ is low while μ^* is high, it indicates that the parameter being considered carries the effects of different signs. In practice, the use of μ^* has been shown to be more convenient when the model output contains several variables [36]. To extract maximum sensitivity information, however, all three of these sensitivity measures may be used [39]. Note that even though the ranking of the input parameters may vary from output to output (when several model outputs are of interest), the Morris EE analysis method may still be useful for identifying a subset of parameters that is non-influential for all model outputs (or plays a smaller role in the whole model). To implement the Morris EE analysis in Step 3, a coupling between FSM (Module "b" in Figure 11) and the RAVEN tool [30] is developed. Details on this computational coupling are given in Section 3.3.

3.2.4 Step 4 – Global Importance Measure Analysis

For the potentially dominant sources of uncertainty and conservatism that are retained in Step 3 above, Step 4 conducts a Global IM analysis to generate a comprehensive ranking based on their influence on the plant risk. Due to the nature of the risk-contributing factors at the level of the simulation inputs and the presence of nonlinearity and interaction effects of the parameters in the fire progression model, the Global IM analysis has to account for (i) uncertainty in the input parameters of the fire model, (ii) nonlinearity and interactions among input parameters in the fire model, and (iii) uncertainty in the risk outputs [27].

To select a proper Global IM method for ranking the input parameters in I-PRA, a literature review has been conducted to identify key attributes that are used to differentiate various types of importance ranking approaches and to utilize these attributes for justifying the selection of a Global IM method for use with the I-PRA Importance Ranking Methodology. Four key attributes have been identified [27], including: (a) level of risk-contributing factors (i.e., component vs. failure-mechanism level), (b) uncertainty of input parameters, (c) uncertainty of the model outputs, and (d) nonlinearity and interactions in the model. Three main types of global sensitivity analysis methods have been identified and their main characteristics are discussed in Section 3.2.4.1. Section 3.2.4.5 summarizes the evaluation of the three types of global sensitivity analysis methods based on their capabilities to address the four key attributes listed above and proposes a Global IM method for the I-PRA Importance Ranking Methodology.

3.2.4.1 Existing Global Methods for Importance Ranking

In literature, global methods for importance ranking include those that are used to (i) conduct "sensitivity analysis" for input parameters at the level of failure mechanisms with respect to the physical performance outputs or the component failure probabilities, and (ii) conduct "importance measure analysis" for the PRA basic events (i.e. at the component level) with respect to the system risk. The multiple levels of "importance measure analysis" in this context (including ''failure mechanism,'' ''components,'' and ''system'') refer to the different layers of accident causation considered in the I-PRA framework (Figure 11). Global methods for importance ranking can be divided into three categories: correlation-based, variance-based, and moment-independent.

3.2.4.2 Correlation-Based Global Sensitivity Analysis Methods

Correlation-based global methods use input-output correlation as a measure of the influence of uncertain inputs on output uncertainty. Importance ranking influential factors (e.g., input parameters) is based on sensitivity measures calculated using correlation coefficients. The most commonly-used correlation coefficients found in literature include Pearson Correlation Coefficient (PEAR), Spearman Correlation Coefficient (SPEAR), Standardized Regression Coefficients (SRCs), and Partial Correlation Coefficients (PCCs) [40-47]. For example, the SCRs indicate the total strength of the linear relationship between the model output and each input parameter, while the PCCs indicate the strength of the linear relationship between the model output and each input parameter after the linear effects of all other input

parameters are removed. These two methods can also be conducted for the rank-transformed data, where they are referred to as the Standardized Rank Regression Coefficients (SRRCs) and Partial Rank Correlation Coefficients (PRCCs), to improve the accuracy of the ranking when the model is a nonlinear but monotonic function [45].

Performance of the correlation-based methods is measured by the coefficient of determination (R_Y^2), which is defined as the ratio of the total sum of squares to the regression sum of squares and represents the fraction of the model variance explained by the regression [40, 41, 44]. A low value of R_Y^2 would signal "a poor regression model." In such cases, the ability of the correlation-based methods to capture the output variability is low, and it would be unrealistic to assess the influence of the input variables based on the correlation coefficients. This typically occurs for nonlinear models and also when interactions among model parameters emerge. Variance-based methods are then developed and utilized to integrate and improve the information obtained by these correlation-based methods.

3.2.4.3 Variance-Based Global Sensitivity Analysis Methods

Variance-based global methods define importance indicators which are independent of model linearity and use the variance of the model output as a basis for assessing uncertainty importance. Importance ranking of influential factors (e.g., parameters) is based on sensitivity measures calculated as the expected reduction in the variance of the model output, given that a specific input parameter (or a specific set of input parameters) is fixed [48, 49]. Common variance-based approaches found in the literature include First-Order Effects (describing the percentage reduction in the output variance that is achieved if an uncertain parameter is fixed [50-53]) and Total Effects (describing the percentage of variance that remains if all parameters, except theone specific parameter is treated as random variable, are fixed [52-54]). For example, the Sobol method [51] is one of the most widely used variance-based techniques which measures sensitivity across the whole input space, deals with nonlinear, and inputs interaction terms within the model. The "total effect index" measures the contribution to the output variance of the input X_i, including all variance caused by interactions of any order with other input variables [51]. Note that, in the variance-based methods, sensitivity measures can be determined for a set of variables as well as for single parameters. This is not possible with the correlation-based methods and represents a methodological advantage for the variance-based methods when compared to the correlation-based methods.

In variance-based global methods, parameters with the highest values of the importance indicator are the most effective in reducing output variance. The interpretation of the variance-based importance measures is, however, somewhat stretched so that they are deemed to measure "the relative importance of each input in driving the uncertainty" [55]. This assumes that the output variance is "sufficient" to describe the output variability. In some cases, the assumption that variance is sufficient to describe uncertainty, however, does not hold and what reflects a decision-maker's state of knowledge of an uncertain quantity is the distribution [55]. Hence, an ideal measure of uncertainty importance should account for changes to the entire distribution, not just to one descriptor of the distribution. To overcome this limitation, other efforts have focused on moment-independent global methods, as discussed below.

3.2.4.4 Moment-Independent Global Sensitivity Analysis Methods

Moment-independent global methods define uncertainty importance measures not by referring to a particular moment of the output; instead, they look at the entire distribution of the output. Two categories of moment-independent methods found in literature are: (i) probability distribution function (pdf)-based methods, and (ii) cumulative distribution function (CDF)-based methods.

Regarding the pdf-based methods, for example, Borgonovo [56] proposed a moment-independent sensitivity indicator, δ_i, which assesses the influence of input parameters on the model output by considering the entire probability distribution of input parameters and model output without relying on correlation coefficients or any moments of the model output. This method uses the difference between the unconditional pdf and conditional pdf, $s(X_i)$, as a measure of sensitivity:

$$s(X_i) = \int \left| f_{Y|X_i}(y) - f_Y(y) \right| dy, \tag{5}$$

where $f_Y(y)$ is the unconditional pdf of the model output Y, while $f_{Y|Xi}(y)$ is the conditional pdf of the model output Y given that the input parameter X_i is fixed at x_i*. By repeating the computation of $s(X_i)$ with different choices of x_i*, the expected value of $s(X_i)$ is computed by

$$E_{X_i}[s(X_i)] = \int f_{X_i}(x_i) \left[\int \left| f_{Y|X_i}(y) - f_Y(y) \right| dy \right] dx_i \tag{6}$$

where $f_{Xi}(x_i)$ is the marginal pdf for input parameter X_i. The moment-independent sensitivity indicator δ_i is then defined by

$$\delta_i = \frac{1}{2} E_{X_i}[s(X_i)] \tag{7}$$

Regarding the cdf-based methods, for instance, Liu and Homma [57] proposed a moment-independent sensitivity indicator, $S_i^{(\mathrm{CDF})}$, which quantifies the influence of input parameters based on the expected change in the cdf of the model output. $S_i^{(\mathrm{CDF})}$ is defined based on the difference between the unconditional cdf $F_Y(y)$ and the conditional cdf given $X_i = x_i^*$, $F_{Y|Xi}(y)$, which is quantified by the area enclosed by these cdfs:

$$A(X_i = x_i^*) = \int_{\forall y} \left| F_{Y|X_i = x_i^*}(y) - F_Y(y) \right| dy \tag{8}$$

Based on the outputs from the replicated calculation of $A(X_i)$, the expected value of $A(X_i)$ is estimated by

$$E[A(x_i)] = \int_{\forall x_i} f_{X_i}(x_i) A(x_i) dx_i \tag{9}$$

The cdf-based sensitivity indicator $S_i^{(\mathrm{CDF})}$ is defined as

$$S_i^{(CDF)} = E[A(X_i)] / |E(Y)| \tag{10}$$

where $E(Y)$ is the expected value of the unconditional output Y [57].

Another example of the cdf-based methods is proposed in Pianosi et al. [58, 59], and called the PAWN sensitivity index. PAWN quantifies the distance between unconditional and conditional cdfs based on the Kolmogorov-Smirnov (KS) statistic, defined by

$$KS(x_i^*) = \max_y \left| F_Y(y) - F_{Y|X_i = x_i^*}(y) \right| \tag{11}$$

The KS statistic depends on the selection of x_i^* where the input parameter X_i is fixed. The PAWN index, denoted by T_i, is defined by considering a statistic of the KS value (e.g., median, maximum) over all possible values of x_i^* [58, 59]:

$$T_i = stat_{x_i}[KS(x_i)] \tag{12}$$

As indicated by Equation (11), the PAWN indicator accounts for the information on the uncertainty of the model output by considering the maximum difference between the unconditional and conditional cdfs of the model output. Other studies on cdf-based sensitivity measures can be found in Refs. [60-62].

3.2.4.5 Comparative Analysis for Global Sensitivity Analysis Methods

The three types of global sensitivity analysis methods discussed above differ in their capabilities to account for the four key attributes that should be addressed in Step 4 of the I-PRA Importance Ranking Methodology, i.e., generating a comprehensive ranking of the risk-contributing factors at the level of simulation model input parameters based on their influence on the plant risk. The four attributes, as previously listed, are (a) level of risk-contributing factors (i.e. component vs. failure-mechanism levels), (b) uncertainty of input parameters, (c) uncertainty of model outputs, and (d) nonlinearity and interactions in the model.

Attribute (a): The Global IM analysis in Step 4 aims to generate the ranking of input parameters of the simulation module in I-PRA at the failure-mechanism level based on their impact on the system risk metrics computed by the plant-specific PRA module. All three types of the global methods discussed in Section 3.2.4.1 satisfy this requirement.

Attribute (b): The input parameters of the simulation models have uncertainty characterized by probability distributions; therefore, the Global IM analysis for I-PRA should be capable of capturing the uncertainty distributions of the input parameters. All three types of the global methods discussed in Section 3.2.4.1 can account for both range and shape of probability distributions for input parameters, as the sensitivity is computed by randomly sampling the input parameters.

Attribute (c): The consideration of uncertainty associated with the risk output is a crucial requirement for the Global IM analysis in Step 4 in order to determine whether the uncertainty in the risk estimates should be reduced, and if so, where to prioritize the efforts on the uncertainty reduction (e.g., reducing uncertainty associated with highly ranked input parameters of the fire model to efficiently reduce the uncertainty in the risk estimates). In considering the uncertainty of the model output, the adequacy of the correlation-based global methods (Section 3.2.4.2) depends on whether the variation of the model output is accurately captured by the selected regression model. Variance-based global methods (Section 3.2.4.3) can also capture uncertainty of the model output using their variance; however, these methods can produce misleading conclusions [55] when (i) input parameters and model output have asymmetric uncertainty distributions and long tails, or (ii) the model output has multiple modes. This limitation is also observed in the correlation-based global methods when the coefficient of determination R_Y^2 is used as a measure of sensitivity because R_Y^2 is defined by the variance of the model output. In contrast, the moment-independent global methods (Section 3.2.4.4) capture the uncertainty of the model output by using its entire probability distribution (pdf or cdf) as a measure of sensitivity. Compared to the cdf-based methods, the pdf-based methods have two limitations in that (i) the construction of empirical pdf (e.g., histogram or kernel density estimation) is affected by user-specified tuning parameters [58] and (ii) compared to the cdf-based methods, a smaller amount of information on uncertainty of the model output (i.e. the maximum distance between conditional and unconditional cdfs) is captured.

Attribute (d): The capability of addressing nonlinearity and interactions in the model, is also an important requirement for the Global IM analysis in Step 4 of the I-PRA Importance Ranking Methodology because the simulation modules in I-PRA are composed of spatiotemporal models of underlying failure mechanisms, most often formed by nonlinear governing equations and involving

interactions among the input parameters. Among the three types of global sensitivity analysis methods, the correlation-based global methods are not adequate for addressing this aspect because their capability deteriorates when the model is a non-monotonic function or when it involves a high degree of interactions [55]. The variance-based and moment-independent global methods, on the other hand, can more accurately capture nonlinearity and interactions by sampling all input parameters simultaneously when quantifying the sensitivity measures.

Based on the evaluation above, the $S_i^{(CDF)}$ method, proposed by Liu and Homma [57], is selected as the most suitable method for the Global IM analysis in I-PRA considering that (i) $S_i^{(CDF)}$ can explicitly address all four attributes discussed above, and (ii) as compared to the pdf-based methods [56] and the cdf-based methods using distance (or norm) between cdfs [58, 59], $S_i^{(CDF)}$ can capture more information on the uncertainty of the model outputs. To implement the Global IM analysis in Step 4, the coupling between FSM and RAVEN (Section 3.3) is equipped with the $S_i^{(CDF)}$ method. The computational procedure for calculating the $S_i^{(CDF)}$ metric using this FSM-RAVEN coupling is discussed in Section 3.3.3.

3.3 Leveraging RAVEN to Develop a Computational Platform for the I-PRA Importance Ranking Methodology

To implement Steps 3 and 4 of the I-PRA Importance Ranking Methodology (Section 3.2), a coupling between FSM (Module "b" in Figure 11, using CFAST/FDS) and RAVEN [30] is developed (hereafter referred to as "FSM-RAVEN coupling," see Figure 12 below). Then, this project, for the first time, integrates the Morris EE analysis and the Global IM analysis [27] with the FSM of the I-PRA framework in RAVEN. Specifically, for Step 3, the FSM-RAVEN coupling is equipped with the Morris EE analysis using an open-source Python library for sensitivity analysis, namely SALib [63]. For Step 4, the FSM-RAVEN coupling is equipped with the $S_i^{(CDF)}$ method by developing a Python script for implementing the Global IM method for I-PRA [27] and interfacing it with the FSM-RAVEN coupling. The following subsection provides more details on the FSM-RAVEN coupling and computational procedures used for implementing the Morris EE analysis and the Global IM ($S_i^{[CDF]}$ method) analysis.

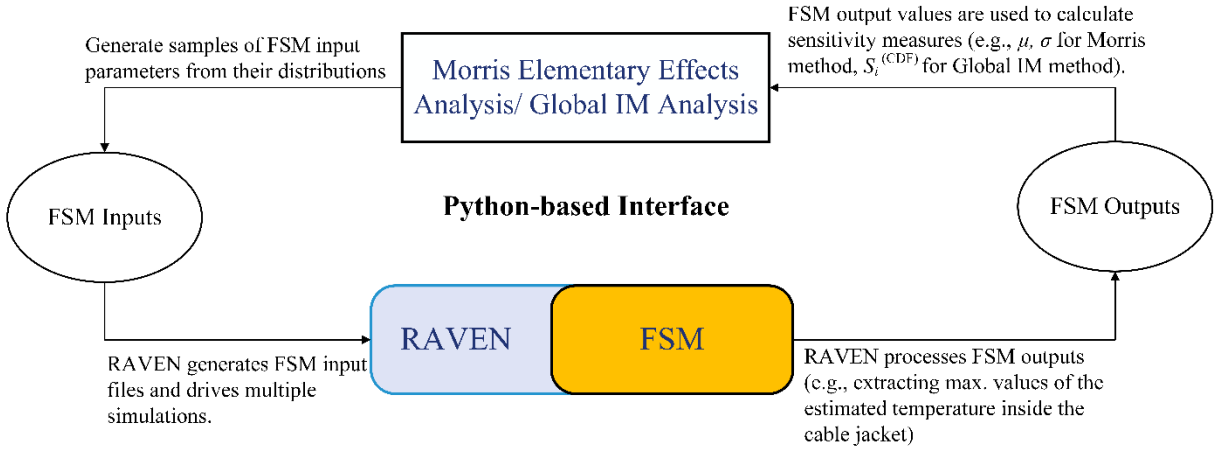

Figure 12: FSM-RAVEN coupling for Morris EE and Global IM analyses.

3.3.1 Coupling FSM and RAVEN

Among the five fire models verified and validated by NRC for fire protection applications in NPPs [4,64], CFAST [38], and FDS [37] are included in the development of the FSM-RAVEN coupling. Between these two, FDS can predict the fire-induced conditions and the physical KPMs for equipment damage with higher resolution; however, its computational cost is much higher than that of CFAST because FDS numerically solves Navier-Stokes equations, which require higher spatiotemporal resolutions compared to the engineering correlations for momentum conservation used in CFAST. As outputs, both CFAST and FDS generate predictions for the evolution of physical KPMs associated with the fire-induced equipment damage, e.g., T_{CB} and q''_{CB} in Figure 11.

As illustrated in Figure 12, in the FSM-RAVEN coupling, RAVEN provides a statistical analysis platform capable of interfacing with FSM and is used for driving simulation jobs with either CFAST or FDS. To perform the Morris EE analysis or the Global IM analysis, the FSM-RAVEN interface, coded in Python, first generates random samples of the FSM input parameters by sampling from their associated distributions (obtained in Step 2 of the I-PRA Importance Ranking Methodology). The selection of the sampling strategy depends on the types of sensitivity analyses used in each step (the Morris EE analysis in Step 3; or the Global IM analysis in Step 4 of the I-PRA Importance Ranking Methodology). The input parameter samples are then provided for RAVEN to execute the FSM simulation runs. Simulation outputs, which include information on the KPMs (e.g., T_{CB} and q''_{CB} of the cable targets), are collected by RAVEN and fed back into the FSM-RAVEN interface to generate fire-induced equipment damage probabilities. Consequently, the Morris EE analysis and the Global IM analysis features equipped in the FSM-RAVEN interface use information on the KPMs and the fire-induced equipment damage to compute corresponding sensitivity measures for each input parameter (i.e., μ and σ for the Morris EE analysis and $S_i^{[CDF]}$ for the Global IM analysis). The FSM-RAVEN interface, when fully integrated into the I-PRA framework, can generate these sensitivity measures with respect to the impact of each input parameter on model outputs obtained at multiple levels of causality in the I-PRA framework. In other words, the sensitivity measures can be generated at the fire simulation output level (i.e., to capture the impact of each input parameter on the physical KPMs such as T_{CB} and q''_{CB}), at the level of equipment damage (i.e., capture the impact of each input parameter on the fire-induced equipment damage probability), or at the level of PRA outputs (to capture the impact of each input parameter on the plant risk metrics such as CDF and LERF).

The FSM-RAVEN interface also provides a valuable tool for the sampling-based uncertainty quantification in Fire I-PRA, which aims at: (i) propagating the uncertainties associated with the FSM input parameters using Monte Carlo simulation and (ii) making the FSM model probabilistic and creating a probabilistic interface between FSM and the plant-specific PRA scenarios. This provides an improvement for the existing Fire PRA which uses a simplified uncertainty analysis approach (i.e., severity factor method [26]).

3.3.2 Computational procedure for Morris EE analysis integrated with FSM-RAVEN

This section provides computational steps for calculating the sensitivity measures μ and σ for the Morris EE analysis (in Step 3 of the I-PRA Importance Ranking Methodology) using FSM-RAVEN coupling (Figure 12). These computational steps are implemented using an open-source Python library for sensitivity analysis, namely SALib [63].

1. Generate a set of realizations of the uncertain input parameters from their associated distributions using the Morris sampling strategy [35, 65].
2. For each realization generated, run the FSM simulation to compute and store the model output, i.e., the KPMs of interest such as TCB and q"CB.
3. Repeat Step 1 and Step 2, above, for N times, with N being the sample size: $N = r * (nX + 1)$, as explained in Section 3.2.3.

4. Calculate the EE for each input parameter using Equation (2) in Section 3.2.3.
5. Estimate the sensitivity measures μ, μ*, and σ for each input parameter using Equations (3) and (4) in Section 3.2.3.

3.3.3 Computational procedure for global Importance measure analysis integrated with FSM-RAVEN

This section provides computational steps for estimating the sensitivity measure $S_i^{(CDF)}$ for the Global IM analysis (in Step 4 of the I-PRA Importance Ranking Methodology) using FSM-RAVEN coupling (Figure 12). The estimation of $S_i^{(CDF)}$ in this study uses a two-loop Monte Carlo simulation technique that was originally used in Liu and Homma [57]. Key steps to performing this two-loop Monte Carlo simulation are summarized below, while details of the implementation can be found in Appendix I of Sakurahara et al. [27].

1. Construct the unconditional cdf of the model output Y, $F_Y(y)$, by Monte Carlo simulation.
2. Calculate the conditional model outputs with the substituted column method [57], following the sub-steps below:
   a. This method begins by developing two matrices (A and B) consisting of random samples of X_i ($i \in \{1,2,\dots,nX\}$) whose size is $nS_1 \times nX$ and $nS_2 \times nX$, respectively. Here, nS_1 and nS_2 represent the sample sizes for the outer and inner loops of the two-loop MC simulation, respectively.
   b. $S_i^{(CDF)}$ is computed by using a new $nS_2 \times nX$ matrix (matrix C) constructed by ''substituting'' one of the columns of matrix B for the corresponding column in matrix A.
   c. Repeat this substitution for all columns of matrix B to obtain a full design matrix of size $(nS_1 \times nS_2 \times nX)$.
   d. Run the FSM simulation to compute and store the corresponding conditional model outputs.
3. Based on the conditional outputs, construct the conditional cdfs of the model output, given that the input parameter X_i is fixed at a certain value x_i*, denoted by $F_{Y|Xi}(y)$.
4. Calculate $A(X_i = x_i^*)$ using Equation (8) in Section 3.2.4.4.
5. Repeat the steps above with the Monte Carlo method using random sampling for the outer loop, i.e., random sampling of x_i*. Based on outputs from the replicated calculation of $A(X_i)$, the expected value of $A(X_i)$ is calculated using Equation (9) in Section 3.2.4.4.
6. Calculate the sensitivity measure $S_i^{(CDF)}$ using Equation (10) in Section 3.2.4.4.

3.3.4 Computational procedure for computation of fire-induced equipment damage probability using FSM-RAVEN

This section provides computational steps for estimating fire-induced equipment damage probability (e.g., fire-induced cable damage probability) using the output obtained from simulation runs. In this procedure, input parameters of the fire simulation model are randomly sampled from their distributions. The simulations are then repeatedly performed with each set of the sampled values to compute the KPMs associated with the fire-induced equipment damage (e.g., maximum temperature inside the cable jacket is selected as the KPM of interest when evaluating fire-induced cable damage). The equipment thermal damage threshold is also randomly sampled from its distribution, and by comparing the KPM of interest against the damage threshold, the fire-induced equipment damage probability can be computed. Key steps of this calculation process are summarized below, while more details can be found in Sakurahara et al. [28, 33].

1. Generate random samples from the input parameters using the simple random sampling. The *i*th set of the input parameters is denoted as $\mathbf{x}^{(i)}$, with $i = 1, 2, \dots, N_i$ where N_i represents a sufficiently large sample size in the Monte Carlo simulation for the simulation input parameters.
2. Run the simulation model using each set of the generated random samples to predict the KPM associated with the fire-induced damage of equipment k, denoted as $T_k^{(i)}$.
3. Generate random samples of the damage threshold from its distribution using the simple random sampling. The *j*th sample of the damage threshold is denoted as $\mathbf{T}_{\text{crt}}^{(j)}, j = 1, 2, \dots, N_j$. Here N_j represents a sufficiently large sample size in the Monte Carlo simulation for the damage threshold sampling.
4. For each $T_k^{(i)}$, use Eq. (13) below to compute the point estimate of the fire-induced cable damage probability, $\hat{p}_{k,i}^*$:

$$\hat{p}_{k,i}^* = \frac{1}{N_j}\sum_{j=1}^{N_j} I\left(T_k^{(i)}, T_{\text{crt}}^{(j)}\right), i = 1,2,\cdots,N_i;\ j = 1, 2, \dots, N_j \tag{13}$$

where the indicator function is defined as:

$$I(a,b) = \begin{cases} 1, & \text{if } a > b \\ 0, & \text{otherwise} \end{cases}. \tag{14}$$

5. Using the $\hat{p}_{k,i}^*$ $(i = 1, 2, \dots, N_i)$ outputs obtained from Eq. (13), construct the empirical histogram for the fire-induced damage probability distribution for equipment k. Based on the setting of the fire simulation model, this constructed histogram represents the uncertainty associated with the fire-induced damage probability of each damage target (equipment) of interest.

3.4 Implementing I-PRA Importance Ranking Methodology in a Case Study and Interpreting Results

This section reports on a case study used in this project to demonstrate the four steps of the I-PRA Importance Ranking Methodology (Section 3.2). The fire scenario in the case study is a typical and realistic NPP fire scenario selected from NUREG-1934 Scenario D (a motor control center panel fire in a switchgear room) [4]. Within the scope of this project, CFAST is used for modeling the fire scenario. This is because (i) CFAST, rather than FDS is more commonly applied in Fire PRAs of NPPs in the U.S, and (ii) the computation with FDS is demanding considering the trials and errors required in the development of the methodology and computational platform.

To minimize the efforts needed for validation of CFAST, this case study closely follows the geometry, dimensions, and material properties used in Appendix D of NUREG-1934 [4], for which the CFAST has been validated using a procedure recommended by the U.S. NRC [2],[3] and NIST [12]. Figure 13 shows the configuration of the fire compartment used in this case study.

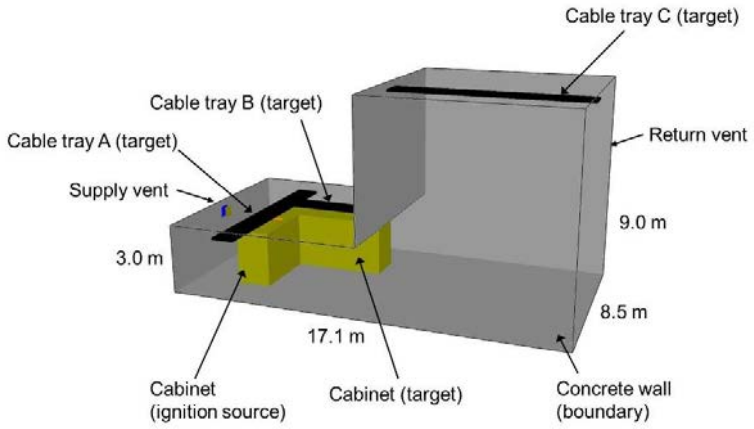

Figure 13: Configuration of the fire compartment used in the case study (adopted from NUREG-1934 Scenario D [4]).

The boundary walls of this fire compartment are made of concrete with a 0.6-m thickness. The material properties of the concrete, including thermal conductivity, specific heat, and density, are treated as random variables. Two electrical cabinets are placed in the fire compartment: one is assumed to be the fire ignition source, while the other is a potential target of fire-induced damage. In addition, three cable trays (A, B, and C in Figure 13) are installed near the ceiling: Cable Tray A is placed directly above the ignition source cabinet, Cable Tray B is installed above the other cabinet, and Cable Tray C is placed in the right portion of the fire compartment which has a higher ceiling. The cable trays are assumed to be filled with cross-linked polyethylene insulated cables with neoprene jackets. These are considered thermoset materials. Each cable is modeled as a cylinder with diameter of 1.5 cm with homogeneous physical properties in accordance with the Thermally-Induced Electrical Failure (THIEF) model proposed in [17]. The cable jacket thickness is treated as a random variable to evaluate its impact on the KPMs of interest. In this case study, six KPMs of interest are the maximum temperature inside the cable jacket (T_{CB}) and maximum heat flux at the surface of the cable jacket (q''_{CB}) of the three target cable trays. More details of this fire scenario can be found in Appendix D to NUREG-1934 [4].

3.4.1 Step 1 – Qualitative analysis of potential sources of uncertainty and conservatism in Fire PRA

For the selected fire scenario, the literature review and engineering judgment process have identified nine input parameters of the fire simulation models (related to the HRR curve, concrete material properties, cable material properties, and fire location) that have potentially significant influences on fire progression. These nine parameters are listed in the second column of Table 3-B.

3.4.2 Step 2 – Quantitative characterization of dominant sources of uncertainty in Fire PRA based on experimental data

For Step 2, based on the analysis of historical fire experiment and test data provided by SNL and previous work by Sakurahara et al. [28], uncertainties associated with the nine input parameters (identified in Step 1) are represented by probability distributions. To obtain these distributions, the Maximum Likelihood Estimation (MLE) method for parameter estimation and the Kolmogorov-Smirnov goodness-of-fit test were used. The nine input parameters and their resulting distributions are listed in the third column of Table 3-B. Note that, due to the lack of data on fire location, this work assumes that the location of the fire source is uniformly distributed along the length of the ignition cabinet.

Table 3-B: List of input parameters treated as random variables and associated uncertainty distributions.

ID	Input Parameters	Probability Distribution	Sources
Input parameters associated with the HRR curve			
X_1	Maximum HRR [kW]	Gamma (α = 0.36, β = 57)	NUREG-2178 [13]
X_2	Time to maximum HRR [minutes]	Uniform (4, 18)	Sakurahara et al. [28], based on experimental data provided in NUREG/CR-6850 [26]
X_3	Duration of max HRR [minutes]	Triangular (0, 0, 20)	Sakurahara et al. [28], based on experimental data provided in NUREG/CR-6850 [26]
X_4	Time to decay [minutes]	Uniform (10, 30)	Sakurahara et al. [28], based on experimental data provided in NUREG/CR-6850 [26]
Input parameters associated with concrete material properties			
X_5	Thermal conductivity of concrete [W/(m K)]	Gamma (α = 30.148, β = 0.099675)	Based on experimental data in Wadsö et al. [66]
X_6	Specific heat of concrete [J/(kg K)]	Gamma (α = 128.389, β = 6.33134)	Based on experimental data in Wadsö et al. [66]
X_7	Density of concrete [kg/m^3]	Gamma (α = 30.4134, β = 83.5117)	Based on experimental data in Wadsö et al. [66]
Input parameters associated with thermoset cable material properties			
X_8	Cable jacket thickness [mm]	Gamma (α = 17.2389, β = 0.077989)	Based on empirical data provided in NUREG/CR-6931 [20]
Input parameters associated with fire source			
X_9	Fire location	Uniform (2.15, 6.35)	Uniformly distributed along the length of the ignition cabinet. Based on engineering judgment.

Notes: for a Gamma distribution, its probability density function is given below:

$$f(x) = \frac{x^{\alpha-1}}{\beta^{\alpha}\,\Gamma(\alpha)} exp\left(\frac{-x}{\beta}\right),$$

where Γ is the Gamma function, and α and β are the shape and scale parameters, respectively.

3.4.3 Step 3 – Quantitative screening of potential sources of uncertainty using Morris EE analysis

In Step 3, the fire scenario first needs to be set up with CFAST. The whole fire compartment (Figure 13) is considered the computational domain for the fire simulation, and is divided into two adjacent compartments in CFAST, one for the low-ceiling area and one for the high-ceiling area (as shown in Figure 13). Each of the two adjacent compartments is then divided into two zones (or control volumes, i.e., an upper layer and a lower layer) in which CFAST assumes the physical characteristics within each zone are homogeneous. Results of the Morris EE analysis with the fire scenario modeled in CFAST are discussed in Section 3.4.3.1.Appendix B includes results of the Morris EE analysis when the fire is modeled with FDS as a preliminary study to investigate how the screening results obtained are influenced by the change of the fire simulation model.

Results of the Morris EE analysis can be sensitive to several factors, including the sampling size and the uncertainty associated with types and parameters of the input parameter distributions. The project team have tested these two factors of the Morris EE analysis for a limited scope which involves only four parameters related to the HRR curve, namely maximum HRR value, time to maximum HRR, duration of maximum HRR, and time to decay (i.e., X_1, X_2, X_3, and X_4 in Table 3-B, respectively). Results of these tests are reported in Appendix B to this report.

3.4.3.1 Input parameter screening analysis using Morris EE analysis method

This section reports on the settings and results of the quantitative screening in Step 3 (using the Morris EE analysis method [35]) for all nine input parameters listed in Table 3-B. The screening aims to identify those input parameters among the ones listed in Table 3-B that have negligible effects on the KPM predictions by the simulation model (i.e., maximum temperature and heat flux at each target cable tray). To compute the EE, the state space of each input parameter is discretized into a p-level grid (with $p = 4$) so that each input parameter X_i can be randomly sampled from its discretized values. As measures of sensitivity, the sample mean (μ), and the sample standard deviation (σ) of the EE analyses are used. Values of these sensitivity measures are obtained by performing 5000 CFAST model executions (nine input parameters and 500 observations of F_i per input factor i). The Morris samples are drawn using the sampling strategy suggested by Campolongo et al. [36]. The computation of the sensitivity measures follows the procedure given in Section 3.3.2.

Figure 10 to Figure 15 below show μ and σ results of this Morris EE analysis for the nine input parameters regarding their influences on the six KPMs of interest, i.e., maximum temperature inside the cable jacket (T_{CB}) and maximum heat flux at the surface of the cable jacket (q''_{CB}) of the three target cable trays A, B, and C. In each figure, in the blue bar chart on the left, the right ends of the blue bars indicate observed point values of μ and the black line segments represent the 95% CIs around them. Table 3-C presents all values of these two sensitivity measure values obtained for nine parameters listed in Table 3-B.

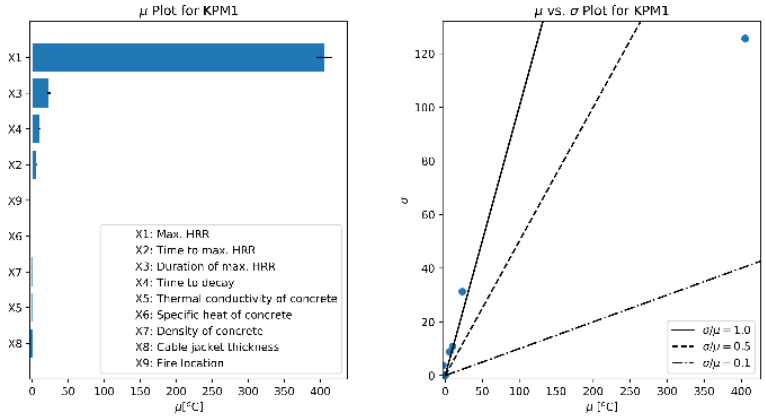

Figure 14: Results of Morris EE analysis for nine input parameters listed in Table 3-B associated with KPM #1 (Cable Tray A Max. Temperature).

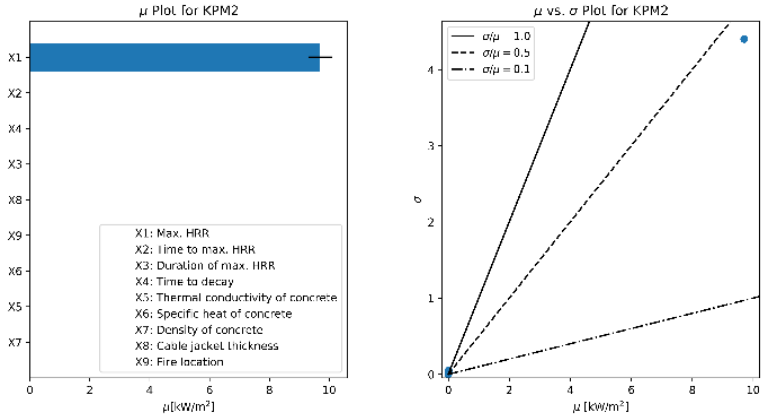

Figure 15: Results of Morris EE analysis for nine input parameters listed in Table 3-B associated with KPM #2 (Cable Tray A Max. Heat Flux).

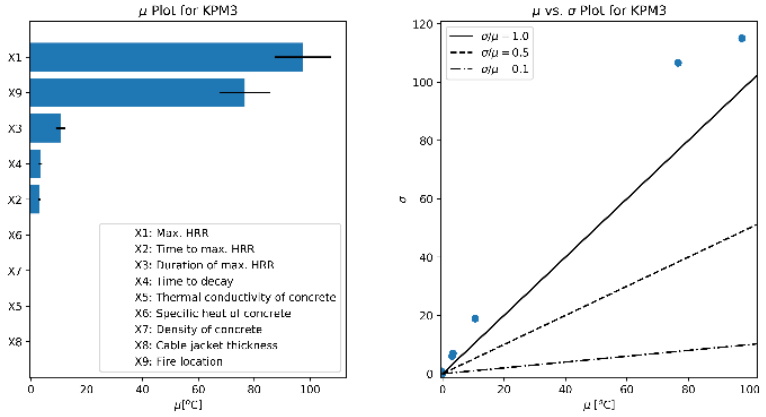

Figure 16: Results of Morris EE analysis for nine input parameters listed in Table 3-B associated with KPM #3 (Cable Tray B Max. Temperature).

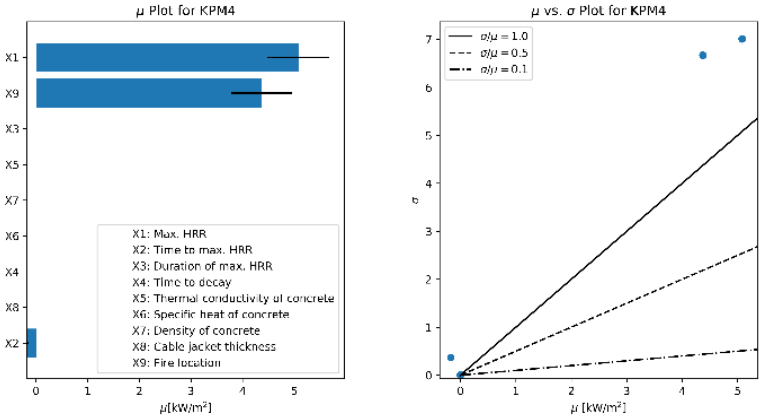

Figure 17: Results of Morris EE analysis for nine input parameters listed in Table 3-B associated with KPM #4 (Cable Tray B Max. Heat Flux).

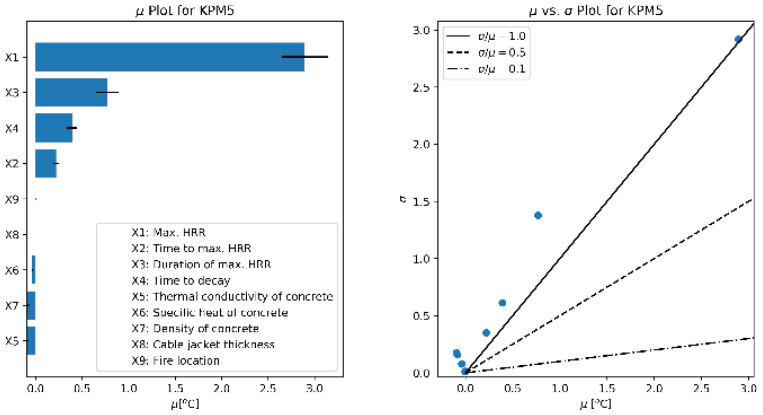

Figure 18: Results of Morris EE analysis for nine input parameters listed in Table 3-B associated with KPM #5 (Cable Tray C Max. Temperature).

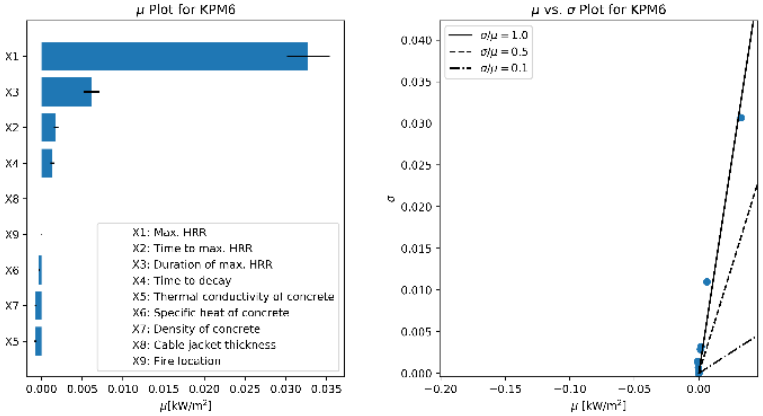

Figure 19: Results of Morris EE analysis for nine input parameters listed in Table 3-B associated with KPM #6 (Cable Tray C Max. Heat Flux).

In practice, to decide whether an input parameter can be screened out, one can apply specific screening criteria and a concept of a threshold area, designed based on both μ and σ, to separate influential input parameters from the non-influential ones. The use of such screening criteria, accounting for both μ and σfacilitates the consideration of both the overall influence of the input parameters on the model output (represented by μ) and the influence of nonlinearity and interactions among input parameters on the model output (represented by σ). For example, the threshold area in this case study is arbitrarily chosen to be an area on the μ vs. σ plot where μ and σ are less than 1% of the corresponding damage criteria (400ºC for the maximum temperature inside the cable jacket [16]; and 11 kW/m^2 for the maximum heat flux at the surface of the cable jacket [9]). Note that, in practice, the design of the threshold area (e.g., 1% chosen above) should consider factors that could affect the accuracy of the simulation model. With the threshold area defined, one can design a screening criterion such as the hypothetical criterion below:

Screening Criterion: If a specific input parameter falls within the non-influential region (i.e., inside the threshold area) for all six KPMs, that input parameter is identified as a non-influential factor in the fire simulation model. Otherwise, if the input parameter falls outside the non-influential regions for any of the six KPMs, that input parameter cannot be considered a non-influential factor (and cannot be screened out).

Using this hypothetical screening criterion for the sensitivity measures μ and σ, one would find that four parameters can be considered as non-influential parameters for all six KPMs: X_5 (i.e., thermal conductivity of concrete), X_6 (i.e., specific heat of concrete), X_7 (i.e., density of concrete), and X_8 (i.e., cable jacket thickness). These input parameters can be screened out and, hence, can be treated as fixed values in the Global IM analysis in Step 4.

Meanwhile, the remaining five input parameters, including X_1, X_2, X_3, X_4 and X_9, are considered for Global IM ranking in Step 4.

Table 3-C: Statistics Results Obtained from the Morris EE Analysis for Nine Parameters Listed in Table 3-B – Fire modeled with CFAST.

		X_1	**X_2**	**X_3**	**X_4**	**X_5**	**X_6**	**X_7**	**X_8**	**X_9**
KPM1 (Cable Tray A Max. Temperature)	μ	405.166	6.038	23.068	10.007	-0.127	-0.057	-0.117	-3.151	0.008
	σ	125.601	8.894	31.243	10.834	0.172	0.082	0.162	3.772	0.13
		X_1	**X_2**	**X_3**	**X_4**	**X_5**	**X_6**	**X_7**	**X_8**	**X_9**
KPM2 (Cable Tray A Max. Heat Flux)	μ	9.698	0.013	0.001	0.011	-0.001	-0.001	-0.002	0	0
	σ	4.398	0.053	0.046	0.049	0.002	0.001	0.002	0	0.001
		X_1	**X_2**	**X_3**	**X_4**	**X_5**	**X_6**	**X_7**	**X_8**	**X_9**
KPM3 (Cable Tray B Max. Temperature)	μ	97.434	3.057	10.593	3.412	-0.151	-0.064	-0.127	-0.371	76.632
	σ	115.032	6.083	18.897	6.96	0.248	0.108	0.201	0.858	106.622

		X_1	X_2	X_3	X_4	X_5	X_6	X_7	X_8	X_9
KPM4 (Cable Tray B Max. Heat Flux)	μ	5.081	-0.175	0.002	0	0.001	0	0.001	0	4.372
	σ	7.011	0.369	0.003	0	0.007	0.003	0.007	0	6.673
		X_1	X_2	X_3	X_4	X_5	X_6	X_7	X_8	X_9
KPM5 (Cable Tray C Max. Temperature)	μ	2.894	0.22	0.769	0.391	-0.095	-0.04	-0.086	-0.006	0
	σ	2.919	0.349	1.376	0.612	0.173	0.078	0.16	0.01	0.013
		X_1	X_2	X_3	X_4	X_5	X_6	X_7	X_8	X_9
KPM6 (Cable Tray C Max. Heat Flux)	μ	0.033	0.002	0.006	0.001	-0.001	0	-0.001	0	0
	σ	0.031	0.003	0.011	0.003	0.001	0.001	0.001	0	0

Note: For input parameters X_i, please refer to Table 3-B.

3.4.4 Step 4 – Global Importance Measures

One practical benefit of applying global sensitivity analysis for importance ranking is that it can be done at multiple levels of detail within the I-PRA framework. This section demonstrates this benefit by looking at the importance rankings obtained at the fire simulation output levels and the risk output level, as discussed in Section 3.4.4.1 and Section 3.4.4.2, respectively.

3.4.4.1 Importance Ranking at the Simulation Output Levels

The cdf-based moment-independent sensitivity measure, $S_i^{(CDF)}$, is quantified for each of the five unscreened input parameters (obtained from the screening analysis in Step 3) with respect to (i) its impact on the KPMs obtained from CFAST simulations, and (ii) its impact on the fire-induced cable damage probabilities calculated from the maximum temperature KPMs and their corresponding damage thresholds. The computation of $S_i^{(CDF)}$ follows the procedure in Section 3.3.3. In calculating the statistics for $S_i^{(CDF)}$ results at these levels, reported in Table 3-D and Table 3-E below, the two-loop Monte Carlo is set up with the sample size for the inner loop $nS_2 = 150$, and the sample size for the outer loop $nS_1 = 30$. The calculation of the fire-induced cable damage probabilities for cable trays A, B, C follows the procedure in Section 3.3.4. In this probability calculation, the case study only considers the thermal damage threshold for the cable trays. Uncertainty associated with the cable thermal damage threshold follows a lognormal distribution with ($\mu = 6.0704$, $\sigma = 0.0872$), obtained for thermoset cables [67].

Table 3-Dbelow shows the statistics of $S_i^{(CDF)}$ estimated for each of the five unscreened input parameters with respect to its influence on the six KPMs (i.e., maximum temperature inside the cable jacket, T_{CB}, and maximum heat flux at the surface of the cable jacket, q''_{CB}, for three cable trays A, B, and C). The 90% confidence intervals (CIs) of $S_i^{(CDF)}$ are calculated using the replicated Monte Carlo simulation and the Bootstrap resampling method (with a sample size of 10,000) [68].

Similarly, Table 3-Ereports on the statistics of $S_i^{(CDF)}$ calculated for each of the five unscreened input parameters with respect to its influence on the fire-induced cable damage probability of cable trays A and B. Note that based on the simulation results, due to its location far from the fire source, cable tray C did not experience fire-induced damage within the scope of this fire scenario. Hence, Table 3-E reports on the statistics of $S_i^{(CDF)}$ calculated for cable trays A and B only.

Table 3-D: $S_i^{(CDF)}$ results calculated for five unscreened input parameters with respect to their influence on each of the six simulation model outputs

Input Parameters		X_1	X_2	X_3	X_4	X_9
KPM1 (Cable Tray A Max. Temperature)	$\bar{S}_i^{(CDF)}$	9.93E-01	1.41E-02	4.54E-02	1.70E-02	1.60E-04
	$S.E.(\bar{S}_i^{(CDF)})$	6.69E-04	1.06E-05	4.98E-05	1.83E-05	1.55E-07
	5th-percentile	8.86E-01	1.23E-02	3.72E-02	1.42E-02	1.36E-04
	95th-percentile	1.11E+00	1.59E-02	5.37E-02	2.01E-02	1.86E-04
		X_1	X_2	X_3	X_4	X_9
KPM2 (Cable Tray A Max. Heat Flux)	$\bar{S}_i^{(CDF)}$	1.16E+00	3.53E-04	4.37E-04	5.51E-04	2.27E-05
	$S.E.(\bar{S}_i^{(CDF)})$	1.07E-03	2.94E-07	3.15E-07	1.07E-06	3.62E-08
	5th-percentile	9.89E-01	3.06E-04	3.86E-04	3.96E-04	1.67E-05
	95th-percentile	1.34E+00	4.03E-04	4.90E-04	7.43E-04	2.85E-05
		X_1	X_2	X_3	X_4	X_9
KPM3 (Cable Tray B Max. Temperature)	$\bar{S}_i^{(CDF)}$	7.34E-01	2.10E-02	6.08E-02	2.37E-02	5.56E-01
	$S.E.(\bar{S}_i^{(CDF)})$	1.47E-03	1.49E-05	5.74E-05	2.52E-05	7.52E-04
	5th-percentile	5.34E-01	1.86E-02	5.14E-02	1.97E-02	4.37E-01
	95th-percentile	1.00E+00	2.35E-02	7.02E-02	2.80E-02	6.86E-01
		X_1	X_2	X_3	X_4	X_9
KPM4 (Cable Tray B Max. Heat Flux)	$\bar{S}_i^{(CDF)}$	1.19E+00	3.92E-03	2.47E-04	0.00E+00	8.47E-01
	$S.E.(\bar{S}_i^{(CDF)})$	3.19E-03	6.19E-06	3.60E-07	0.00E+00	1.16E-03
	5th-percentile	7.72E-01	2.94E-03	1.90E-04	0.00E+00	6.66E-01
	95th-percentile	1.80E+00	4.99E-03	3.09E-04	0.00E+00	1.05E+00
		X_1	X_2	X_3	X_4	X_9
KPM5 (Cable Tray C Max. Temperature)	$\bar{S}_i^{(CDF)}$	2.64E-02	9.89E-04	3.15E-03	1.95E-03	1.94E-05
	$S.E.(\bar{S}_i^{(CDF)})$	8.89E-05	8.17E-07	2.72E-06	2.11E-06	2.44E-08
	5th-percentile	1.49E-02	8.55E-04	2.70E-03	1.60E-03	1.57E-05
	95th-percentile	4.34E-02	1.12E-03	3.60E-03	2.30E-03	2.37E-05
		X_1	X_2	X_3	X_4	X_9
KPM6 (Cable Tray C Max. Heat Flux)	$\bar{S}_i^{(CDF)}$	1.87E-02	4.85E-04	1.56E-03	3.90E-04	1.54E-05
	$S.E.(\bar{S}_i^{(CDF)})$	6.30E-05	3.63E-07	1.33E-06	4.12E-07	2.13E-08
	5th-percentile	1.03E-02	4.25E-04	1.33E-03	3.23E-04	1.21E-05
	95th-percentile	3.07E-02	5.45E-04	1.77E-03	4.60E-04	1.91E-05

Note: For input parameters X_i, please refer to Table 3-B.

Table 3-E: S_i (CDF) results calculated for five unscreened input parameters with respect to their influence on the fire-induced cable damage probabilities

[Ranking] Input Parameters		**[1] X_1**	**[4] X_2**	**[2] X_3**	**[3] X_4**	**[5] X_9**
Cable Tray A Damage Probability	$\bar{S}_i^{(CDF)}$	8.57E-02	2.57E-03	8.17E-03	7.46E-03	8.07E-05
	$S.E.(\bar{S}_i^{(CDF)})$	1.66E-04	1.87E-06	1.05E-05	9.77E-06	8.40E-08
	5th-percentile	5.96E-02	2.26E-03	6.46E-03	5.91E-03	6.76E-05
	95th-percentile	1.14E-01	2.88E-03	9.90E-03	9.11E-03	9.54E-05
[Ranking] Input Parameters		**[1] X_1**	**[4] X_2**	**[3] X_3**	**[5] X_4**	**[2] X_9**
Cable Tray B Damage Probability	$\bar{S}_i^{(CDF)}$	2.36E-03	9.84E-05	3.98E-04	4.32E-05	9.42E-04
	$S.E.(\bar{S}_i^{(CDF)})$	1.47E-05	3.68E-07	1.41E-06	2.64E-07	3.39E-06
	5th-percentile	4.47E-04	3.84E-05	1.79E-04	5.52E-06	4.38E-04
	95th-percentile	5.17E-03	1.62E-04	6.41E-04	9.15E-05	1.54E-03

Note: The ranking in this table is based on point estimates of the calculated $\bar{S}_i^{(CDF)}$. One should, however, note that if the confidence intervals are overlapped, the difference in the rankings would not be statistically significant.

The results in Table 3-D and Table 3-E shows that X_1 (maximum HRR) is consistently ranked as the most important input parameter with respect to its impact on all of the six KPM outputs, as well as its impact on the fire-induced cable damage probabilities. This observation indicates that the uncertainty associated with X_1 contributes the most to the variation in the cdfs of the six KPMs and the fire-induced cable damage probabilities.

Among the other four parameters, it can be seen that X_9 (fire location) has considerable impact on the KPMs and damage probability associated with Cable Tray B, while its impact on those outputs associated with Cable Trays A and C is the smallest among the five parameters. This observation can be explained by the locations of the cable trays inside the fire compartment. Cable Tray A runs right above and along the ignition source cabinet; therefore, when the fire location is varied in Global IM, the damage target associated with Cable Tray A is always assumed to be right above the fire. Cable Tray C is located far away from the ignition source; hence, the impact of the fire location, when it is varied along the ignition source cabinet, on the Cable Tray C's KPMs and damage probability is negligible. On the other hand, Cable Tray B is located close to the ignition source cabinet, installed at perpendicular angle. Therefore, the minimum distance from Cable Tray B to the ignition source, when the fire location is varied along the ignition source cabinet, also varies significantly. For these reasons, X_9 has a large impact on the KPMs and the damage probability for Cable Tray B, while it has a negligible impact on Cable Trays A and C. Regarding X_2 (time to maximum HRR), X_3 (time at maximum HRR), and X_4 (time to decay), their rankings vary depending on the specific output of interest. Note that, when comparing the ranking of two parameters, if their confidence intervals are overlapped, one may not conclude with certainty that one parameter is more important than the other. For example, X_1 and X_9 have overlapped confidence interval with respect to their impact on cable tray B damage probability (Table 3-E); hence, one may not conclude with absolute certainty if X_1 is more important than X_9. In such case, the sample size can be increased to reduce the overlap between the two confidence intervals. In practice, one would need to conduct a thorough convergence study to determine what a sufficiently large sample size would be that would guarantee statistically sound ranking results. In this project, this convergence study is not of particular interest; rather, this analysis is meant to demonstrate the feasibility of the I-PRA Importance Ranking Methodology and its supporting computational platform.

3.4.4.2 Importance Ranking at the System Risk Level

This section covers the global importance ranking at the level of risk estimate, i.e., ranking of the five unscreened input parameters (X_1, X_2, X_3, X_4 and X_9) with respect to their impact on the risk output. To demonstrate the quantification procedure, the risk importance ranking is generated for a hypothetical Fire PRA model shown in Figure 20. In this hypothetical model, the initiating event of interest is a fire-induced Small Break Loss-of-Coolant Accident (SBLOCA) in a PWR plant, assumed to be triggered by a pressurizer's stuck-open Pressure Operated Relief Valve (PORV). The safety systems involved in this hypothetical model include the High Pressure Injection System (HPIS), Reduce Pressure (RP), and the Low Pressure Injection System (LPIS). It is assumed that following the occurrence of the SBLOCA, the reactor is successfully tripped. Note that the global risk importance ranking analysis is not bounded by the complexity of the PRA model; however, for demonstration purpose, other relevant safety systems such as the Residual Heat Removal System, the Containment Fan Cooling System are not considered in this hypothetical model for simplification.

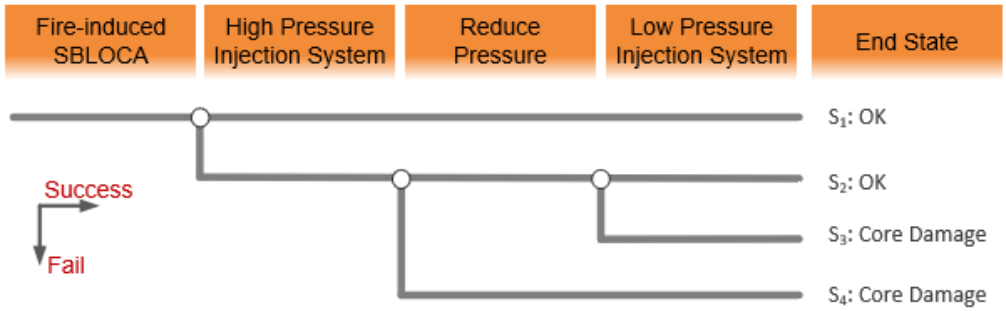

Figure 20: A Hypothetical Fire PRA Model

The HPIS and LPIS are further modeled with simplified Fault Trees in Figure 21 and Figure 22, respectively. For simplification, failure of the RP system is modeled as a single pivotal event.

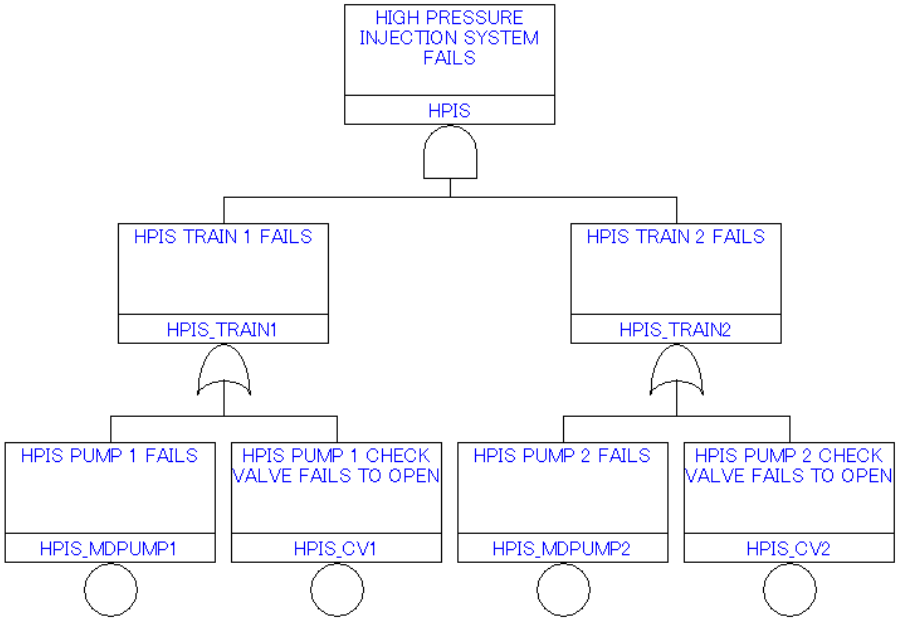

Figure 21: Fault Tree for the High Pressure Injection System

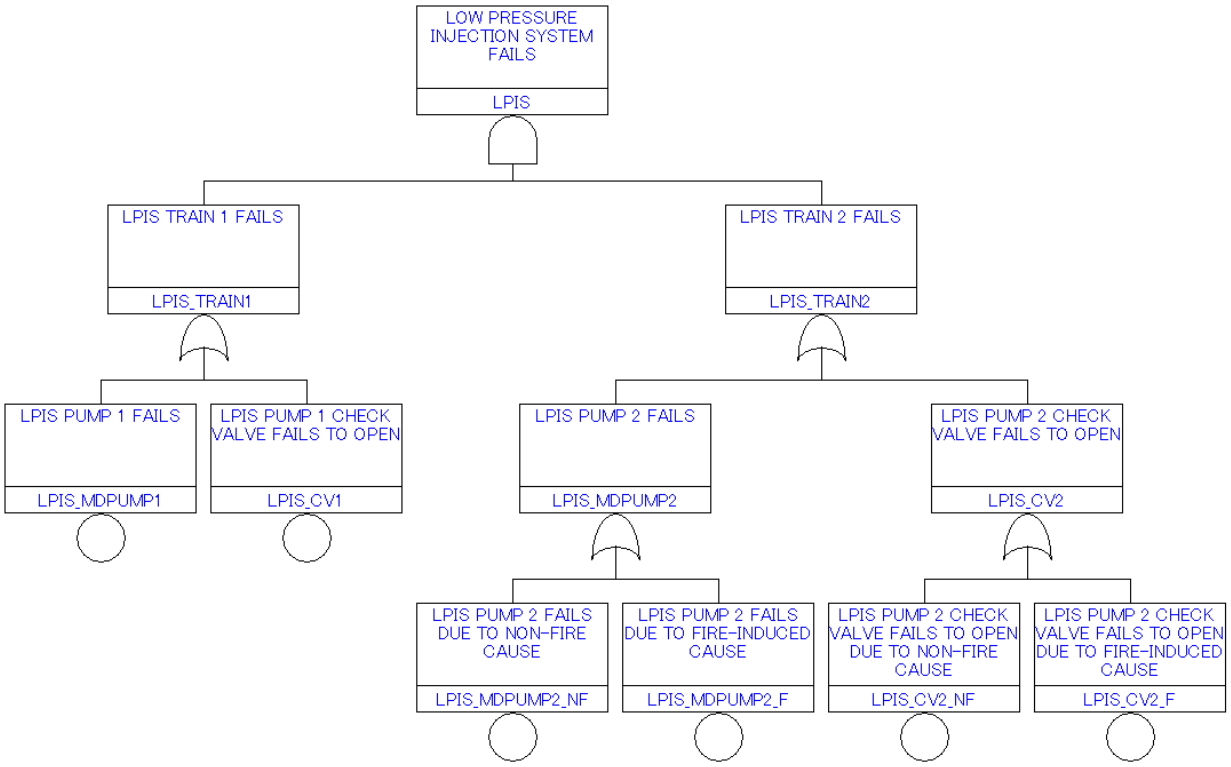

Figure 22: Fault Tree for the Low Pressure Injection System

Identifying the Fire PRA components and the associated cable raceways is a critical task in Fire PRA. Table 3-F summarizes the relationships, considered in this case study, among the components of the hypothetical Fire PRA model (Figure 20 to Figure 22) and the target cable trays A, B, C in the switchgear room fire scenario (Figure 13).

- The ignition frequency of the electrical cabinet, f (FIRE), is assumed to be 0.03 [1/year] using a point estimate (mean value) of the Bin 15 ignition frequency provided in NUREG-2169 [69].
- The control and power cables associated with LPIS_CV2 are placed in cable tray A. Damage to cable tray A is assumed to cause the fire-induced failure of this valve. The fire-induced failure of this valve should be added to the PRA model as a basic event "LPIS_CV2_F," as shown in Figure 22. This case study considers "Fail to open" as the functional failure mode of concern, and it is assumed that, if cable tray A is damaged, "LPIS_CV2_F" occurs with certainty. This assumption is conservative yet has been widely applied in Fire PRAs for NPPs to simplify the circuit failure analysis.
- The control and power cables associated with LPIS_MDPUMP2 are placed in cable tray B. The fire-induced failure of this pump should be added to the PRA model as a basic event "LPIS_MDPUMP2_F," as shown in Figure 22. It is assumed that, given fire-induced damage to cable tray B, the function of this pump is lost with certainty. Cable tray B is assumed to be filled with thermoset-insulated conductor cables. NUREG/CR-7150 Volume 2 [70] provides a probability distribution which represents the epistemic uncertainty associated with the conditional probability of spurious actuation, given the fire-induced damage to the associated cable. In this case study, the mean value of the probability distribution (0.47) is used as the point estimate of the conditional probability of spurious actuation of pressurizer PORVs, given fire-induced damage to cable tray B and the fire occurrence.

- The pressurizer PORV control cable is assumed to be placed in cable tray B. The fire-induced damage to cable tray B may cause a sustained hot short circuit and spurious opening of the pressurizer PORV, which may lead to a SBLOCA. Spurious actuation of the pressurizer PORV is assumed to be sustained long enough to cause a SBLOCA condition. The PORVs are assumed to be solenoid-operated valves controlled by a double break control circuit for ungrounded AC (with individual control power transformers) and may experience the fire-induced spurious operation due to a hot short circuit.

Table 3-F: Mapping among the Fire-induced Damage Targets and PRA Equipment and Events

Damage Targets	PRA Equipment	Failure Mode	PRA Event	PRA Input
Cable Tray A	LPIS Train 2 Check Valve (LPIS_CV2)	Fail to open	LPIS_CV2_F	*Pr(LPIS_CV2_F)*
Cable Tray B	LPIS Train 2 Motor-driven Pump (LPIS_MDPUMP2)	Loss of function	LPIS_MDPUMP2_F	*Pr(LPIS_MDPUMP2_F)*
	Pressurizer PORV	Spurious actuation due to hot short circuit	Initiating Event (FireSBLOCA)	*f (FireSBLOCA) [per year]*

Notes: for notations of the events, please refer to Figure 22.

In some minimal cut sets of the Core Damage scenarios, it appears that a joint damage probability of two cable trays, i.e., $Pr(CBB\ and\ CBA \mid FIRE)$, needs to be estimated. In this report, this joint damage probability is calculated based on the simulation outputs considering the impact of the shared fire-induced conditions on the damage state of the two cable trays. More details on the implementation can be found in Sakurahara et al. [33].

By leveraging the I-PRA methodological framework and the Global IM computational procedure in Section 3.3.3 (when the model output of interest is the plant risk estimate) that are integrated in the I-PRA Importance Ranking methodology, the Global IM results at the risk output level can be obtained. Table 3-G reports the $S_i^{(\mathrm{CDF})}$ results calculated for the five unscreened CFAST input parameters with respect to their influence on the Core Damage Frequency of the hypothetical PRA model. Results for all nine input parameters are included in Table C-3 in Appendix C.

Table 3-G: $S_i^{(\mathrm{CDF})}$ results calculated for five unscreened input parameters with respect to their influence on the risk output (Core Damage Frequency of the hypothetical PRA model)

Ranking	Input parameters	$\overline{S}_i^{(CDF)}$	$S.E.(\overline{S}_i^{(CDF)})$	90% CIs
#1	X_1 (Max. HRR)	2.92E-08	1.95E-10	(5.20E-09, 6.74E-08)
#2	X_9 (Fire Location)	1.06E-08	3.40E-11	(5.47E-09, 1.66E-08)
#3	X_3 (Time at max. HRR)	4.36E-09	1.60E-11	(1.91E-09, 7.20E-09)
#4	X_2 (Time to max. HRR)	1.24E-09	4.52E-12	(5.06E-10, 2.00E-09)
#5	X_4 (Time to Decay)	7.55E-10	3.50E-12	(2.37E-10, 1.37E-09)

Notes: The small orders of magnitude for the $S_i^{(CDF)}$ results in Table 3-G are due to the use of Equation (9) instead of Equation (10) (which calculates normalized $S_i^{(CDF)}$ values). The ranking in this table is based on point estimates of the calculated $\bar{S}_i^{(CDF)}$. One should, however, note that if the confidence intervals are overlapped, the difference in the rankings would not be statistically significant.

As can be seen in Table 3-G, two parameters X_1 (max. HRR) and X_9 (fire location) are identified as the most important input parameters with respect to the impact on the risk core damage frequency (of the hypothetical PRA model). This observation can help inform decision makers as to where to focus additional research and experiment efforts to reduce the epistemic uncertainties associated with these two parameters. In fact, the importance of X_1 helps explain recent efforts that have been made to refine and characterize the maximum HRR of electrical enclosure fires [71] more realistically. On the other hand, the observed importance of X_9 indicates that, in reducing the epistemic uncertainty associated with fire location, more fire experiments may need to be conducted, in which the studied fires are considered to ignite at various locations within the switchgear room (e.g., on different electrical cabinets, at various heights). Such considerations need to be accounted for during the design of experiments to achieve the greatest effect on improving the understanding of the fire location and its impact while satisfying limited budget or resource constraints.

3.4.5 Concluding Remarks: Contributions and Benefits

The SoTeRiA Laboratory at UIUC was the first to conduct quantitative screening using the Morris EE method and to compute the moment-independent Global IM for Fire PRA of NPPs [27, 28, 72]. This current research has advanced the previous studies by the SoTeRiA Laboratory at UIUC [27, 28, 72] by:

- Developing methodological steps for the I-PRA Importance Ranking Methodology (section 3.2) that generate a structured relationship among uncertainty analysis, Morris EE screening analysis, and Global IM analysis;
- Developing a RAVEN-based automated computational platform for implementing the I-PRA Importance Ranking Methodology for Fire PRA of NPPs; and
- Applying the I-PRA Importance Ranking Methodology to a case study. The results showed that, among the sources of uncertainty associated with the nine input parameters of the fire simulation model (listed in Table 3-B), the Morris Elementary Effects analysis was able to screen out four insignificant parameters, i.e., X_5 (thermal conductivity of concrete), X_6 (specific heat of concrete), X_7 (density of concrete), and X_8 (cable jacket thickness). Among the five unscreened parameters, the Global IM analysis results indicated that X_1 (max. HRR) and X_9 (fire location) are the most important parameters.

Recently, EPRI published a technical report [Ref.] on uncertainty quantification for Fire PRA of NPPs. The EPRI report [73] conducted the identification, review and screening, characterization, and propagation of uncertainty sources in the existing Fire PRA models. Uncertainty quantification was performed using Monte Carlo simulation. Additionally, the risk importance measure ranking of the uncertainty sources was obtained based on the Monte Carlo simulation outputs using the correlation coefficients and the variance of the risk outputs as measures of sensitivity.

In the EPRI report [73], simulation outputs were analyzed in the spreadsheets equipped with a statistical plugin to generate the PRA inputs for each fire scenario, such as the probabilities of the fire-induced damage states. Those PRA inputs were then plugged into the PRA software, where the plant risk metrics were computed. In the "external" linkage between plant PRA and underlying simulations generated by EPRI [73], uncertainty sources were ranked based on their contribution to each fire scenario, and the rankings then aggregated. The study [73] measured the degree of uncertainty using the correlation coefficients and the variance; thus, various sources of uncertainty could be analyzed individually and then be aggregated by analytical methods for uncertainty propagation (e.g., the variance formula for error propagation).

The following summarizes benefits as well as future work of the current research by UIUC, INL, and SNL (UIUC-INL-SNL) and highlights how this research can be complementary to the EPRI study [73]:

i. In literature, it is recognized that the correlation-based and variance-based importance measures may result in misleading ranking, especially when input parameters and model outputs have asymmetric uncertainty distributions with fat and long tails. The observations from the CFAST and FDS outputs in the UIUC research showed that, depending on the initial and boundary conditions of the fire scenarios, fire-induced damage could have a very small probability and could be dominated by the tail of the uncertainty distribution. For instance, in the case study (Section 3.4), the physical KPMs for cable tray B have skewed probability distributions, and the cable damage probability is dominated by the upper tail of those uncertainty distributions; hence, the accuracy of the correlation-based and variance-based methods is questionable. To select an appropriate sensitivity/importance measure analysis method for the I-PRA Importance Ranking Methodology, scientific justifications (Section 3.2.4.5) are provided based on a thorough review of the existing sensitivity analysis methods (Section 3.2.4.1). In this research (UIUC-INL-SNL), a cdf-based moment-independent global method, $S_i^{(CDF)}$, is selected since it can address the four attributes (Attributes a to d discussed in Section 3.2.4.5), including (a) the level of risk-contributing factors to be ranked, (b) uncertainty of input parameters, (c) uncertainty of model outputs, and (d) non-linearity and interactions, and can be more accurate than correlation-based and variance-based global methods.

ii. The I-PRA Importance Ranking Methodology includes quantitative screening of the uncertainty sources using the Morris EE method (Step 3 in Section 3.2.3). To go beyond one-way sensitivity analysis methods commonly used in the current PRA practices, the Morris EE method provides a robust distinction between influential vs. non-influential factors since it can explicitly address both main effects and the effects by nonlinearity and interaction through a randomized one-at-a-time sampling scheme.

iii. This research (UIUC-INL-SNL) has developed a RAVEN-based automated computational platform that can integrate the plant PRA scenarios, underlying simulations (e.g., a fire progression model), quantitative screening (using the Morris EE method), and the Global IM analysis into a "unified" framework:

   - The unified RAVEN-based computational platform can generate the ranking of input parameters considering multiple key scenarios simultaneously, rather than considering one scenario at a time followed by post-aggregation. Although the analytical post-aggregation of uncertainties could be applicable when the uncertainties are measured by the correlation coefficients and the variance, the correlation-based/variance-based global methods can be inaccurate compared to the moment-independent global methods, particularly under the conditions explained above. For the moment-independent global methods, it is not possible to derive an analytical formula for uncertainty propagation, unless the model of interest is a simple additive or multiplicative function of input parameters; hence, a unified computational platform that integrates the plant PRA model with the underlying simulations is required.
   - The unified computational platform, developed in this research, contributes to more explicit and accurate treatment of dependencies at multiple levels of Fire PRA, such as those at the levels of physical inputs, multiple targets, multiple spurious actuations, and PRA basic events. In the I-PRA framework, the Interface Module can treat multi-level dependencies by using the simulation-informed approach for dependency analysis developed in the previous research by the SoTeRiA Laboratory at UIUC [33].

- The RAVEN-based automated computational platform facilitates the sampling-based uncertainty quantification in Fire I-PRA, which aims at: (i) propagating the uncertainties associated with the FSM input parameters using Monte Carlo simulation and (ii) making the FSM model probabilistic and creating a probabilistic interface between FSM and the plant-specific PRA scenarios.
- The unified RAVEN-based computational platform can provide both “industry-wide” and "plant-specific" rankings of uncertainty sources. The industry-wide ranking may not be the same as the plant-specific ranking. The I-PRA computational platform, developed in this research, is designed in a way that alternate models for the plant-specific PRA and the underlying simulations can be plugged in; hence, it can provide a possibility for industry to easily redo the analysis for a specific plant. This automated computational platform would be helpful if a plant uses the I-PRA ranking methodology to identify the plant-specific dominant sources of uncertainty and to inform the plant-specific risk-informed decision-making.

iv. This research has done Morris EE analysis using both FDS and CFAST. As can be seen in Table B-3 in Appendix B, the absolute magnitudes of the sensitivity metrics (μ and σ) obtained when using FDS are different from those obtained when using CFAST (Table 3-C). One possibility is that this disagreement stems from the differences between the FDS and CFAST model resolutions. For example, a significant difference between FDS and CFAST in predicting the maximum heat flux and cable temperature is that FDS has a “finer” spatial resolution as all of its geometrical entities are divided into rectilinear grid cells and described by defining their coordinates in the computational domain; CFAST, on the other hand, is a two-zone model where the vertical dimension of the fire compartment is divided into two discrete layers. It should also be noted that NUREG-1934 indicated a reservation on the applicability of CFAST to Scenario D (Figure 13) due to multiple reasons related to the fire conditions that may not be suitable for CFAST. To thoroughly investigate the underlying causes of the differences and how they affect the results of the Morris Elementary Effects analysis, further study is needed.

3.5 Future Work or Enhancements

3.5.1 Uncertainty Scope

Future research should extend the scope of uncertainty sources beyond the input parameters of the fire models, e.g., the uncertainties associated with ignition frequencies, cable fire spread, detection and suppression, electrical circuit failure likelihoods, and model uncertainty. For instance, as an initial research phase to demonstrate the implementation of the I-PRA Importance Ranking Methodology, the illustrative case study (Section 3.4of this report) has not considered detection and suppression. The I-PRA framework, however, is capable of accounting for these contributions as discussed in Sakurahara et al. [27, 30, 74] and Bui et al. [75]. While the illustrative case study only considered the potential sources of uncertainties associated with the Fire Propagation Model, future research needs to analyze and rank the uncertainty sources associated with the other modules/submodules of I-PRA. In addition, further research should be conducted to establish a theoretical and methodological foundation for analyzing aleatory and epistemic uncertainties separately in the I-PRA Importance Ranking Methodology.

3.5.2 RAVEN Computational Platform

Future research will advance the RAVEN-based computational platform to have an explicit connection to the physical phenomena data and the underlying experimental design parameters that contribute to the epistemic uncertainties associated with the simulation models and their input parameters. With this advancement, sensitivity analysis and parametric study can be performed to examine, for example, the impact of the experimental design parameters on the plant risk outputs. This type of analysis helps decision makers understand which refinements of physical phenomena data can provide the largest benefit to improving the realism of PRA and to reducing the uncertainty associated with the PRA outputs.

3.5.3 PRA Software Integration

In future research, to generate an automated linkage to a full-scope plant PRA, PRA software (e.g., SAPHIRE) should be integrated into the RAVEN-based computational platform developed in this project. This advancement will offer an automated and unified computational platform that can be applied directly for comprehensive uncertainty analysis and risk importance measure ranking in Fire PRAs by the nuclear industry and NRC. One of the main methodological challenges in the integration of the full-scope plant PRA is the treatment of dependent failures due to the shared or correlated causal factors at multiple levels, such as physical inputs, fire-human interactions, cable damage, circuit failures, and component failures. This current research has partially addressed the dependency at the cable damage level, i.e., a joint failure event of two cable trays (Section 3.4.4.2). To generate a reliable interface with the full-scope plant PRA, future research should implement the simulation-informed dependency treatment methodology in the I-PRA framework [64] for the other levels of dependencies.

3.5.4 Additional Significant Scenarios

The illustrative case study (Section 3.4.1) only considers one fire scenario (i.e., one fire zone and one ignition source). Future research should scale up the analysis by applying the I-PRA Importance Ranking Methodology and the RAVEN-based computational platform developed in this research to other NPP risk-significant fire scenarios that can include multiple ignition sources and intervening combustibles. The EPRI [73] study uses three case studies for the uncertainty analysis.

3.5.5 Time Dependent Scenario Modeling

Both INL and UIUC are researching dynamic probabilistic risk assessment (DPRA) methods for fire analysis and how to apply these insights to existing models and future methodologies. As mentioned in Section 3.1, the I-PRA methodological framework (Figure 11) developed by UIUC integrates simulation models of the underlying human and physical failure mechanisms with the existing plant PRA through a probabilistic interface [28, 74]. The dynamic coupling [75, 76] between the human performance and the physical failure simulation in I-PRA is similar in its nature to simulation-based PRA (or dynamic PRA).Methods being researched can be applied for advanced reactors and new plants as industry and the regulatory agency deem advantageous, using dynamic with static coupling or fully simulation-based/dynamic PRA. Meanwhile, the Interface Module (‘e’ in Figure 11) in the I-PRA offers the possibility of reliably using dynamic simulation approaches linked with the existing PRA of aging plants. The I-PRA risk importance ranking offered in this report can provide valuable information for efficiently (i) enhancing the realism of Fire PRA for existing plants [77] and (ii) supporting the development of Fire DPRA for advanced reactors and new plants.

Dynamic modeling can more accurately model some aspects of fire scenarios, such as operator actions and manual suppression. Changes in time-related data, such as the HRR curves can have a large effect in dynamic modeling. Future work of a DPRA model using varied input data can show the correlation of this data and operation procedures. This will further identify key areas and show the justification for reducing uncertainty of specific input data.

Recently, DPRA has been implemented in nuclear safety to capture timing aspects that are difficult to represent in currently used, purely numerical methods. Some recent DPRA can also employ physics-based simulator codes to accurately model physical phenomena with system dynamics. These physics-based simulator codes, like FDS, are coupled with DPRA codes that monitor and control the simulation (e.g., Event Model Risk Assessment using Linked Diagrams [EMRALD]). The latter codes, in particular, introduce both deterministic (e.g., system control logic and operating procedures) and stochastic (e.g., component failures and variable uncertainties) elements into the simulation.

A typical DPRA analysis involves the following four steps:

1. Sampling values of a set of parameters from the uncertainty space of interest
2. Simulating the system behavior for that specific set of parameter values
3. Analyzing the set of simulation runs
4. Visualizing the correlations of time contributing values and simulation outcome.

Step 1 is typically performed by randomly sampling from a given distribution (i.e., Monte Carlo) or selecting such parameter values as inputs from the user (i.e., Dynamic Event Tree). In Step 2, a simulation run is performed using the values sampled in Step 1. These values typically affect the timing and sequencing of events that occur during the simulation. Some codes sample values during the simulation run, combining Steps 1 and 2. The objective of Step 3 is to identify the correlations between timing and sequencing of events with simulation outcomes (such as maximum core temperature). In a classical PRA (event tree/fault tree based) environment, such analysis is performed by observing and ranking the minimal cut sets that contribute to a top event (e.g., core damage). In a DPRA environment, however, data generated is more heterogeneous since it consists of both (a) temporal profiles of state variables and (b) timing of specific events. Clustering and visually displaying failure data over time and space is a new research topic and it is especially relevant when analyzing time or order-dependent sequences, such as operator actions.

4. REFERENCES

[1] Performance-Based Standard for Fire Protection for Light Water Reactor Electric Generating Plants, NFPA 805. 2001.
[2] Salley MH, Kassawara RP. Verification and Validation of Selected Fire Models for Nuclear Power Plant Applications: Fire Dynamics Simulator (FDS) (NUREG-1824, Volume 7). 2007.
[3] Salley MH, Lindeman A. Verification and Validation of Selected Fire Models for Nuclear Power Plant Applications - Final Report (NUREG-1824, Supplement 1). 2016.
[4] Salley MH, Wachowiak R. Nuclear Power Plant Fire Modeling Analysis Guidelines (NPP FIRE MAG) - Final Report (NUREG-1934, EPRI 1023259). 2012.
[5] Commission USNR. NRC/Industry Workshop on Improving Realism in Fire PRAs. Washington, DC2017.
[6] Olivier TJ, Nowlen SP. A Phenomena Identification and Ranking Table (Pirt) Exercise for Nuclear Power Plant Fire Model Applications (NUREG/CR-6978, SAND2008-3997P). Washington, DC; 2008.
[7] Smith CL, Wood ST, O'Neal D. Systems Analysis Programs for Hands-on Integrated Reliability Evaluations (SAPHIRE) Version 8: Overview and Summary. Idaho National Laboratory and Office of Nuclear Regulatory Research, U.S. Nuclear Regulatory Commission; 2011.
[8] al Be. Review of the Diablo Canyon Probabilistic Risk Assessment, (NUREG/CR-5726). U.S. Nuclear Reglatory Commission, Office of Nuclear Regulatory Research; 1994.
[9] Iqbal N, Salley MH, Weerakkody S. FDT: Fire Dynamics Tools (FDT): Quantitative Fire Hazard Analysis Methods for the U.S. Nuclear Regulatory Commission Fire Protection Inspection Program, Final Report (NUREG-1805). U.S. Nuclear Regulatory Commission; 2004.
[10] Peacock RD, Reneke PA, Forney GP. CFAST - Consolidated Model of Fire Growth and Smoke Transport (Version 7) Volume 2: User's Guide. National Institute of Standards and Technology; 2017.
[11] Gay L. User Guide of MAGIC Software V4.1.1. France EdF HI82/04/022/B, Electricité de France; 2005.
[12] McGrattan K, al e. Fire Dynamics Simulator Technical Reference Guide, Volume 3: Validation. National Institute of Standards and Technology, VTT Technical Research Centre of Finland; 2013.
[13] Commission USNR. Refining and Characterizing Heat Release Rates from Electrical Enclosures during Fire (RACHELLE-FIRE). U.S. Nuclear Regulatory Commission, Office of Nuclear Regulatory Research, NUREG/CR-2178; 2016.

[14] Bareham S, McGrattan K. Heat Release Rates of Electrical Enclosure Fires (HELEN-FIRE), (NUREG/CR-7197). Division of Risk Analysis, US Nuclear Regulatory Commission; 2016.
[15] Nowlen SP, Wyant FJ. Cable Respose to Live Fire (CAROLFIRE) Volume 1: Test Descriptions and Analysis of Circuit Response Data. U.S. Nuclear Regualtory Commission, Office of Nuclear Regulatory Research, NUREG/CR-6931; 2008.
[16] Nowlen S, Wyant F. Cable Response to Live Fire (CAROLFIRE), Volume 2: Cable Fire Response Data for Fire Model Improvement. U.S. Nuclear Regualtory Commission, Office of Nuclear Regulatory Research, NUREG/CR-6931; 2008.
[17] Nowlen S, Wyant F, McGrattan K. Cable Response to Live Fire (CAROLFIRE), NUREG/CR-6931. Washington, DC: U.S. Nuclear Regulatory Commission; 2008.
[18] Commission USNR. Characterization of Fire-Induced Circuit Faults. U.S. Nuclear Regulatory Commission; 2002.
[19] Institute EPR. Spurious Actuation of Electrical Circuits due to Cable Fires. Electric Power Research Institute; 2002.
[20] McGrattan K. Cable Response to Live Fire (CAROLFIRE) Volume 3: Thermally-Induced Electrical Failure (THIEF) Model. NUREG/CR-6931; 2008.
[21] Commission USNR. Kerite Analysis in Thermal Environment of FIRE (KATE-Fire): Test Resuls. U.S. Nuclear Regualtory Commission, Office of Nuclear Regulatory Research, NUREG/CR-7102; 2012.
[22] Commission USNR. Direct Current Electrical Shorting in Response to Exposure Fire (DESIREE-Fire): Test Results. U.S. Nuclear Regulatory Commission, Office of Nuclear Regulatory Research, NUREG/CR-7100; 2012.
[23] Commission USNR. Cable Heat Release, Ignition, and Spread in Tray Installations during Fire (CHRISTIFIRE), Phase 1: Horizontal Trays. U.S. Nuclear Regulatory Commission, Office of Nuclear Regulatory Research, NUREG/CR-7010; 2012.
[24] Commission USNR. Cable Heat Release, Ignition, and Spread in Tray Installations during Fire (CHRISTIFIRE), Phase 2: Vertical Shafts and Corridors. U.S. Nuclear Regulatory Commission, Office of Nuclear Regulatory Research, NUREG/CR-7010; 2013.
[25] Commission USNR. Guidance on the Treatment of Uncertainties Associated with PRAs in Risk-Informed Decision Making. U.S. Nuclear Regulator Commission, Office of Nuclear Regulatory Research, NUREG-1855; 2009.
[26] Commission USNR. EPRI/NRC-RES Fire PRA Methodology for Nuclear Power Facilities Volume 2: Detailed Methodology (NUREG/CR-6850, ADAMS Accession No. ML052580118). 2005.
[27] Sakurahara T, Reihani S, Kee E, Mohaghegh Z. Global Importance Measure Methodology for Integrated Probabilistic Risk Assessment. Proceedings of the Institution of Mechanical Engineers, Part O: Journal of Risk and Reliability. 2019.
[28] Sakurahara T, Mohaghegh Z, Reihani S, Kee E, Brandyberry M, Rodgers S. An Integrated Methodology for Spatio-Temporal Incorporation of Underlying Failure Mechanisms into Fire Probabilistic Risk Assessment of Nuclear Power Plants. Reliability Engineering and System Safety. 2018;169:242-57.
[29] Bui H, al e. Integrated Probabilistic Risk Assessment (I-PRA) Importance Ranking for Fire PRA of Nuclear Power Plants. Transaction of American Nuclear Society (ANS) Winter Meeting and Technology Expo. Washington, DC2019.
[30] Alfonsi A, al e. RAVEN Theory Manual. Idaho National Laboratory; 2019.
[31] Sakurahara T, Mohaghegh Z, Reihani S, Kee E. Methodological and Practical Comparison of Integrated Probabilistic Risk Assessment (I-PRA) with the Existing Fire PRA of Nuclear Power Plants. Nuclear Technology. 2018;204:354-77.
[32] Consulting A. Riskman for Windows, Version 15.0. Irvine, CA: ABS Consulting 2014.
[33] Sakurahara T, Schumock G, Reihani S, Kee E, Mohaghegh Z. Simulation-Informed Probabilistic Methodology for Common Cause Failure Analysis. Reliability Engineering & System Safety. 2019;185:84-99.

[34] Bui H, Sakurahara T, Reihani S, Kee E, Mohaghegh Z. Spatiotemporal Integration of an Agent-Based First Responder Performance Model with a Fire Hazard Propagation Model for Probabilistic Risk Assessment of Nuclear Power Plants. ASCE-ASME Journal of Risk and Uncertainty in Engineering Systems: Part B Mechanical Engineering, Special Issue on Human Performance & Decision-making in Complex Industrial Environments. 2019.
[35] Morris MD. Factorial sampling plans for preliminary computational experiments. Technometrics. 1991;33:161-74.
[36] Campolongo F, Cariboni J, Saltelli A. An effective screeening design for sensitivity analysis of large models. Environmental Modelling & Software. 2007;22:1509-18.
[37] McGrattan K, al e. Fire Dynamics Simulator (Version 6) User's Guide. National Institue of Standards and Technology; 2013.
[38] Peacock RD, McGrattan K, Forney GP, Reneke PA. CFAST—Consolidated Fire and Smoke Transport (Version 7)—Volume 1: Technical Reference Guide. NIST Technical Note 1889v1 (National Institute of Standards and Technology, Gaithersburg, MD) 2016.
[39] Saltelli A, al e. Global sensitivity analysis: the primer: John Wiley & Sons; 2008.
[40] Iman RL, Conover WJ. A Measure of Top-Down Correlation. Technometrics. 1987;29:351-7.
[41] Saltelli A, Marivoet J. Non-parametric statistics in sensitivity analysis for model output: a comparison of selected techniques. Reliability Engineering & System Safety. 1990;28:229-53.
[42] Helton JC. Uncertainty and sensitivity analysis techniques for use in performance assessment for radioactive waste disposal. Reliability Engineering & System Safety. 1993;42:327-67.
[43] Hamby DM. A review of techniques for parameter sensitivity analysis of environmental models. Environmental Monitoring and Assessment. 1994;32:135-54.
[44] Borgonovo E. Measuring uncertainty importance: investigation and comparison of alternative approaches. Risk analysis. 2006;26:1349-61.
[45] Helton JC, Johnson JD, Sallaberry CJ, Storlie CB. Survey of sampling-based methods for uncertainty and sensitivity analysis. Reliability Engineering & System Safety. 2006;91:1175-209.
[46] Ikonen T, Tulkki V. The importance of input interactions in the uncertainty and sensitivity analysis of nuclear fuel behavior. Nuclear Engineering and Design. 2014;275:229-41.
[47] Ikonen T. Comparison of global sensitivity analysis methods – Application to fuel behavior modeling. Nuclear Engineering and Design. 2016;297:72-80.
[48] Hora SC, Iman RL. Comparison of Maximus/Bounding and Bayes/Monte Carlo for fault tree uncertainty analysis (SAND85-2389). Hawaii Univ., Hilo (USA); Sandia National Labs., Albuquerque, NM (USA); 1986.
[49] Iman RL, Hora SC. A Robust Measure of Uncertainty Importance for Use in Fault Tree System-Analysis. Risk Analysis. 1990;10:401-6.
[50] Sobol′ IM. On sensitivity estimation for nonlinear mathematical models. Matematicheskoe Modelirovanie. 1990;2:112-8.
[51] Sobol′ IM. Sensitivity estimates for nonlinear mathematical models. Mathematical Modeling and Computational Experiment Model, Algorithm, Code. 1993;1:407.
[52] Saltelli A, Tarantola S, Campolongo F. Sensitivity analysis as an ingredient of modeling. Statistical Science. 2000;15:377-95.
[53] Saltelli A. Sensitivity analysis for importance assessment. Risk Analysis. 2002;22:579-90.
[54] Homma T, Saltelli A. Importance measures in global sensitivity analysis of nonlinear models. Reliability Engineering & System Safety. 1996;52:1-17.
[55] Borgonovo E, Plischke E. Sensitivity analysis: A review of recent advances. European Journal of Operational Research. 2016;248:869-87.
[56] Borgonovo E. A new uncertainty importance measure. Reliability Engineering & System Safety. 2007;92:771-84.
[57] Liu Q, Homma T. A New Importance Measure for Sensitivity Analysis. J Nucl Sci Technol. 2010;47:53-61.

[58] Pianosi F, Wagener T. A simple and efficient method for global sensitivity analysis based on cumulative distribution functions. Environmental Modelling & Software. 2015;67:1-11.
[59] Pianosi F, Wagener T. Distribution-based sensitivity analysis from a generic input-output sample. Environmental Modelling & Software. 2018;108:197-207.
[60] Borgonovo E, Aliee H, Glaß M, Teich J. A new time-independent reliability importance measure. European Journal of Operational Research. 2016;254:427-42.
[61] Cui L, Lu Z, Wang Q. Parametric sensitivity analysis of the importance measure. Mechanical Systems and Signal Processing. 2012;28:482-91.
[62] Borgonovo E, Zentner I, Pellegri A, Tarantola S, de Rocquigny E. On the importance of uncertain factors in seismic fragility assessment. Reliability Engineering & System Safety. 2013;109:66-76.
[63] Herman JD, Usher W. SALib: An open-source Python library for Sensitivity Analysis. J Open Source Software. 2017;2:97.
[64] U.S. Nuclear Regulatory Commission. Verification and Validation of Selected Fire Models for Nuclear Power Plant Applications, Volume 1: Main Report (NUREG-1824). In: (RES) OoNRR, editor. Rockville, MD2007.
[65] Campolongo F, Cariboni J, Saltelli A. An effective screening design for sensitivity analysis of large models. Environmental Modelling & Software. 2007;22:1509-18.
[66] Wadsö L, Karlsson J, Tammo K. Thermal properties of concrete with various aggregates. Cement and Concrete Research; 2012.
[67] Taylor GJ. Evaluation of critical nuclear power plant electrical cable response to severe thermal fire conditions [Master's thesis]: University of Maryland, College Park; 2012.
[68] Efron B, Tibshirani RJ. An introduction to the bootstrap: CRC press; 1994.
[69] Melly N, Lindeman A. Nuclear Power Plant Fire Ignition Frequency and Non-Suppression Probability Estimation Using the Updated Fire Events Database-United States Fire Event Experience Through 2009 (NUREG-2169, EPRI 3002002936). 2015.
[70] Subudhi M, Martinez-Guridi G, Taylor G, Salley MH, Wachowiak R, Lindeman A. Joint Assessment of Cable Damage and Quantification of Effects from Fire (JACQUE-FIRE)- Volume 2: Expert Elicitation Exercise for Nuclear Power Plant Fire-Induced Electrical Circuit Failure (NUREG/CR-7150, EPRI 3002001989, and BNL-NUREG-98204-2012; Volume 2). Brookhaven National Laboratory; Office of Nuclear Regulatory Research, U.S. Nuclear Regulatory Commission; and Electric Power Research Institute (EPRI); 2014.
[71] U.S. Nuclear Regulatory Commission. Refining And Characterizing Heat Release Rates From Electrical Enclosures During Fire (RACHELLE-FIRE), Volume 1: Peak Heat Release Rates and Effect of Obstructed Plume (NUREG-2178). Washington DC: U.S. Nuclear Regulatory Commission; 2015.
[72] Sakurahara T, Reihani SA, Mohaghegh Z, Brandyberry M, Kee E, Rodgers S, et al. Integrated PRA methodology to advance fire risk modeling for nuclear power plants. European Safety and Reliability Conference (ESREL). Zürich, Switzerland2015.
[73] Electric Power Research Institute. A Practical Approach for Addressing Uncertainty in Fire Probabilistic Risk Assessment Modeling (EPRI 3002003188). Palo Alto, CA.: EPRI; 2020.
[74] Mohaghegh Z, Kee E, Reihani S, Kazemi R, Johnson D, Grantom R, et al. Risk-Informed Resolution of Generic Safety Issue 191. International Topical Meeting on Probabilistic Safety Assessment and Analysis (PSA2013)2013.
[75] Bui H, Sakurahara T, Reihani S, Kee E, Mohaghegh Z. Spatiotemporal Integration of an Agent-Based First Responder Performance Model with a Fire Hazard Propagation Model for Probabilistic Risk Assessment of Nuclear Power Plants. ASCE-ASME Journal of Risk and Uncertainty in Engineering Systems: Part B Mechanical Engineering. 2020;6.
[76] Sakurahara T, Reihani S, Kee E, Mohaghegh Z. Human Reliability Analysis (HRA)-based Method for Manual Fire Suppression Analysis in an Integrated Probabilistic Risk Assessment. ASCE-ASME Journal of Risk and Uncertainty in Engineering Systems: Part B Mechanical Engineering, Special Issue on Human Performance & Decision-making in Complex Industrial Environments. 2020;6.

[77] Bui H, Sakurahara T, Pence J, Reihani S, Kee E, Mohaghegh Z. An algorithm for enhancing spatiotemporal resolution of probabilistic risk assessment to address emergent safety concerns in nuclear power plants. Reliability Engineering & System Safety. 2019;185:405-28.
[78] Taylor G. Evaluation of Critical Nuclear Power Plant Electrical Cable Response to Severe Thermal Fire Conditions. U.S. Nuclear Regulatory Commission; 2012.
[79] Efron B, Tibshirani RJ. An introduction to the bootstrap. CRC press; 1994.

APPENDIX A

The uncertainty of parameters in the fire modeling effort can be analyzed through input of probability distributions. Initially, the fire modeling was evaluated with parameters for which the uncertainty was formally characterized through probability distributions. The peak HRR of different cable/fuel types was characterized as a gamma distribution with the following parameters[13]:

Table A-1. Peak HRR probability distribution parameters.

Parameter	Fuel Type	Distribution	Alpha	Beta
Peak HRR (kW)	TS/QTP/SIS	Gamma	0.36	57
	TP	Gamma	1.21	30

The next parameters are the time to maximum heat release rate, the duration time of the maximum heat release rate, and the decay time. These input parameters are treated as random variables and the associated distributions are listed in [31]:

Table A-2. HRR timing probability distribution parameters.

Parameter	Distribution	Parameter 1	Parameter 2	Parameter 3
Time to Maximum HRR (min)	Uniform	4	18	N/A
Duration of Maximum HRR (min)	Triangular	0	0	20
Time to Decay (min)	Uniform	10	30	N/A

The cable thermal fragility probability distribution was determined numerically using NRC sponsored test data [78]. The distribution parameters are shown in.

Table A-3. Cable thermal fragility probability distribution parameters.

Parameter	Distribution	Mean	Standard Deviation	p Value
Cable Thermal Fragility (°C)	Lognormal	6.0704	0.0872	0.8905

The uncertainty associated with a second set of parameters was also evaluated in the fire modeling effort. The first set were parameters associated with concrete material properties, including thermal conductivity, specific heat, and density. The variability of these parameters for concrete samples with different aggregate recipes is shown in [66]:

Table A-4. Concrete material properties of samples with different aggregate recipes.

Sample	Density (kg/m^3)	Thermal Conductivity (W/mK)	Specific Heat (J/kgK)
REF	2240	2.24	795
MAG	3650	2.57	734
GRA	1890	3.52	810
GAM	2810	3.85	875
ST1	2330	2.57	828
ST2	2441	2.95	828
BRA	2520	2.71	694
COP	2438	3.63	939

A gamma distribution was fit to the parameters in this limited data set. Because the simulations in which these distributions are used are primarily for illustrative purposes, the large CIs associated with the fitted distributions were deemed to be acceptable. shows the distribution parameters for each of the concrete material properties. through show the proposed gamma distribution compared to the empirical distribution and the resulting p value for each distribution.

Table A-5. Concrete material property distribution parameters.

Parameter	Distribution	p Value	Parameter 1	Parameter 2
Density	Gamma	0.66571	a=30.4134	b=83.5117
Thermal Conductivity	Gamma	0.85516	a=30.148	b=0.099675
Specific Heat	Gamma	0.9836	a=128.389	b=6.33134

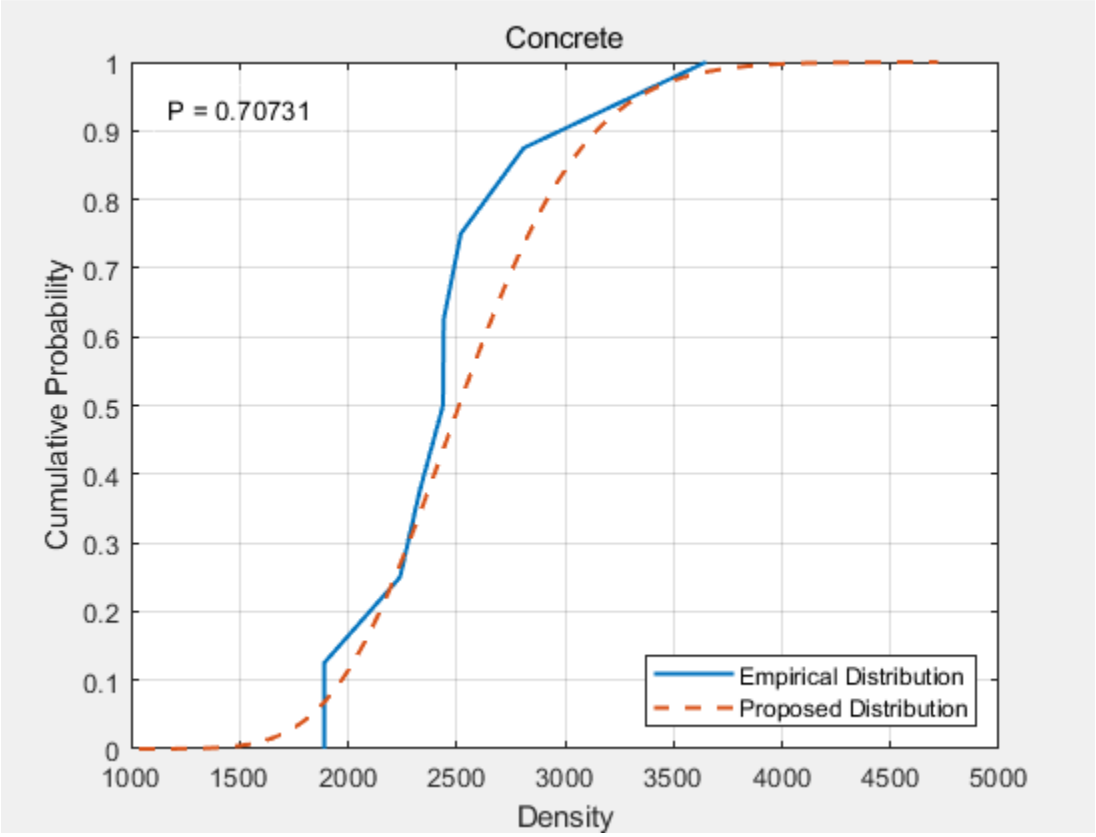

Figure A-1. Concrete density cumulative probability distribution.

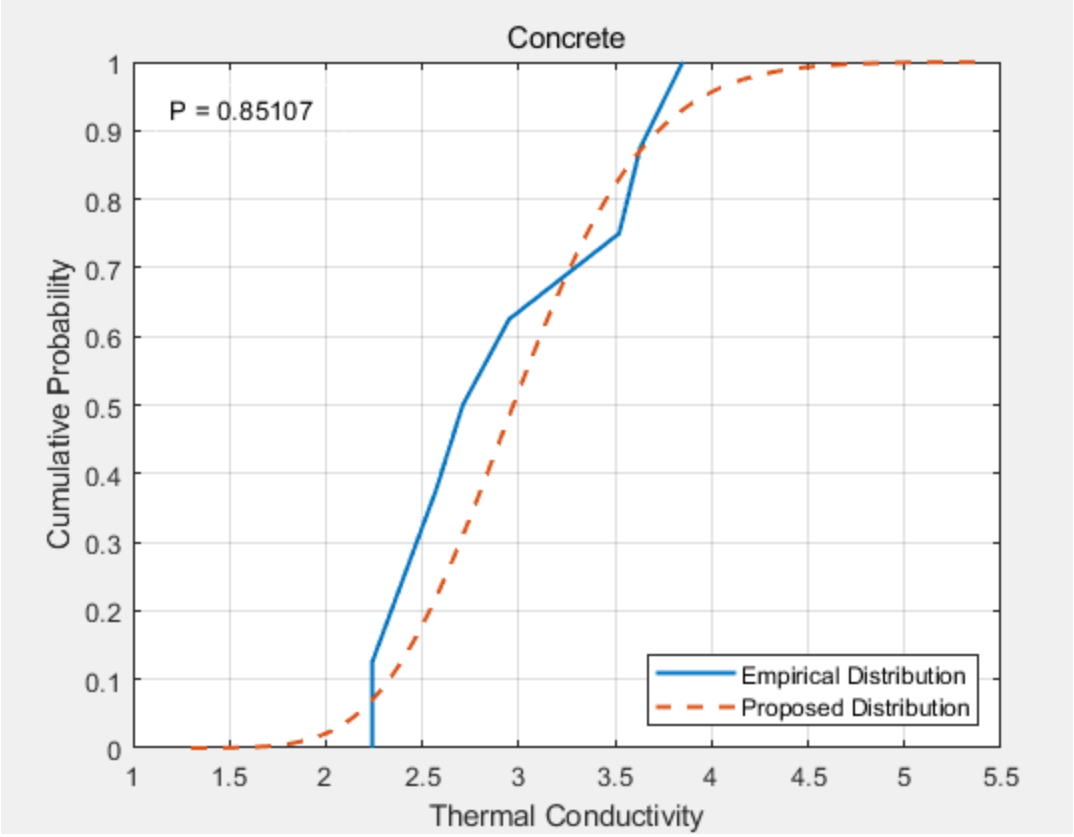

Figure A-2. Concrete thermal conductivity cumulative probability distribution.

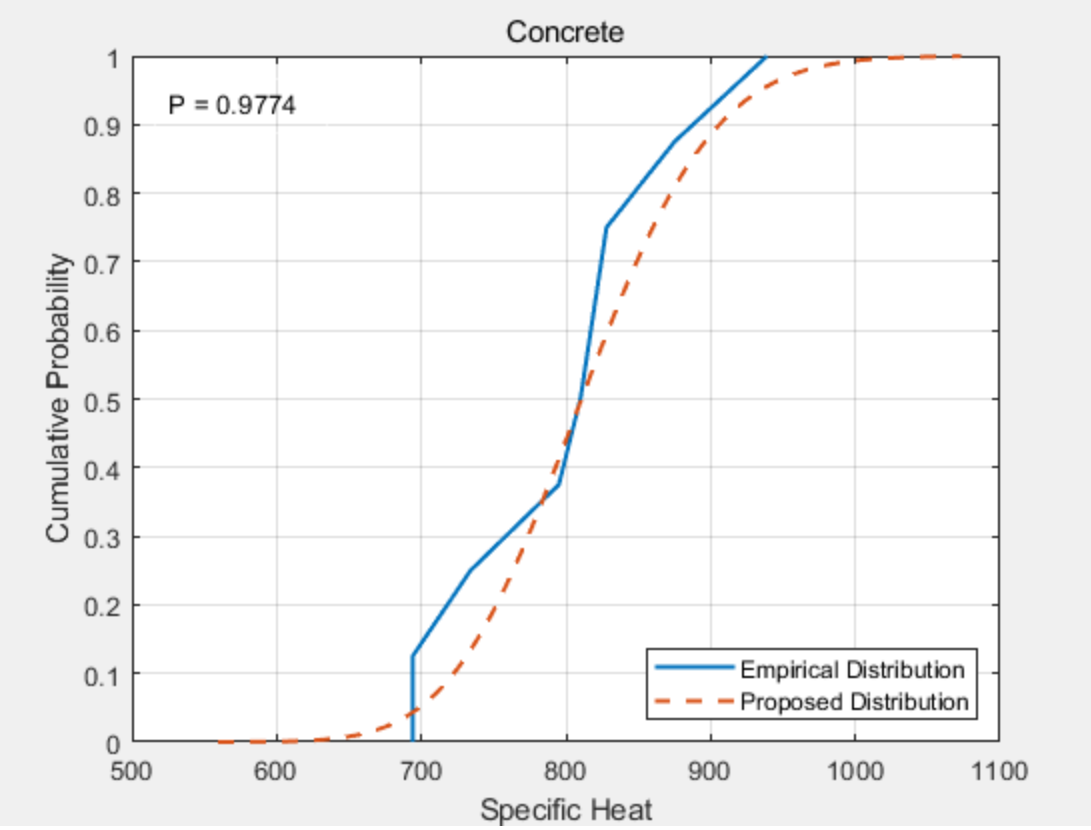

Figure A-3. Concrete specific heat cumulative probability distribution.

The next set were parameters associated with thermoset cable material properties, including insulation thickness, jacket thickness, outer diameter, and bulk density. The variability of these parameters for thermoset cables is shown in [20]:

Table A 6. Thermoset cable material properties.

Cable Number	Cable Description (Insulation/Jacket/No. Conductors)	Cable Classification	Insulation Thickness (mm)	Jacket Thickness (mm)	Outer Diameter (mm)	Bulk Density (kg/m3)
3	XLPE/PVC, 7/C	Mixed	0.8	1.5	15.1	2166
2	EPR/CPE, 7/C	Thermoset	0.8	1.5	15.1	2232
7	XLPE/CSPE, 2/C	Thermoset	0.6	1.1	7.9	1993
8	XLPO/XLPO, 7/C	Thermoset	0.5	0.9	12.2	2743
9	SR/Aramid Braid, 7/C	Thermoset	1.3	1	14.5	2168
10	XLPE/CSPE, 7/C	Thermoset	0.8	1.5	15	2321
11	VITA-LINK, 7/C	Thermoset	1.5	2	19	1656
13	XLPE/CSPE, 12/C	Thermoset	0.6	1.1	12.7	1825
14	XLPE/CSPE, 3/C	Thermoset	1.1	1.5	16.3	2538

A gamma distribution was fitted to the parameters in this limited data set. Because the simulations in which these distributions are used are primarily for illustrative purposes, the large CIs associated with the fitted distributions were deemed to be acceptable. shows the distribution parameters for each of the thermoset cable material properties. through show the proposed gamma distribution compared to the empirical distribution and the resulting p value for each distribution.

Table A-7. Thermoset cable material property distribution Parameters.

Parameter	Distribution	p Value	Parameter 1	Parameter 2
Insulation Thickness	Gamma	0.64805	a=8.18389	b=0.108614
Jacket Thickness	Gamma	0.5374	a=17.2389	b=0.077989
Outer Diameter	Gamma	0.65443	a=20.4278	b=0.69513
Bulk Density	Gamma	0.95733	a=46.8602	b=46.5735

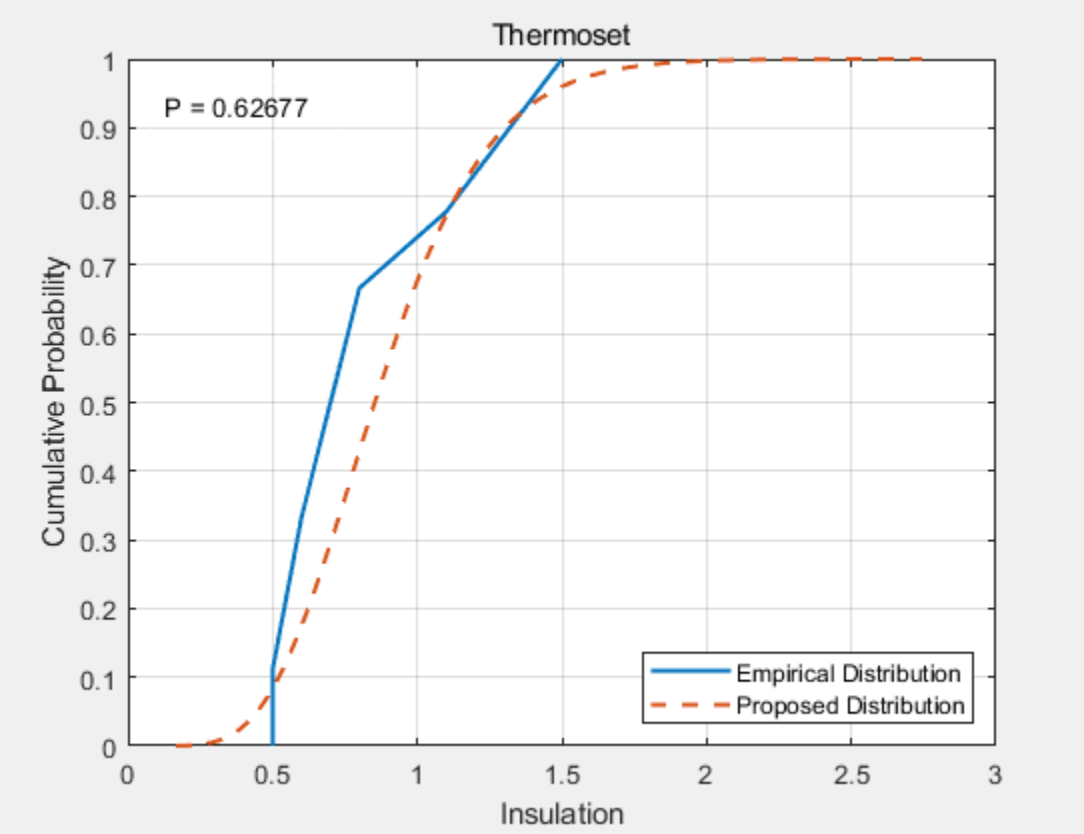

Figure A-4. Thermoset cable insulation thickness cumulative probability distribution.

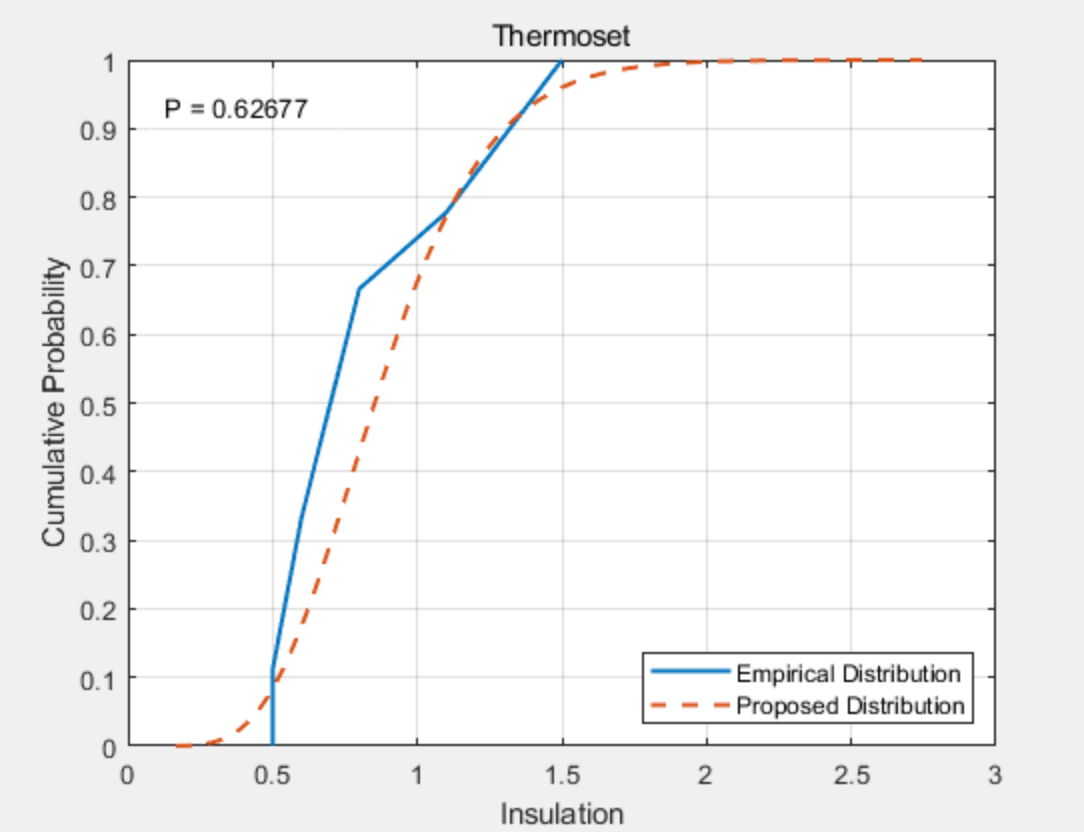

Figure A-5. Thermoset cable jacket thickness cumulative probability distribution.

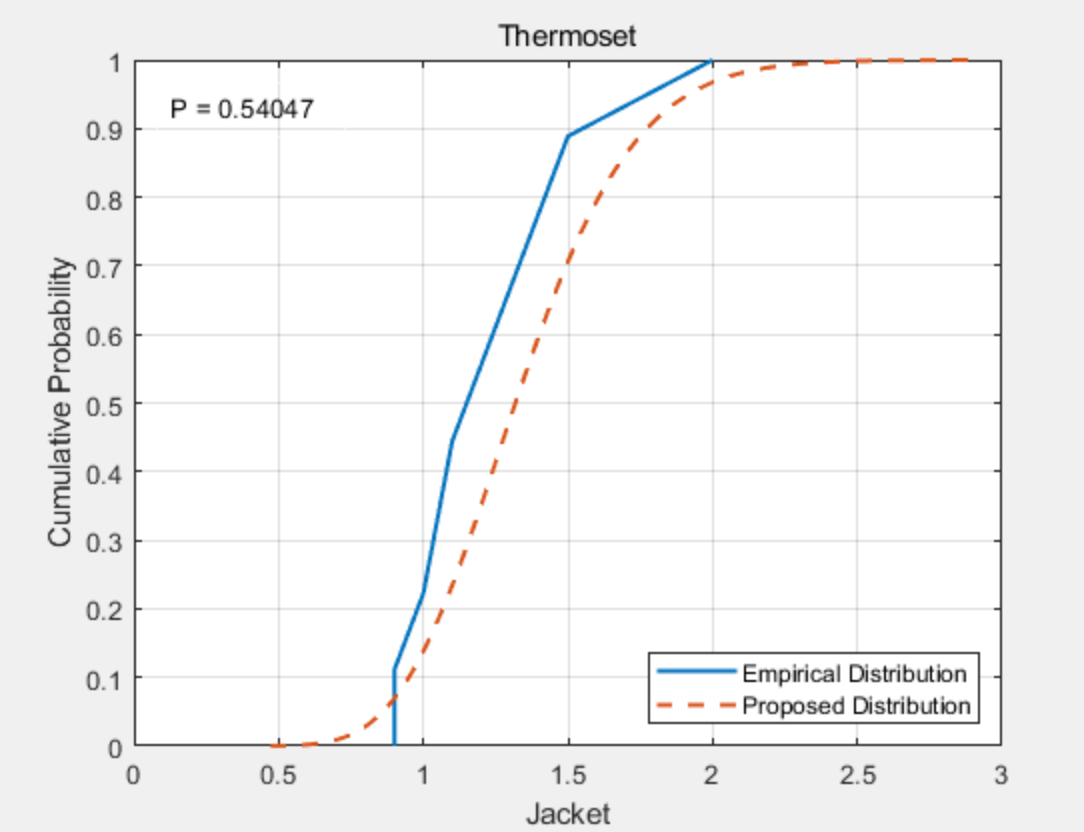

Figure A-6. Thermoset cable outer diameter cumulative probability distribution.

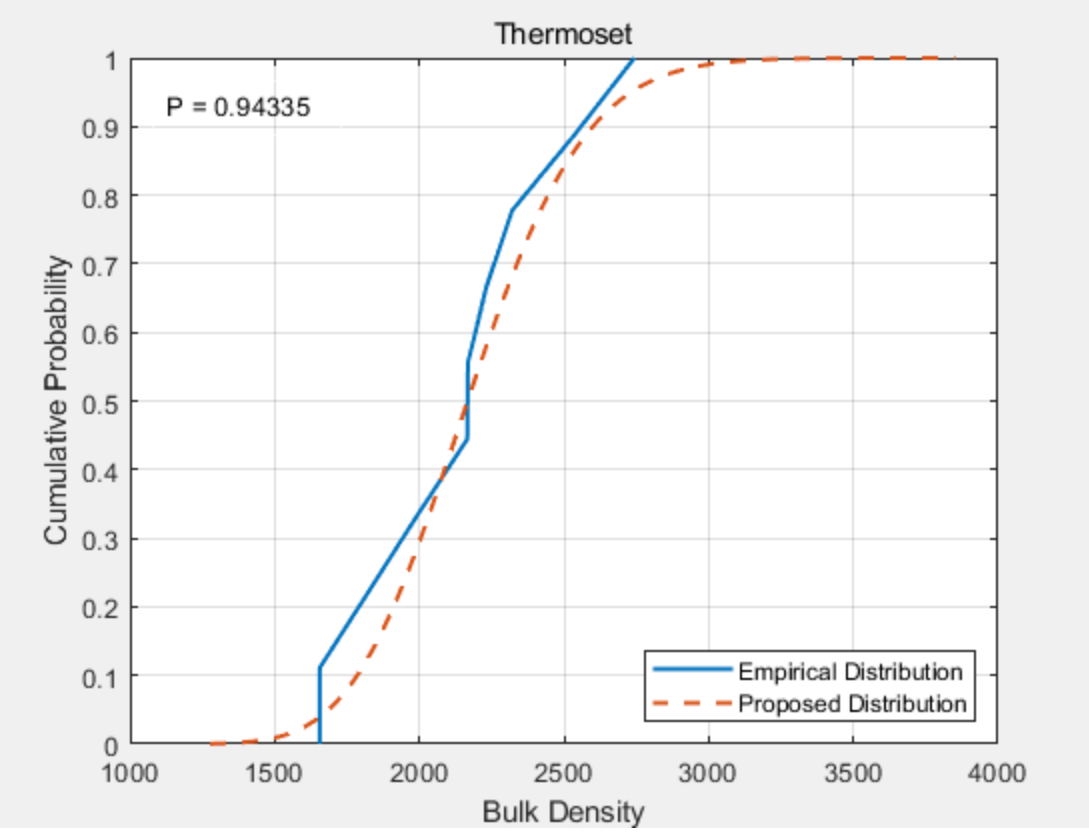

Figure A-7. Thermoset cable bulk density cumulative probability distribution.

The last set was made up of parameters associated with thermoplastic cable material properties, including insulation thickness, jacket thickness, outer diameter, and bulk density. The variability of these parameters for thermoplastic cables is shown in [20]:

Table A-8. Thermoplastic cable material properties.

Cable Number	Cable Description (Insulation/Jacket/No. Conductors)	Cable Classification	Insulation Thickness (mm)	Jacket Thickness (mm)	Outer Diameter (mm)	Bulk Density (kg/m3)
1	PVC/PVC, 7/C	Thermoplastic	0.5	1.1	12.4	2680
4	PVC/PVC, 2/C	Thermoplastic	0.7	1	7	1668
5	PVC/PVC, 3/C	Thermoplastic	0.9	1.5	15.2	2532
6	PVC/PVC, 12/C	Thermoplastic	0.5	1.1	11.3	1948
12	TEF/TEF, 7/C	Thermoplastic	0.4	0.5	10.2	3578
15	PE/PVC, 12/C	Thermoplastic	0.8	1.1	15	2152

A gamma distribution was fit to the parameters in this limited data set. Because the simulations in which these distributions are used are primarily for illustrative purposes, the large CIs associated with the fitted distributions were deemed to be acceptable. shows the distribution parameters for each of the thermoplastic cable material properties. through show the proposed gamma distribution compared to the empirical distribution and the resulting p value for each distribution.

Table A-9. Thermoplastic cable material property distribution parameters.

Parameter	Distribution	p Value	Parameter 1	Parameter 2
Insulation Thickness	Gamma	0.74622	a=12.2996	b=0.0514923
Jacket Thickness	Gamma	0.4857	a=10.3509	b=0.101441
Outer Diameter	Gamma	0.96185	a=15.6428	b=0.757539
Bulk Density	Gamma	0.99789	a=16.4843	b=147.191

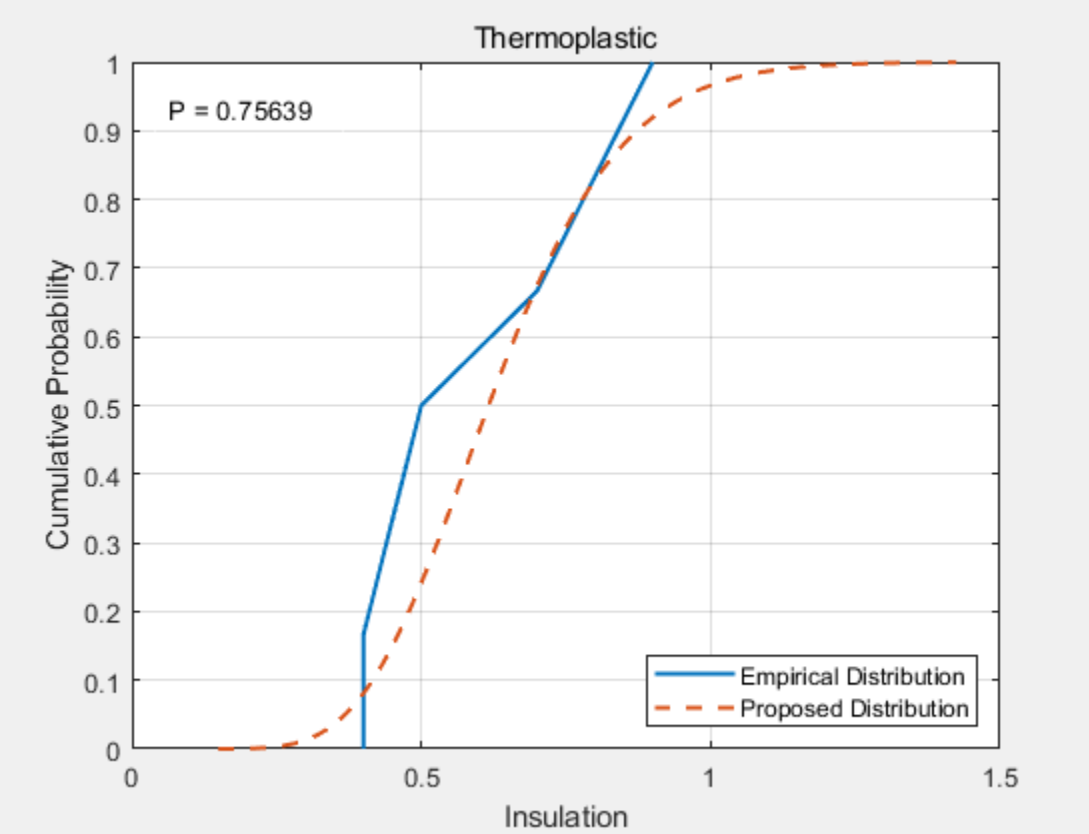

Figure A-8. Thermoplastic cable insulation thickness cumulative probability distribution.

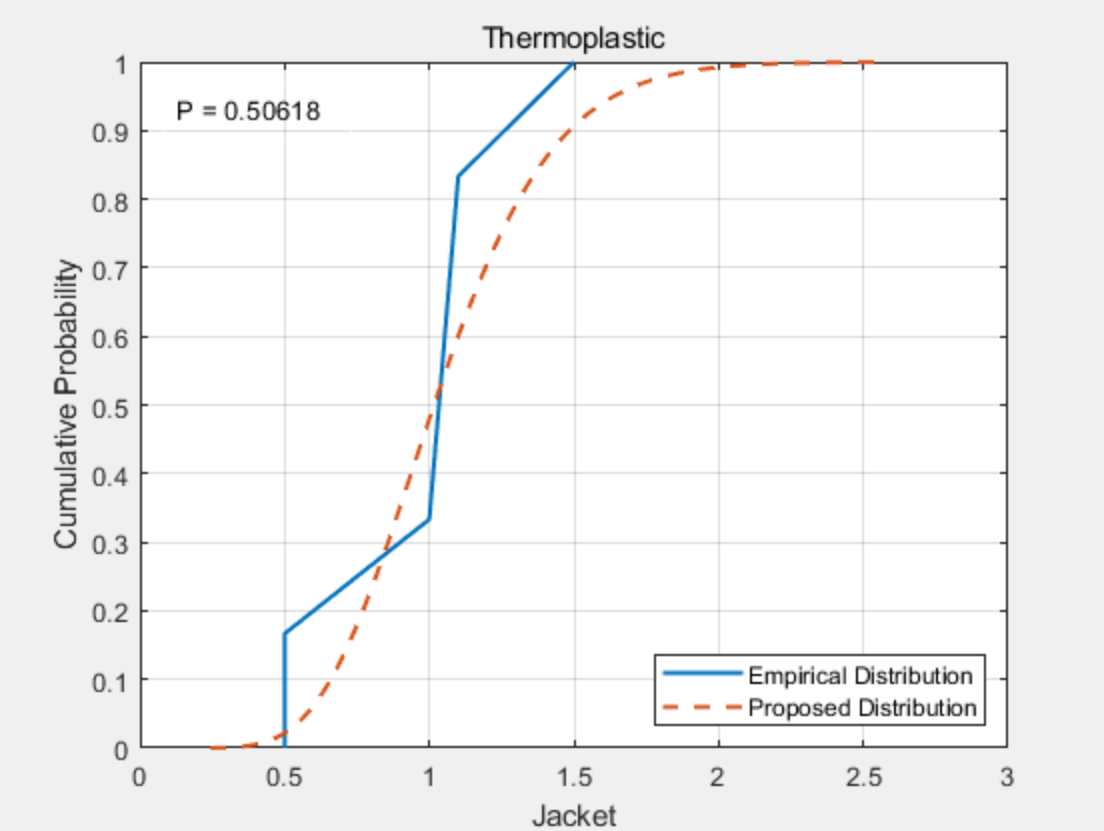

Figure A-9. Thermoplastic cable jacket thickness cumulative probability distribution.

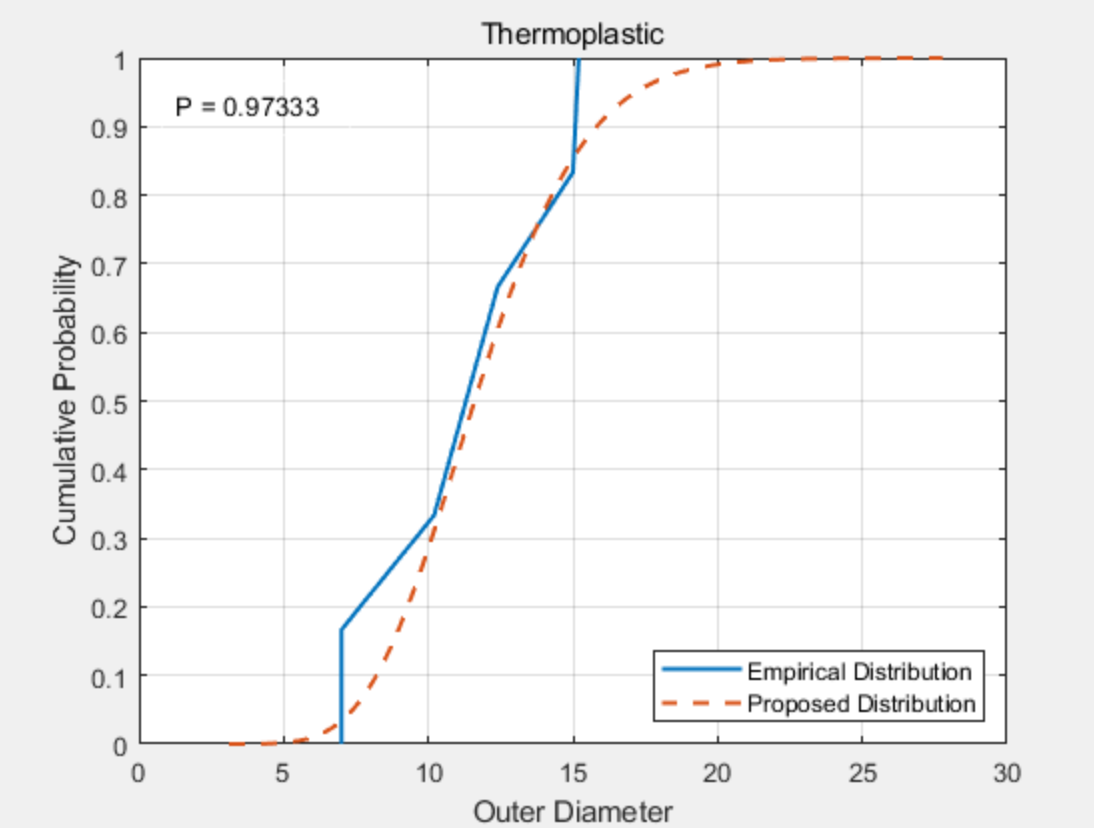

Figure A-10. Thermoplastic cable outer diameter cumulative probability distribution.

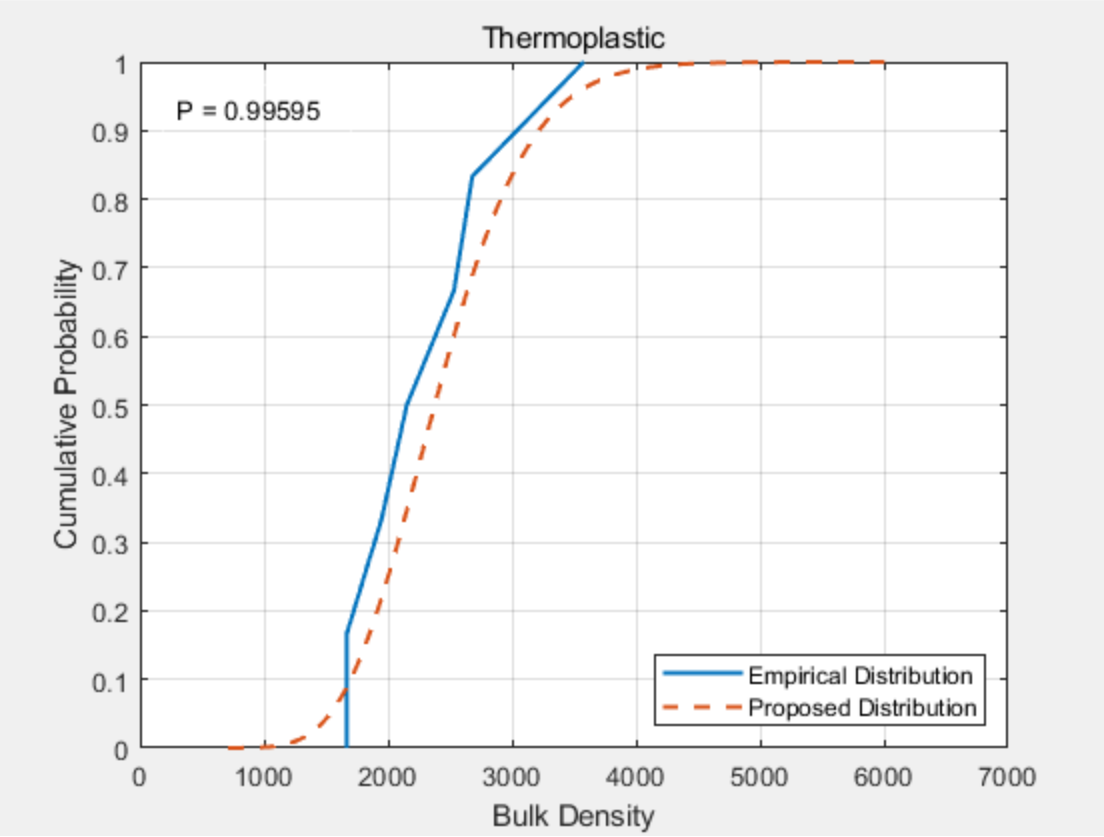

Figure A-11. Thermoplastic cable bulk density cumulative probability distribution.

APPENDIX B

Sections B.1 and B.2 of this appendix report on the results of two sensitivity tests that are conducted to study the impact of the Morris sampling size and the uncertainty associated with types and parameters of the input parameter distributions on the results of the Morris EE analysis (Section 3.4.3). These two tests are limited to involve only four parameters related to the HRR curve, namely maximum HRR value, time to maximum HRR, duration of maximum HRR, and time to decay (i.e., X_1, X_2, X_3, and X_4 in Table 3-B in Section 3.4.2, respectively). The fire simulation model with FDS is used for these two tests and their results are discussed below.

Section B.3 reports on the results of the input parameter screening analysis using Morris EE analysis method when the fire scenario is modeled with FDS.

B.1. Convergence study on Morris sampling size

Sample size in the Morris EE analysis is a function of the number of input parameters treated as random variables and the number of observations of F_i quantified through the input space[35],[36]. By varying the number of observations, a convergence study on the Morris sampling size has been done. Four different Morris sampling sizes were tested: N = 25, N = 50, N = 75, and N = 100. To evaluate the degree of confidence in the estimated μ and σ, it is important to obtain the CIs associated with their point estimates. For each sample size N, results obtained from the N iterative FDS simulations can be considered as independent and identically distributed random samples of the point estimates of μ and σ. Using the Bootstrap resampling method[79], the 95% Confidence Interval (CI) around the point estimates of μ and σ can be computed. Table B-1 shows the point estimates and 95% CIs of μ and σ obtained for the four input parameters regarding their influences on KPM #3 (maximum temperature of Cable Tray B) for the four Morris sampling sizes.

Table B-1: Statistics results for different Morris sampling sizes (obtained using Bootstrap resampling method with 1000 resamples) associated with KPM #3 (maximum temperature of Cable Tray B).

ID	Parameters	Statistics	Morris Sampling Sizes			
			N = 25	N = 50	N = 75	N = 100
X_1	Maximum HRR	μ (95% CI)	38.437 (13.331, 63.543)	38.571 (24.184, 52.958)	42.372 (29.199, 55.545)	34.525 (22.966, 46.084)
		σ (95% CI)	32.300 (17.041, 47.559)	23.809 (18.734, 28.884)	27.327 (22.882, 31.772)	27.562 (23.024, 32.100)
X_2	Time to maximum HRR	μ (95% CI)	1.223 (-0.749, 3.195)	1.621 (-0.019, 3.261)	0.878 (0.006, 1.750)	1.137 (0.456, 1.818)
		σ (95% CI)	2.453 (0.144, 4.762)	2.844 (0.885, 4.803)	1.733 (0.641, 2.825)	1.546 (1.137, 1.955)
X_3	Duration of max HRR	μ (95% CI)	7.698 (1.108, 14.288)	5.734 (1.955, 9.513)	5.696 (2.722, 8.670)	4.885 (2.330, 7.440)
		σ (95% CI)	8.625 (4.191, 13.059)	6.387 (4.797, 7.977)	6.146 (4.158, 8.134)	6.197 (4.603, 7.791)
X_4	Time to decay	μ (95% CI)	0.706 (-0.213, 1.625)	2.086 (0.186, 3.950)	2.345 (0.924, 3.766)	3.421 (2.012, 4.830)
		σ (95% CI)	1.161 (0.257, 2.065)	3.085 (1.382, 4.788)	2.914 (1.954, 3.874)	3.241 (2.583, 3.899)

The widths of the 95% CIs of μ and σ, as shown in Table B-1, generally decrease when the Morris sampling size increases. The results in Table B-1, however, have shown that the ranking order of the four parameters based on the magnitudes of their associated μ and σ values is stable for the four tested sampling sizes. Based on the magnitudes of μ, for example, input parameter X_1 (max. HRR) is the most influential parameter on the Cable Tray B maximum temperature (among the four parameters being considered) due to its highest μ value. However, when considering the CIs around the μ values estimated for these four parameters, one should pay attention to the overlaps (if any) among these CIs. For example, with N = 25, the CIs for μ values associated with X_1 and X_3 are overlapped, which indicates that with this sampling size, it cannot be concluded with statistical significance that X_1 has a greater influence on the output as compared to X_3. At larger sampling sizes, for example, $N \geq 50$, this overlap, however, is no longer present and one can make such conclusion with statistical significance. At this stage, statistical thresholds have not been applied on the obtained statistical measures for determining an "optimal" sample size required for generating statistically stable estimates of μ and σ. Use of statistical thresholds should be considered in a practical application. Regarding the effect of nonlinearity and interactions among the input parameters, the results in Table B-1 have shown that the σ values obtained for all four parameters are relatively high as compared to their μ values. This implies that there are nonlinearity and interaction effects among these input parameters. Note that when considering the values of σ, one should also consider their CIs and pay attention to the overlaps among the CIs (if any).

B.2. Sensitivity of the Morris EE analysis results to changes in the characteristics of input parameter distributions

Based on different sources of data, there may be uncertainty associated with the type and parameters of the probability distribution assigned to each input parameter listed in Table 3-B in Section 3.4.2. To evaluate the sensitivity of the Morris EE analysis results to this type of uncertainty, a limited-scope sensitivity test which involves four key input parameters (X_1, X_2, X_3, and X_4 in Table 3-B) was conducted. In this test, only these four input parameters are treated as random variables in the Morris EE analysis settings. Probability distributions assigned for X_2 and X_3 are kept the same as those listed in Table 3-B. For X_1, two probability distributions are tested: (i) the distribution listed in Table 3-B, which was obtained from NUREG-2178 [71]; (ii) a distribution obtained from NUREG/CR-6850 [26] for electrical fires in multiple cable bundles with qualified cable inside vertical cabinets, which is represented by a gamma distribution with $\alpha = 0.7$, $\beta = 216$. Regarding X_4, by conducting the Kolmogorov-Smirnov test to fit selected distributions to the experimental data provided in NUREG/CR-6850 [26], two alternative distributions are not rejected and, hence, are considered in this test: (i) the distribution listed in Table 3-B, and (ii) a triangular distribution with lower bound LB = 10, upper bound UB = 30, and mode value of 17. In total, four combinations of input parameter distributions have been tested as summarized in Table B-2.

Table B-2: Combinations of input parameter distributions for testing the sensitivity of Morris EE analysis results.

ID	X_1 (Maximum HRR) Distributions	X_4 (Time to decay) Distributions
1	Gamma ($\alpha = 0.36$, $\beta = 57$)	Uniform (10, 30)
2	Gamma ($\alpha = 0.36$, $\beta = 57$)	Triangular (10, 17, 30)
3	Gamma ($\alpha = 0.7$, $\beta = 216$)	Uniform (10, 30)
4	Gamma ($\alpha = 0.7$, $\beta = 216$)	Triangular (10, 17, 30)

Notes: In these four combinations, distributions for X_2 and X_3 are kept the same as reported in Table 3-B (Section 3.4.2).

Representative results of this sensitivity test are reported in Figures B-1 through B-4 below, which show results on the influences of the four input parameters (X_1, X_2, X_3, and X_4) on the maximum temperature of Cable Tray B obtained for the four combinations listed in Table B-2 (with N = 75), respectively. In each of these four figures, in the bar chart on the left, the right ends of the blue bars indicate observed point values of μ and the black line segments represent the 95% CIs around them.

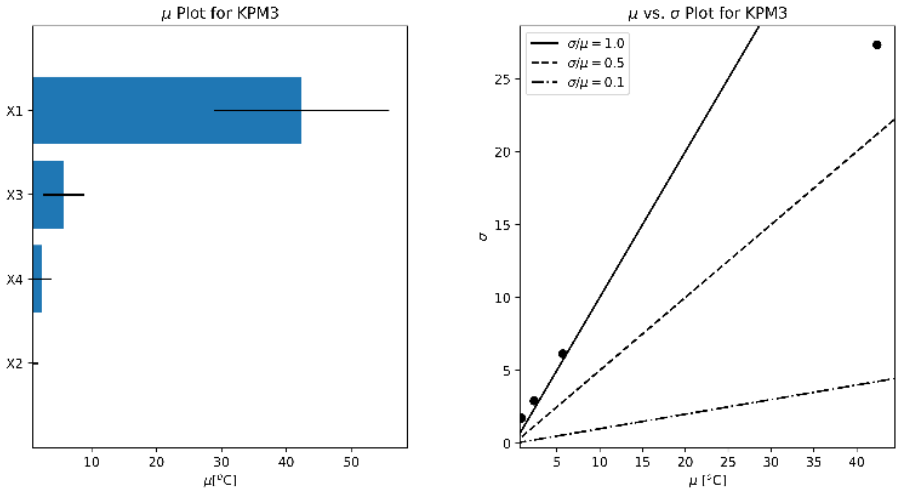

Figure B-1: Sensitivity measures obtained for KPM #3 (Cable Tray B Max. Temperature) – Combination #1.

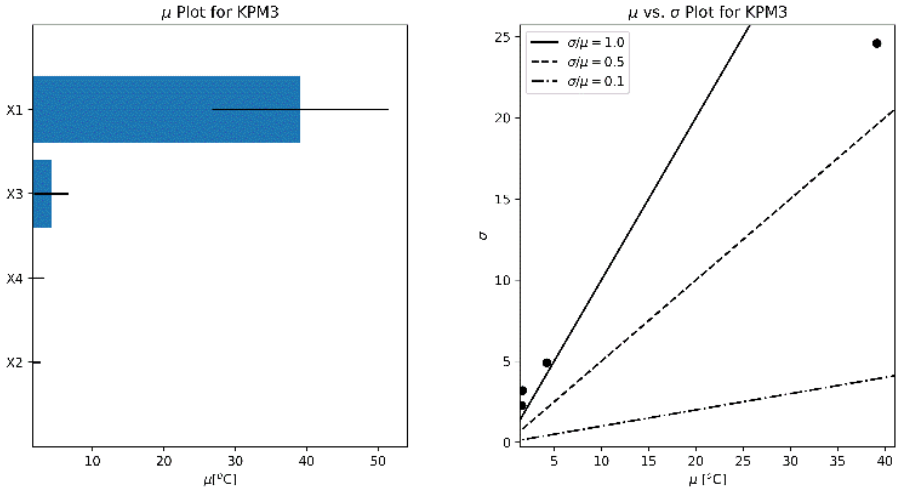

Figure B-2: Sensitivity measures obtained for KPM #3 (Cable Tray B Max. Temperature) – Combination #2.

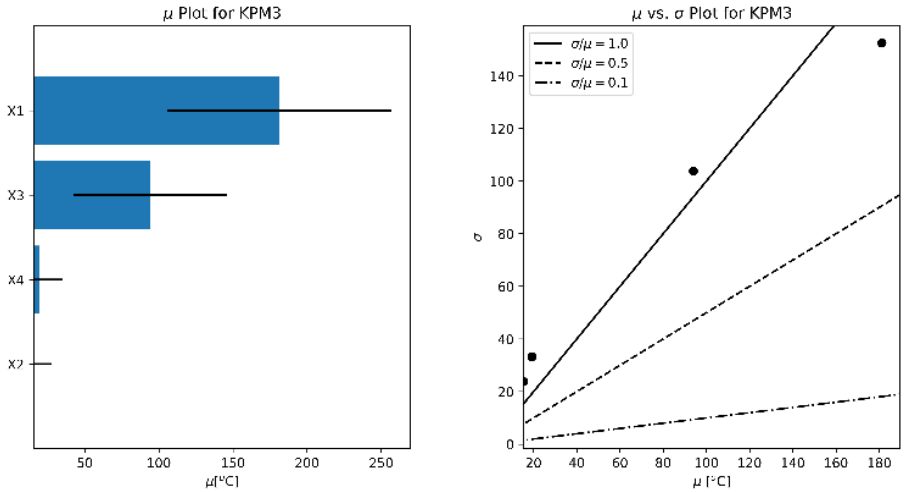

Figure B-3: Sensitivity measures obtained for KPM #3 (Cable Tray B Max. Temperature) – Combination #3.

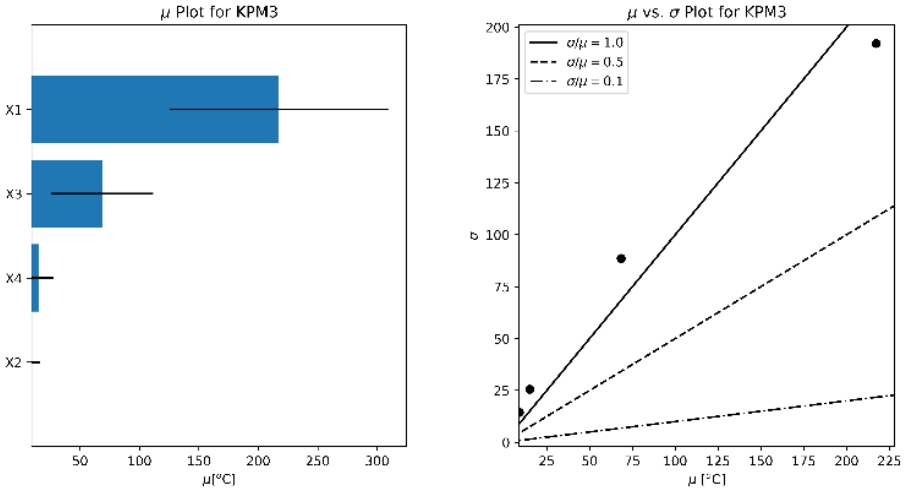

Figure B-4: Sensitivity measures obtained for KPM #3 (Cable Tray B Max. Temperature) – Combination #4.

Figures B-1 to B-4 show that the ranking obtained for the four parameters (based on their μ values) in the four tested combinations seems to follow the same order. It is, however, noted that in Figure B-3, the 95% CIs obtained for X_1 and X_3 are overlapped, which indicates that it cannot be simply concluded that X_1 has a higher influence on the KPM #3 as compared to X_3. To make such conclusion, one would need to reduce the width of the 95% CIs to avoid the overlap. This reduction may be achieved by increasing the Morris sampling size. By varying the distribution of X_4, there are, however, noticeable changes in the magnitudes of μ associated with X_1 and X_3. This result indicates additional experimental data for X_4 (i.e., time to decay) should be collected to develop an accurate distribution for this parameter. By varying the distribution of X_1, significant changes were observed in the magnitudes of μ associated with all input parameters. This result could provide an explanation for the motivation behind recent research efforts to more realistically refine and characterize the maximum HRR of electrical enclosure fires [13]. The observations obtained from this sensitivity test also imply the presence of interaction effects among the parameters, which highlights the need for Global IM analysis. Note that, in the current scope of work, the

NSP is not considered (i.e., assumed to be unity). Should the analysis consider the suppression curve (based on NUREG/CR-6850), it may change the observations obtained in this test.

B.3. Input parameter screening analysis using Morris EE analysis method

This section reports on the settings and results of the quantitative screening in Step 3 (using the Morris EE analysis method [35]) for all nine input parameters listed in Table 3-B when the fire scenario is modeled with FDS. The screening aims to identify input parameters among those listed in Table 3-B that have negligible effects on the KPM predictions by the simulation model (i.e., maximum temperature and heat flux at each target cable tray). To compute the EE, the state space of each input parameter is discretized into a p-level grid (with $p = 4$) so that each input parameter X_i can be randomly sampled from its discretized values. As measures of sensitivity, the sample mean (μ) and the sample standard deviation (σ) of the EE are used.

Values of the sensitivity measures are obtained by performing 150 FDS model executions (9 input parameters and 15 observations of F_i per input factor i). The Morris samples are drawn using the sampling strategy suggested by Campolongo et al. [36]. Due to an intensive computational resource demand associated with the use of FDS, a parallel simulation using the Message Passing Interface (MPI) is recommended to efficiently perform the FDS runs. An optimal mesh resolution (i.e., spatial grid cell size) for the FDS simulation model is adopted from Sakurahara et al. [28].

Figure B-5 to Figure B-10 below show μ and σ results of this Morris EE analysis for the nine input parameters regarding their influences on the six KPMs of interest, i.e., maximum temperature inside the cable jacket (T_{CB}) and maximum heat flux at the surface of the cable jacket (q''_{CB}) of the three target cable trays A, B and C. In each figure, in the blue bar chart on the left, the right ends of the blue bars indicate observed point values of μ and the black line segments represent the 95% CIs around them. Table B-3 reports numerical results of these sensitivity measures, μ, and σ.

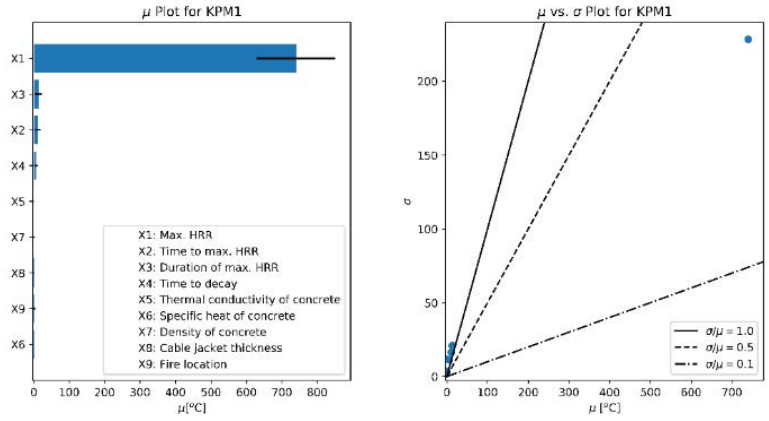

Figure B-5: Results of Morris EE analysis for nine input parameters listed in Table 3-B associated with KPM #1 (Cable Tray A Max. Temperature)

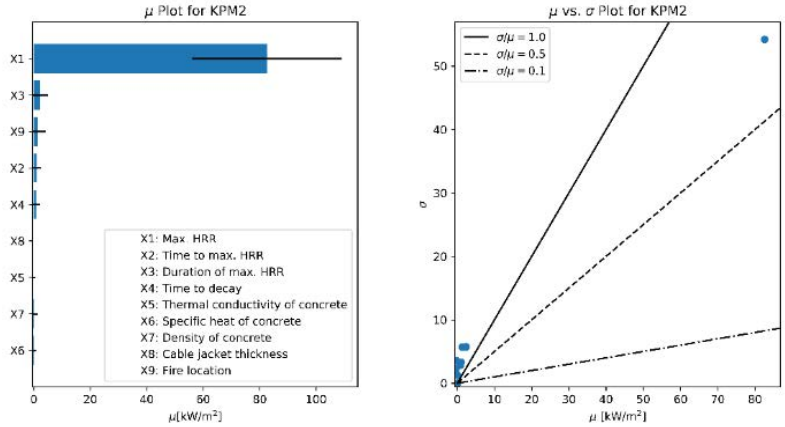

Figure B-6: Results of Morris EE analysis for nine input parameters listed in Table 3-B associated with KPM #2 (Cable Tray A Max. Heat Flux)

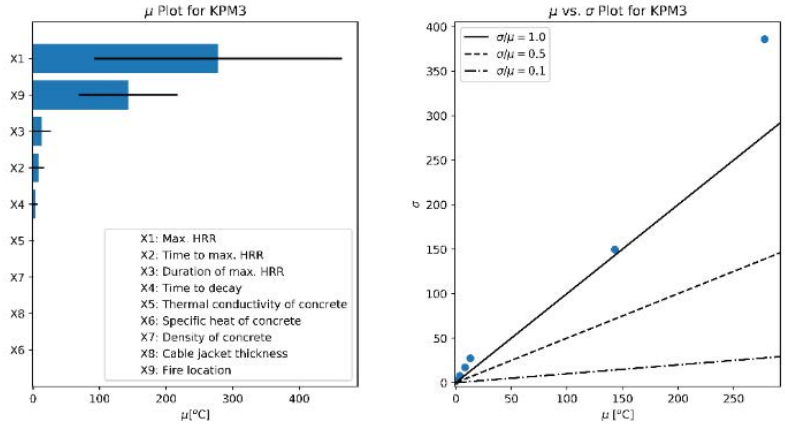

Figure B-7: Results of Morris EE analysis for nine input parameters listed in Table 3-B associated with KPM #3 (Cable Tray B Max. Temperature)

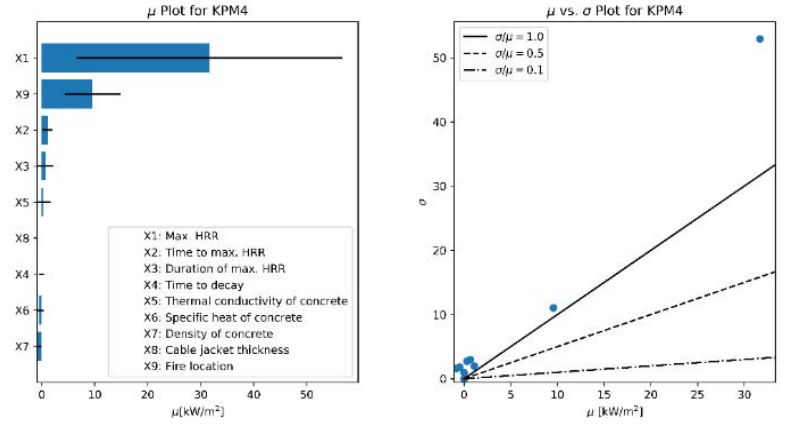

Figure B-8: Results of Morris EE analysis for nine input parameters listed in Table 3-B associated with KPM #4 (Cable Tray B Max. Heat Flux)

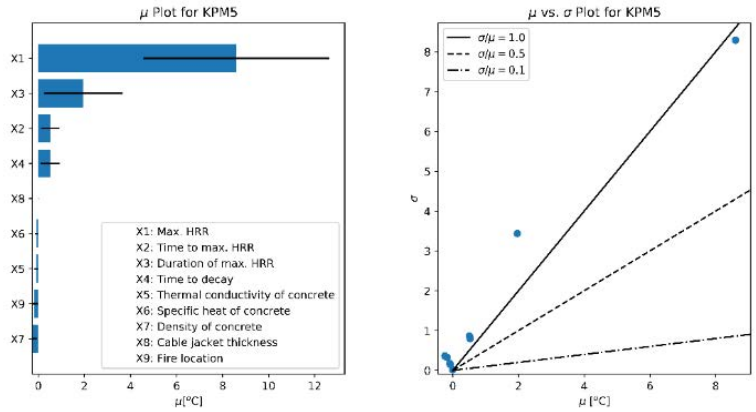

Figure B-9: Results of Morris EE analysis for nine input parameters listed in Table 3-B associated with KPM #5 (Cable Tray C Max. Temperature)

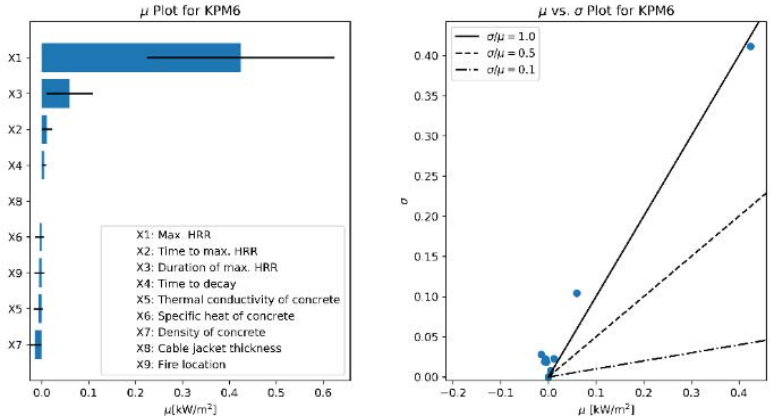

Figure B-10: Results of Morris EE analysis for nine input parameters listed in Table 3-B associated with KPM #6 (Cable Tray C Max. Heat Flux)

Table B-3: Statistics Results Obtained from the Morris EE analysis for Nine Parameters Listed in Table 3-B, sorted by μ* values – Fire modeled with FDS.

		X_1	X_2	X_3	X_4	X_5	X_6	X_7	X_8	X_9
KPM1 (Cable Tray A Max. Temperature)	μ	739.92	11.182	13.129	6.162	0.406	-2.513	0.367	-0.814	-1.614
	σ	228.444	16.408	20.916	11.357	2.158	3.341	3.489	1.993	11.773
		X_1	X_2	X_3	X_4	X_5	X_6	X_7	X_8	X_9
KPM2 (Cable Tray A Max. Heat Flux)	μ	82.584	0.99	2.348	0.824	-0.085	-0.396	-0.3	0	1.326
	σ	54.206	3.292	5.723	2.868	1.31	2.254	3.552	0	5.704
		X_1	X_2	X_3	X_4	X_5	X_6	X_7	X_8	X_9
KPM3 (Cable Tray B Max. Temperature)	μ	277.753	8.402	13.089	3.545	0.03	-0.424	-0.233	-0.364	143.016
	σ	385.849	17.136	27.342	7.516	2.099	1.472	1.532	1.357	149.702

		X_1	X_2	X_3	X_4	X_5	X_6	X_7	X_8	X_9
KPM4 (Cable Tray B Max. Heat Flux)	μ	31.669	1.09	0.661	-0.004	0.317	-0.461	-0.838	0	9.579
	σ	52.921	1.979	2.987	0.967	2.713	1.803	1.599	0	11.049
		X_1	X_2	X_3	X_4	X_5	X_6	X_7	X_8	X_9
KPM5 (Cable Tray C Max. Temperature)	μ	8.604	0.525	1.962	0.506	-0.092	-0.078	-0.245	-0.007	-0.18
	σ	8.295	0.804	3.438	0.863	0.17	0.152	0.364	0.021	0.328
		X_1	X_2	X_3	X_4	X_5	X_6	X_7	X_8	X_9
KPM6 (Cable Tray C Max. Heat Flux)	μ	0.425	0.012	0.06	0.005	-0.008	-0.004	-0.015	0	-0.005
	σ	0.411	0.023	0.104	0.008	0.019	0.018	0.028	0	0.022

Note: For input parameters X_i, please refer to Table 3-B.

As can be seen in Table B-3, the absolute magnitudes of the three sensitivity metrics (μ, and σ) obtained when using FDS are different from those obtained when using CFAST (Table 2). One possibility is that this stems from the differences between the FDS and CFAST model resolutions. For example, a significant difference between FDS and CFAST in predicting the maximum heat flux and cable temperature is that FDS has a "finer" spatial resolution as all of its geometrical entities are divided into rectilinear grid cells and described by defining their coordinates in the computational domain; CFAST, on the other hand, is a two-zone model where the vertical dimension of the fire compartment is divided into two discrete layers. It should also be noted that NUREG-1934 indicated a reservation on the applicability of CFAST to Scenario D (Figure 13) due to multiple reasons related to the fire conditions that may not be suitable for CFAST. To thoroughly investigate the underlying causes of the differences and how they affect the results of the Morris EE analysis, further study is needed.

APPENDIX C

This appendix reports on the full results the Global IM analysis done for nine input parameters listed in Table 1. Table C-1 shows $S_i^{(CDF)}$ results calculated for each of the 9 input parameters with respect to its influence on each of the six KPMs considered in this case study (i.e., maximum temperature inside the cable jacket, T_{CB}, and maximum heat flux at the surface of the cable jacket, q''_{CB}, for three cable trays A, B, and C). Meanwhile, Table C-2 reports on the $S_i^{(CDF)}$ results calculated with respect to the influence of the input parameters on the fire-induced cable damage probabilities. Table C-3 reports on the $S_i^{(CDF)}$ results calculated with respect to the influence of the input parameters on the risk output (i.e., Core Damage Frequency of the hypothetical PRA model in Section 3.4.4). The 90-percentile confidence intervals (CI) of $S_i^{(CDF)}$ are calculated using the replicated Monte Carlo simulation and the Bootstrap resampling method [68].

Table C-1: $S_i^{(CDF)}$ results calculated for nine input parameters with respect to their influence on each of the six simulation model outputs

Input Parameters		**X_1**	**X_2**	**X_3**	**X_4**	**X_5**	**X_6**	**X_7**	**X_8**	**X_9**
KPM1 (Cable Tray A Max. Temperature)	$\bar{S}_i^{(CDF)}$	9.93E-01	1.41E-02	4.54E-02	1.70E-02	8.05E-05	3.90E-05	9.08E-05	4.48E-03	1.60E-04
	$S.E.(\bar{S}_i^{(CDF}$	6.69E-04	1.06E-05	4.98E-05	1.83E-05	9.96E-08	6.83E-08	1.44E-07	5.91E-06	1.55E-07
	5th-percentile	8.86E-01	1.23E-02	3.72E-02	1.42E-02	6.43E-05	2.85E-05	6.84E-05	3.56E-03	1.36E-04
	95th-percentile	1.11E+00	1.59E-02	5.37E-02	2.01E-02	9.70E-05	5.08E-05	1.16E-04	5.49E-03	1.86E-04
		X_1	**X_2**	**X_3**	**X_4**	**X_5**	**X_6**	**X_7**	**X_8**	**X_9**
KPM2 (Cable Tray A Max. Heat Flux)	$\bar{S}_i^{(CDF)}$	1.16E+00	3.53E-04	4.37E-04	5.51E-04	7.24E-05	3.55E-05	8.93E-05	0.00E+00	2.27E-05
	$S.E.(\bar{S}_i^{(CDF}$	1.07E-03	2.94E-07	3.15E-07	1.07E-06	8.42E-08	7.53E-08	1.03E-07	0.00E+00	3.62E-08
	5th-percentile	9.89E-01	3.06E-04	3.86E-04	3.96E-04	5.93E-05	2.34E-05	7.29E-05	0.00E+00	1.67E-05
	95th-percentile	1.34E+00	4.03E-04	4.90E-04	7.43E-04	8.70E-05	4.83E-05	1.07E-04	0.00E+00	2.85E-05
		X_1	**X_2**	**X_3**	**X_4**	**X_5**	**X_6**	**X_7**	**X_8**	**X_9**
KPM3 (Cable Tray B Max. Temperature)	$\bar{S}_i^{(CDF)}$	7.34E-01	2.10E-02	6.08E-02	2.37E-02	3.38E-04	2.00E-04	4.33E-04	2.08E-03	5.56E-01
	$S.E.(\bar{S}_i^{(CDF}$	1.47E-03	1.49E-05	5.74E-05	2.52E-05	3.60E-07	3.13E-07	3.78E-07	2.49E-06	7.52E-04
	5th-percentile	5.34E-01	1.86E-02	5.14E-02	1.97E-02	2.80E-04	1.48E-04	3.72E-04	1.69E-03	4.37E-01
	95th-percentile	1.00E+00	2.35E-02	7.02E-02	2.80E-02	3.98E-04	2.52E-04	4.95E-04	2.50E-03	6.86E-01
		X_1	**X_2**	**X_3**	**X_4**	**X_5**	**X_6**	**X_7**	**X_8**	**X_9**

KPM4 (Cable Tray B Max. Heat Flux)	$\bar{S}_i^{(CDF)}$	1.19E+00	3.92E-03	2.47E-04	0.00E+00	1.40E-04	5.14E-05	2.24E-04	0.00E+00	8.47E-01
	$S.E.(\bar{S}_i^{(CDF}$	3.19E-03	6.19E-06	3.60E-07	0.00E+00	2.60E-07	1.70E-07	3.07E-07	0.00E+00	1.16E-03
	5th-percentile	7.72E-01	2.94E-03	1.90E-04	0.00E+00	9.92E-05	2.47E-05	1.75E-04	0.00E+00	6.66E-01
	95th-percentile	1.80E+00	4.99E-03	3.09E-04	0.00E+00	1.85E-04	8.04E-05	2.77E-04	0.00E+00	1.05E+00
		X_1	**X_2**	**X_3**	**X_4**	**X_5**	**X_6**	**X_7**	**X_8**	**X_9**
KPM5 (Cable Tray C Max. Temperature)	$\bar{S}_i^{(CDF)}$	2.64E-02	9.89E-04	3.15E-03	1.95E-03	2.38E-04	1.35E-04	3.32E-04	2.84E-05	1.94E-05
	$S.E.(\bar{S}_i^{(CDF}$	8.89E-05	8.17E-07	2.72E-06	2.11E-06	1.58E-07	1.07E-07	3.49E-07	2.63E-08	2.44E-08
	5th-percentile	1.49E-02	8.55E-04	2.70E-03	1.60E-03	2.12E-04	1.17E-04	2.77E-04	2.43E-05	1.57E-05
	95th-percentile	4.34E-02	1.12E-03	3.60E-03	2.30E-03	2.64E-04	1.53E-04	3.92E-04	3.29E-05	2.37E-05
		X_1	**X_2**	**X_3**	**X_4**	**X_5**	**X_6**	**X_7**	**X_8**	**X_9**
KPM6 (Cable Tray C Max. Heat Flux)	$\bar{S}_i^{(CDF)}$	1.87E-02	4.85E-04	1.56E-03	3.90E-04	1.21E-04	7.03E-05	1.69E-04	0.00E+00	1.54E-05
	$S.E.(\bar{S}_i^{(CDF}$	6.30E-05	3.63E-07	1.33E-06	4.12E-07	8.36E-08	4.71E-08	1.60E-07	0.00E+00	2.13E-08
	5th-percentile	1.03E-02	4.25E-04	1.33E-03	3.23E-04	1.07E-04	6.27E-05	1.44E-04	0.00E+00	1.21E-05
	95th-percentile	3.07E-02	5.45E-04	1.77E-03	4.60E-04	1.35E-04	7.81E-05	1.97E-04	0.00E+00	1.91E-05

Table C-2: S_i (CDF) results calculated for nine input parameters with respect to their influence on the fire-induced cable damage probabilities

Input Parameters		**X_1**	**X_2**	**X_3**	**X_4**	**X_5**	**X_6**	**X_7**	**X_8**	**X_9**
Cable Tray A Damage Probability	$\bar{S}_i^{(CDF)}$	8.57E-02	2.57E-03	8.17E-03	7.46E-03	5.32E-05	2.87E-05	7.08E-05	3.07E-03	8.07E-05
	$S.E.(\bar{S}_i^{(CDF}$	1.66E-04	1.87E-06	1.05E-05	9.77E-06	4.06E-08	2.30E-08	5.48E-08	4.61E-06	8.40E-08
	5th-percentile	5.96E-02	2.26E-03	6.46E-03	5.91E-03	4.65E-05	2.49E-05	6.20E-05	2.36E-03	6.76E-05
	95th-percentile	1.14E-01	2.88E-03	9.90E-03	9.11E-03	5.99E-05	3.26E-05	7.98E-05	3.88E-03	9.54E-05
		X_1	**X_2**	**X_3**	**X_4**	**X_5**	**X_6**	**X_7**	**X_8**	**X_9**
Cable Tray B	$\bar{S}_i^{(CDF)}$	2.36E-03	9.84E-05	3.98E-04	4.32E-05	8.13E-08	4.31E-08	1.69E-07	2.29E-05	9.42E-04

Damage Probability	$S.E.(\bar{S}_i^{(CDF}$	1.47E-05	3.68E-07	1.41E-06	2.64E-07	7.91E-10	4.18E-10	9.18E-10	7.84E-08	3.39E-06
	5th-percentile	4.47E-04	3.84E-05	1.79E-04	5.52E-06	0.00E+00	0.00E+00	4.29E-08	1.06E-05	4.38E-04
	95th-percentile	5.17E-03	1.62E-04	6.41E-04	9.15E-05	2.44E-07	1.29E-07	3.34E-07	3.65E-05	1.54E-03

Table C-3: S_i (CDF) results calculated for nine input parameters with respect to their influence on the risk output (of the hypothetical PRA model in Section 3.4.4.2)

Input Parameters		**X_1**	**X_2**	**X_3**	**X_4**	**X_5**	**X_6**	**X_7**	**X_8**	**X_9**
Core Damage Frequency	$\bar{S}_i^{(CDF)}$	2.92E-08	1.24E-09	4.36E-09	7.55E-10	1.23E-12	6.58E-13	8.69E-12	3.63E-10	1.06E-08
	$S.E.(\bar{S}_i^{(CDF}$	1.95E-10	4.52E-12	1.60E-11	3.50E-12	1.19E-14	6.38E-15	5.93E-14	1.34E-12	3.40E-11
	5th-percentile	5.20E-09	5.06E-10	1.91E-09	2.37E-10	0.00E+00	0.00E+00	1.29E-12	1.53E-10	5.47E-09
	95th-percentile	6.74E-08	2.00E-09	7.20E-09	1.37E-09	3.68E-12	1.95E-12	2.04E-11	5.98E-10	1.66E-08